Design and synthesis of benign, N- and O-containing, organic ligands for surface engineering

Robert Phillip Renz

Doctor of Philosophy

University of Edinburgh

2007

Declaration

I declare that I have composed this thesis and the work it refers to has been carried out by myself, except where referenced to another.

Robert Renz

May 2007

Abstract

This thesis is concerned with the development of new organic ligands as corrosion inhibitors. The introductory chapter presents a review of the chemistry involved in the corrosion of metal surfaces. Chapter 2 considers the requirements necessary to develop new ligands. The ligand-surface complex must have a high thermodynamic and kinetic stability. The inclusion of multifunctionality allows the potential for intermolecular ligand-ligand or ligand-surface secondary bonding which can generate a multisite attachment mode of binding. For example, Irgacor 419©, 3-(4-methylbenzoyl)-propionic acid, is used commercially in surface coatings as a corrosion inhibitor. Its efficacy is rationalised by the strong binding of the carboxylic acid group to iron(III) atoms and the secondary bonding of the keto group to a surface hydroxyl. Its bromo-analogue, 3-(4-bromobenzoyl)-propionic acid, was studied for use in Quartz Crystal Microbalance studies. Use of a QCM and the adsorption isotherm of a ligand from a solution phase onto high surface area solid substrate, goethite, were considered as analytical techniques to investigate ligand-surface interactions.

Chapter 3 considers the synergistic corrosion inhibition effect obtained by combining two knonwn corrosion inhibitors for mild steel, 2-hydroxyl-5-nonyl-benzaldehyde oxime (P50 oxime) and polyisobutylene succinic anhydride (PIBSA) which has been patented by ICI. Reactions between salicyaldehyde or benzaldehyde oxime and succinic or glutaric anhydride are shown to result in ring opening and generation of a series of ligands, including salicyaldehyde *O*-(4-carboxypropanoyl) oxime and benzaldehyde *O*-(5-carboxybutanoyl) oxime. A search of the CSD shows that salicylaldoximes and similar structures have a propensity for formation of polynuclear complexes. Measurement of adsorption isotherms on goethite indicate that the inclusion of a phenolic hydroxyl to these oxime ester molecules allows them to generate multilayers when attaching to iron(III) oxide surfaces which is useful in generating hydrophobic thick-films. The absence of a phenol to surface interaction in surface binding is supported by the binding of 2-hydroxy-benzaldehyde-*O*-methyl-oxime being weaker than that of 2-hydroxy-benzaldehyde oxime. In addition, these are both weaker than

P50 oxime suggesting that the corrosion resistance synergism observed when combining P50 oxime with PIBSA is partly due to the high number of alkyl chain groups held in close proximity to the surface which assists in forming films with good hydrophobicity.

In the fourth chapter, the synthesis of several benzoic acid derivatives was used to determine the effect of the systematic introduction of cooperative intermolecular bonding groups to a ligand. In addition, the inclusion of a sulfur atom was used to allow adsorption isotherm determination to be carried out using ICP-OES. The binding strength of 4-[3-(4-Methylsulfanyl-phenyl)-ureido]-benzoic acid, as determined by adsorption isotherms, is considerably higher than that of 4-ethylsulfanyl benzoic acid. A series of methionine derivates generated 2-[4-(1-Carboxy-3-methylsulfanyl-propylcarbamoyl)-benzoylamino]-4-methylsulfanyl-butyric acid, which has a large number of surface ligating and hydrogen bonding groups. This ligand forms a very stable ligand-surface assembly and has a tendency to create second or further layers.

Carboxylic acids with a single carbon atom link to a carbonyl group are considered in chapter 5. Adsorption isotherm determinations demonstrate that 2-(4-chloro-phenyl) malonic acid binds more strongly to goethite that the commercial reagent, Irgacor 419©, and much more strongly than (4-chloro-phenyl) acetic acid. Molecular modelling identifies surface binding modes which could account for the higher stability of the malonate surface complexes. The most plausible models involve multisite attachment with a binucleating mode which leaves on carboxylic acid group free to form hydrogen bonds to adjacent ligands or, a trinucleating arrangement with malonate in its dianionic form. The development of commercial corrosion inhibitors is considered. A propensity for decarboxylation, observed when attempting to prepare polynuclear complexes as model compounds and when attempting to prepare new 2-substituted malonic acids may limit their efficacy in surface protection and surface engineering.

I dedicate this thesis to my parents to say thank you for everything.

Acknowledgements

My biggest thank you goes to my supervisor Professor Peter Tasker, firstly for giving me the opportunity to do a PhD and for all the help and advice during it. I am sure that with all my tasty results, extension of deadlines, listening and learning from all the digressions, that I have done enough character building over the past few years to face the working world. I have really enjoyed my time as a PhD student, except the smelly thiol accident, and appreciate the fact that I have been allowed to do one.

I'd like to thank all the departmental staff who have helped with the analysis of my compounds, particularly John Millar for his advice with NMR, Ronald Brown for BET surface area determinations and Stuart the glassblower for making me a special beaker for the QCM. Demonstrating in the 1st year lab was worth it just to here Elaine the technician's dry sense of humour once a week. Thanks to Dr. Simon Parsons, Fraser White for X-ray structural analysis and the remaining crystallography department for checking my crystals that weren't suitable.

I would also like to thank my family and especially my parents for being supportive, and for the financial help over the past few months, and to all my friends who have provided me with much entertainment.

Finally, a thank you to everyone in the Tasker group for providing such a nice place to work despite the radio discussion - Ross (Wee)! I'd also like to mention Christine and Rachel who have helped with reading my thesis, your comments were really appreciated and to Jy who has provided so much organic knowledge and was happy to provide the information freely, you really made the last year much easier. Also, thank you Rachel for your hilarity and to Vesna for being a constant tea break companion.

Contents

Contents

Appendix

Ligand index

1	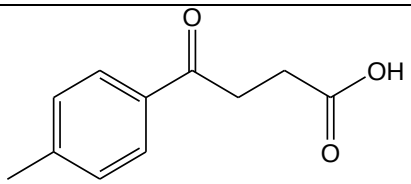	3-(4-methylbenzoyl)-propionic acid
2	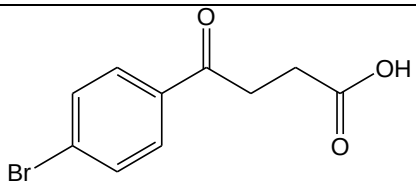	3-(4-bromobenzoyl)-propionic acid
3	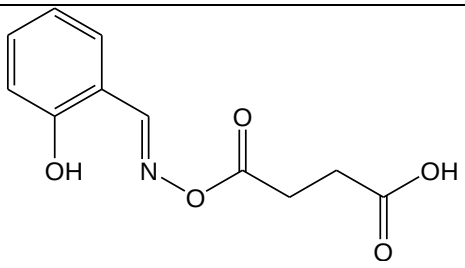	salicylaldehyde-*O*-(4-carboxypropanoyl) oxime
4	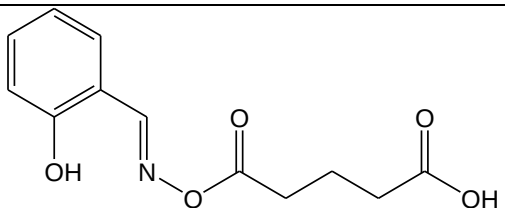	salicylaldehyde-*O*-(5-carboxybutanoyl) oxime
5	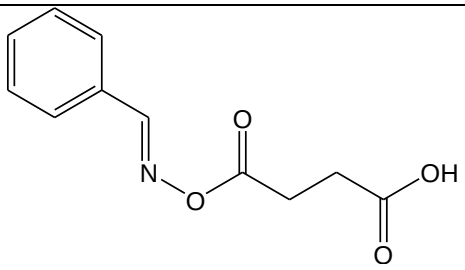	benzaldehyde-*O*-(4-carboxypropanoyl) oxime
6	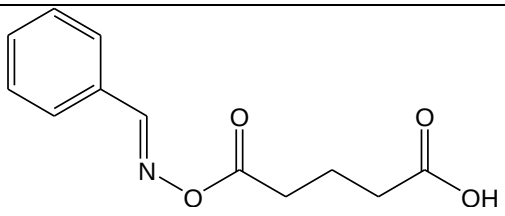	benzaldehyde-*O*-(5-carboxybutanoyl) oxime

7	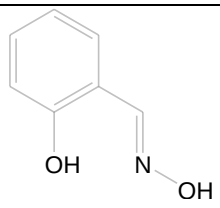	salicylaldoxime
8	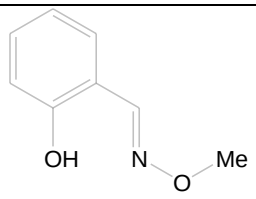	salicylaldehyde-*O*-methyl-oxime
9	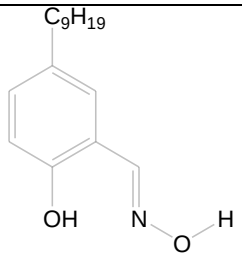	5-nonyl salicylaldoxime (P50 oxime)
10		4-Ethylsulfanyl-benzoic acid
11	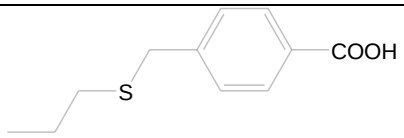	4-Propylsulfanylmethyl-benzoic acid
12	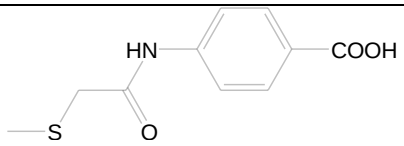	4-(2-Methylsulfanyl-acetylamino)-benzoic acid
13	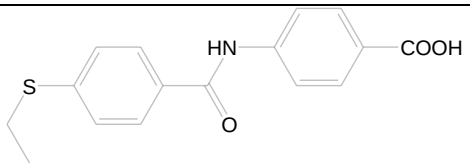	4-(4-Ethylsulfanyl-benzoylamino)-benzoic acid
14	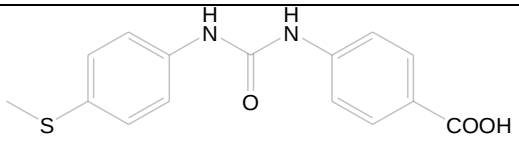	4-[3-(4-Methylsulfanyl-phenyl)-ureido]-benzoic acid

15	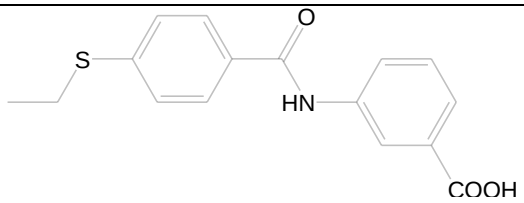	N-(4-ethylsulfanyl-phenyl)-isophthalamic acid
16	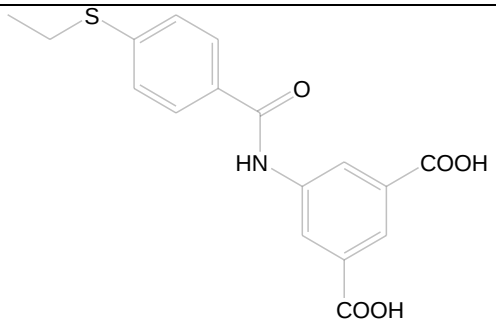	3-(4-Ethylsulfanyl-benzoylamino)-5-(1-hydroxy-vinyl)-benzoic acid
17	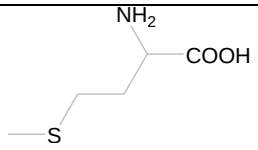	DL-methionine
18	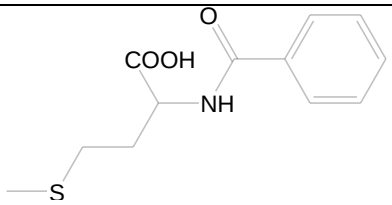	2-Benzoylamino-4-methylsulfanyl-butyric acid
19	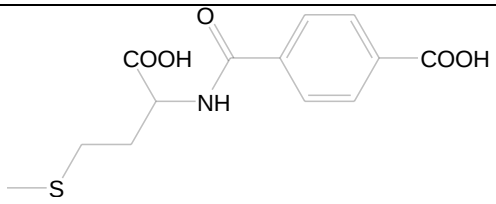	N-(1-Carboxy-3-methylsulfanyl-propyl)-terephthalamic acid
20	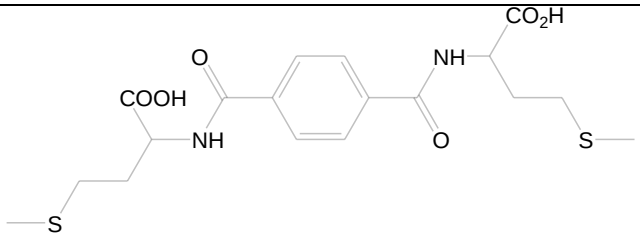	2-[4-(1-Carboxy-3-methylsulfanyl-propylcarbamoyl)-benzoylamino]-4-methylsulfanyl-butyric acid
21	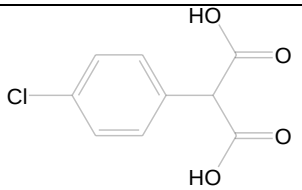	2-(4-chlorophenyl)-malonic acid

22	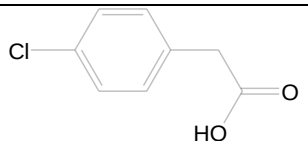	4-cholorphenyl acetic acid

Abbreviations

δ	chemical shift
°	degrees
°C	degree centigrade
$	dollars
ε	extinction coefficient (UV)
<	less than
≤	less than or equal to
>	more than
≥	more than or equal to
%	percent
±	plus or minus
√	square route
λ	wavelength (UV)
ν	wavenumber (IR)
A	*maximum* surface coverage (adsorption isotherms)
Å	Angstrom
AES	Auger Electron Spectroscopy
Ar	aromatic (NMR)
bs	broad singlet (NMR)
ca.	*circa* (approximately)
$CDCl_3$	deuterated chloroform
cf.	compare
cis	*cisoid*
cm^{-1}	wavenumber
conc.	concentrated

CSD	Cambridge Structural Database
d	doublet (NMR)
D_2O	deuterated water
DCM	dichlormethane
dd	doublet of doublets (NMR)
DMSO	dimethylsulfoxide
e.g.	for example
ES	Electrospray
et al.	*et alli* (and others)
EtOH	ethanol
EU	European Union
EXAFS	Extended X-ray Absorption Fine Spectroscopy
FAB	Fast Atom Bombardment
g	gram
HCl	hydrochloric acid
HOMO	Highest Occupied Molecular Orbital
hr	hour
Hz	Hertz
i.e.	that is
ICP-OES	Inductively Coupled Plasma Optical Emission Spectroscopy
in situ	in the natural place
in vacuo	under vacuum
IR	Infrared
J	coupling constant (NMR)
K	equilibrium adsorption constant
K	Kelvin
KBr	Potassium Bromide
kJ mol^{-1}	kilojoules per mole
lit.	literature

LUMO	Lowest Occupied Molecular Orbital
m	multiplet (NMR)
M	Molar
m	*meta*
m.p.	melting point
m/z	mass per unit charge
m^2	metres squared
$m^2\ g^{-1}$	metres squared per gram
Me	methyl
μm	micrometres
mg	milligrams
MHz	Mega Hertz
min	minute
ml	millilitre
mmHg	millimetres of mercury
mmol	millimoles
mol	moles
mol dm^{-3}	moles per decimetre cubed
mol g^{-1}	moles per gram
MS	Mass Spectrometry
MW	molecular weight
nm	nanometre
NMR	Nuclear Magnetic Resonance
o	*ortho*
p	*Para*
P50 oxime	5-nonylsalicylaldoxime
pH	$-\log_{10}[H^+]$
Ph	Phenyl
PIBSA	poly isobutylene succinic anhydride

p*K*a	-$\log_{10}$[acid dissociation constant]
ppm	parts per million
q	quartet (NMR)
QCM	quartz crystal microbalance
r	radius
s	singlet (NMR)
s	seconds
SAM	self assembled monolayer
SEERS	Surface Enhanced Electronic Raman Spectroscopy
sin	sine (trigonometry)
STM	Scanning Tunnelling Microscopy
t	triplet (NMR)
T	temperature
trans	*transoid*
UV/Vis	Ultraviolet/Visible
V	volts
wt	weight
wt %	weight percentage
XPS	X-ray Photoelectron Spectroscopy
y	surface coverage (adsorption isotherms)

Contents

1 Corrosion Inhibition

Formed in stars, iron is the most abundant element by mass of the Earth.[1] In its elemental form it exists as a shiny grey metallic substance, see Figure 1-1. In the first billions years of life on the Earth, the environment was anaerobic.[2] As plants evolved and started the process of photosynthesis of carbon dioxide with water, the Earth's atmosphere became oxygen rich and the iron was oxidised. The process known as rusting had begun. As mankind developed, it passed through the stone and bronze ages to reach the iron age, where the skills of obtaining iron from its oxide were discovered.[3] Iron will always want to return to its oxidised state unless forced to do otherwise.

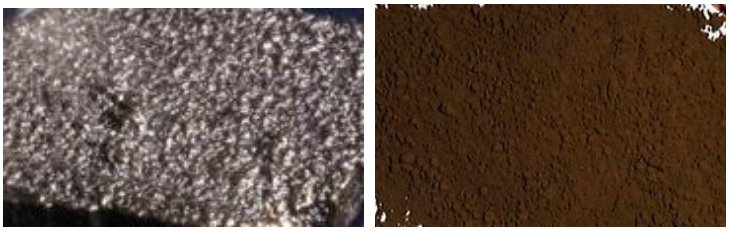

Figure 1-1 Pure metallic iron and powdered iron oxide[4]

The work described in this thesis aimed to develop ligands that prevent rusting. This introductory chapter discusses the uses of metals, in particular iron, and the effect of surrounding environments. The chemistry of metal corrosion and protection is reviewed with a view to introducing the concept of benign organic corrosion inhibitors. Possible methods for screening new compounds as suitable ligands, investigation of the mode of action of corrosion inhibition described in an ICI patent and the development of new ligands and their mode of action are considered in the remaining chapters.

1.1 Metals

The wide variation of properties of metals and their alloys, means they are used extensively as materials in various industries, see, for example, Figure 1-2. Soft, malleable metals with low abundance in the Earth, such as gold and silver are often

used in jewellery. Other soft metals, such as copper, are more abundant and also good conductors of heat and electricity are often used in electrical industries. Metals with higher strength can be used for mechanical or building purposes. Steel, an alloy of iron containing carbon has very high strength and low cost and is used where weight is not a problem, aluminium alloys are also strong but are much lighter and are used in aircraft construction.

Figure 1-2 Various uses of metals. From top left, gold in decorative masks,[5] copper electrical wires,[6] and steel in bridge construction.[7]

Metals used in structural applications are often exposed to an aqueous environment and are subject to oxidation and corrosion. Even with processes to minimise corrosion it is still a widespread and very expensive problem and has been estimated to cost the US between $50 billion and $100 billion a year.[8] In some cases, corrosion can occur to such a large extent that structures have to be rebuilt or have parts replaced which can be problematic. Figure 1-3 shows an example of a severe case of corrosion that has occurred to such an extent that a large section has corroded away.

Figure 1-3 Example of severe corrosion at the top of a tower[9]

1.2 Corrosion

The are various forms of corrosion which can occur are shown in Figure 1-4.[10] Although uniform corrosion accounts for most of the damage other forms are problematic, particularly in the context of structural failures, and much more difficult to predict and control. Determination of corrosion is carried out in a variety of ways ranging from visual inspection to use of modern spectroscopy.

Different corrosion processes occur depending on the local environment of the surface. For example, galvanic corrosion is specific to situations where two metals with different electrochemical potentials are in contact with each other. Other localised forms of corrosion can cause difficulties since they can cause structural failures and often occur via an iterative process as described below.

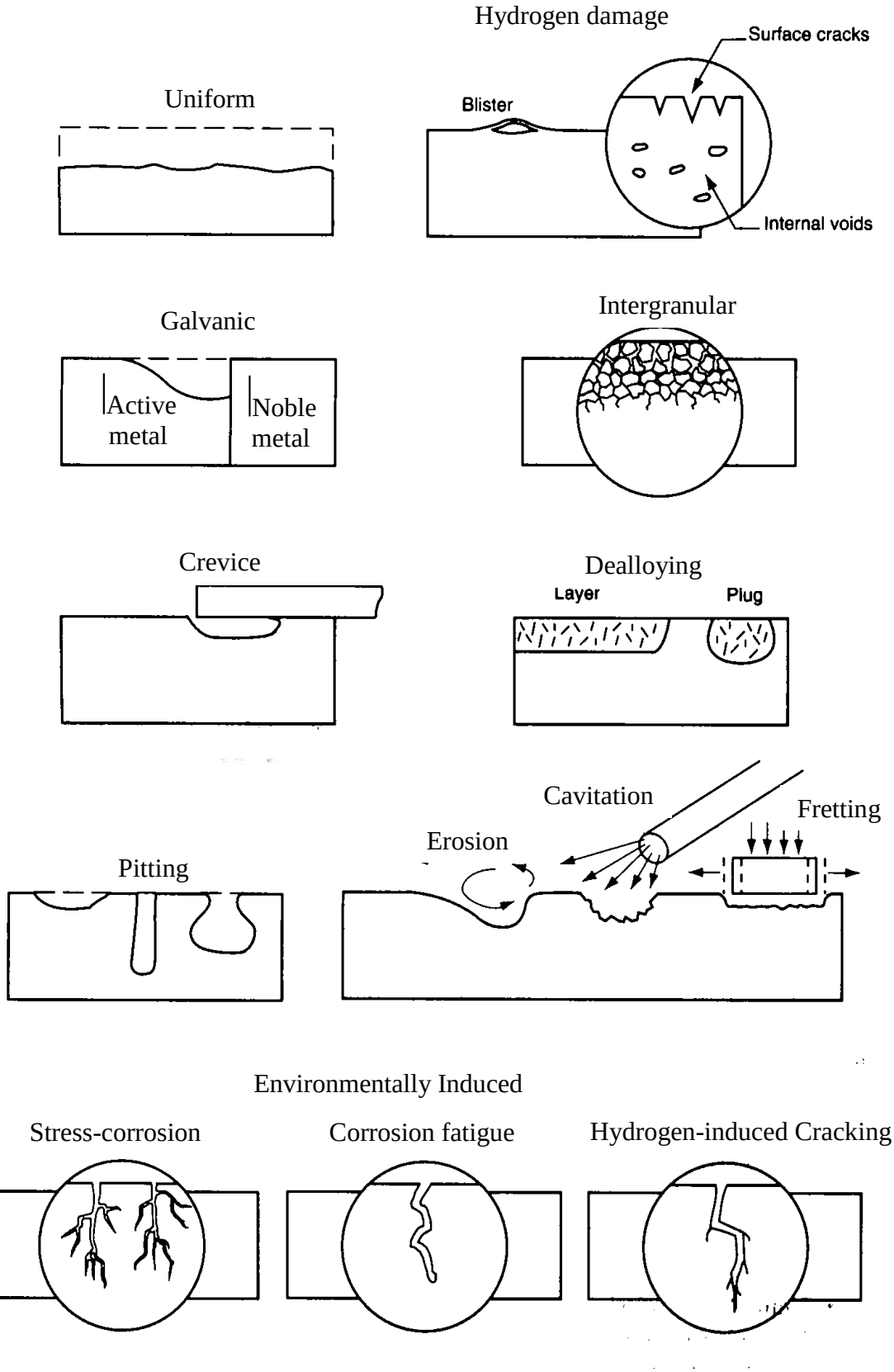

Figure 1-4 Various forms of corrosion[10]

Pitting corrosion can be initiated by defects on the surface, for example, a cathodic site surrounded by normal surface which acts as an anode.[11] This creates a local potential difference cell. Once a hole is started, the products of the redox reaction are not removed and a build up of ions occurs which increases the corrosion rate.[12] Post examination of the pit reveals the uncorroded cathode as shown in Figure 1-5. Other pitting corrosion affects result from mechanical ruptures such as scratches or chips of a corrosion-resistant coating.

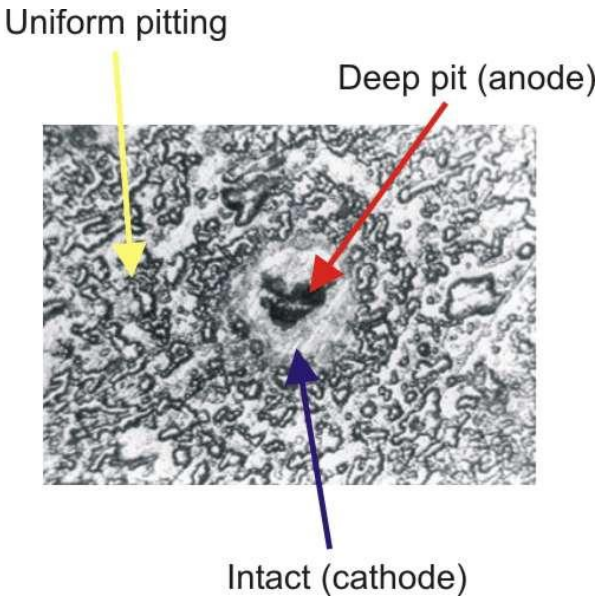

Figure 1-5 Example of a pitted aluminium surface produced by exposing a specimen of aluminium A92519 to 3.5% NaCl during seven days.[11] The width of the picture is approximately 1mm.

Often dealloying occurs when one element is preferentially dissolved over another. In the case of cast iron, an iron alloy containing carbon, the metal is removed leaving a brittle graphite skeleton. This skeleton is then filled with insoluble corrosion products. This material allows the alloy to retain its appearance and shape but is structurally weaker. Often testing is carried out by scraping of the surface to reveal the crumbling of the iron beneath.

In all forms of aqueous corrosion, the reactions can be thought of as electrochemical.[13] The water in the system acts as an electrolyte and transfers the electrons between the cathode and anode. The metal oxidation is the anodic reaction and occurs according to equation 1.

$$M \rightarrow M^{n+} + ne^{-} \qquad \text{Equation 1}$$

This has a corresponding cathodic reaction involving a species which is reduced. This is commonly dissolved oxygen in neutral or acidic aqueous solutions. The reduction equation occurs according to equation 2.

$$O_2 + 2H_2O + 4e^{-} \rightarrow 4OH^{-} \qquad \text{Equation 2}$$

In the absence of all other reduction reactions water itself can undergo reduction according to equation 3.

$$2H_2O + 2e^{-} \rightarrow H_2 + 2OH^{-} \qquad \text{Equation 3}$$

In some cases, the oxidized metal ion may react with oxygen to form a protective oxide coating. This is known as passivation.[14] This coating acts as a barrier to further anodic reaction. However, this passive film is usually very thin and fragile and its loss leads to localised forms of corrosion. The properties of these passive films are not well understood which has delayed the control and prevention of the localised forms of corrosion that occur where the passive layer is broken down. The properties of these passive films are usually determined by chemical or electrochemical methods, however these are difficult to interpret.[15] *Ex-situ* surface data has a different structure due to dehydration of the surface film.

1.3 Corrosion testing

One of the main problems with the prediction of corrosion is the length of time it takes to occur. It is a reasonably slow process and happens over many years.[16] Often, archaeology studies are useful since they give information about materials which

have been exposed to weathering conditions for a long time. However, industry is constantly designing new alloys and these products do not have the benefit of long term analysis. Consequently some other methods are required for determination of their usefulness in terms of their corrosion resistance.

Accelerated testing, carried out in laboratories, is typically used to give some indication of the corrosion which can occur. There are many patents in the literature regarding equipment and techniques used in corrosion testing.[17] In practice, metals are used in a wide variety of environments and as such, experimental conditions for laboratory testing need to reflect these.[18] These can involve high temperature effects, spray tests, deposit attack and galvanic effects. The atmosphere surrounding the metals in the tests is also important; the uses of humid or polluted atmospheres are common. Alternatively, metals can be immersed in a range of corrosive solutions with differing degrees of immersion: total, partial or intermittent.

Although useful for providing an insight on the effectiveness of corrosion prevention measures, laboratory conditions are often not truly representative of those found in the atmosphere. Some companies therefore carry out corrosion testing by leaving small samples of alloys, known as coupons, at various locations.[19] These include industrial, rural, and marine environments as shown in Figure 1-6. The mass lost by each is then determined and allows a prediction of the structural integrity of the alloy, prior to failure. Difficulties exist in analysis of the corrosion products due to the different oxides that can be present on structures. It is also important and useful to know how, and under what conditions, these products form and transform.

Oxy hydroxides are commonly found in atmospheric corrosion products whereas others tend to form under more specific exposure conditions. Different spectroscopic techniques are often used for a variety of functions.[16] Mossbauer, micro Raman, X-ray diffraction and IR can give oxide identification and measurement of each fraction present. Corrosion coating impurity content and morphology require use of electron probe micro-analysis (EPMA), energy and dispersive X-ray analysis (EDS) and SEM.

Figure 1-6 Metal samples left at marine environments for corrosion testing[20]

In addition to corrosion which occurs at the surface of metals exposed to the atmosphere, many industrial processes such as those in oil and petroleum refineries contain structures in which metals are exposed to extreme environments such as reactive gases at high temperatures.[21] Good predictions of the corrosion rates, assists in the management of the lifetime of structures. However, due to the large number of alloys and corrosive environments possible, it is difficult to generate suitable data to assess engineering lifetimes. Important aspects such as equipment and process design, operation, alloy selection and design are all influenced by the lifetimes of the materials used. Most previously high temperature data reported are given in terms of weight change per area for short exposures with inadequately defined exposure conditions. These often do not relate directly to thickness of corroded metal which is needed to asses the strength of equipment components.

Two of the major problem reactions which occur in these systems are oxidation and sulfidation. Oxidation occurs at high temperatures (>300^0C) in oxidising gases in combustors, process heaters and burners.[22] Most alloys have an increasing penetration rate with increasing temperature. Sulfidation reactions occur in gases containing sulfides at temperatures slightly lower than oxidations (>200^0C). They occur in crude distillation columns, petroleum coking units and sulfur removal plants.[23] The reactions are confirmed by X-ray diffraction of the surface or analysis of the gas composition. Mixed sulfidation/oxidation reactions occur on alloys

containing elements such as Cr and Al upon exposure to hot gases containing mix of CO, CO_2, -COS, H_2, H_2O, H_2S gases. These are found in hydrocrackers, coal, oil, coke gasifiers and sulfur removal plants.[22, 23] The corrosion products are mixtures of sulfides and oxides. Pure Fe, Ni or low alloy steels, rarely undergo mixed sulfidation/oxidation reactions, it is usually one or the other.

The development of software that includes a database and thermochemical calculation programs and which uses corrosion data from well-controlled conditions to predict corrosion for alloys over a range of high temperature environments is reported by John *et. al*.[21] The four main tasks defined in the project are:

1. "Software development: including additions to corrosion data, distribution and instruction on use by a company called Humberside Solution
2. Thermochemical modelling: Centre for Research in Computational Thermochemistry of Ecole Polytechnic de Montreal evaluate the available thermochemical data to produce consistent data sets that improve accuracy of predictions of mechanism by determinination of the most stable corrosion products of alloys.
3. Corrosion Testing: Determination of corrosion under well defined conditions and store in defined formats.
4. Procedure for Corrosion Predictions: the stable corrosion products and the equilibrium gas composition for a given combination of alloy and exposure conditions are calculated using the software from the information collected on the alloy composition and corrosive environment. Computations using the ChemApp program from F*A*C*T(ref 25) considers the thermodynamic solution behaviours of the solid and liquid alloys and the solid and liquid corrosion products. The software assists identification of the likely corrosion mechanisms by knowing the stable corrosion products, alloy in question and the gas thermochemistry. "

1.4 Current methods used to combat corrosion

There are several methods commonly used to combat corrosion. These include protective coatings, cathodic protection or use of inhibitors.[10]

1.4.1 Passive film formation

If the metal will spontaneously form a passive oxide layer then an electrochemical potential can be applied to oxidise the metal further and increase the thickness of the oxide layer.[24] It has been established that the quality of this passive film in terms of its ion and electron transport properties, or its structure and chemistry, determines the dissolution rate of passive metals in a given environment.[25] This dissolution rate often determines the lifetime of structural materials.

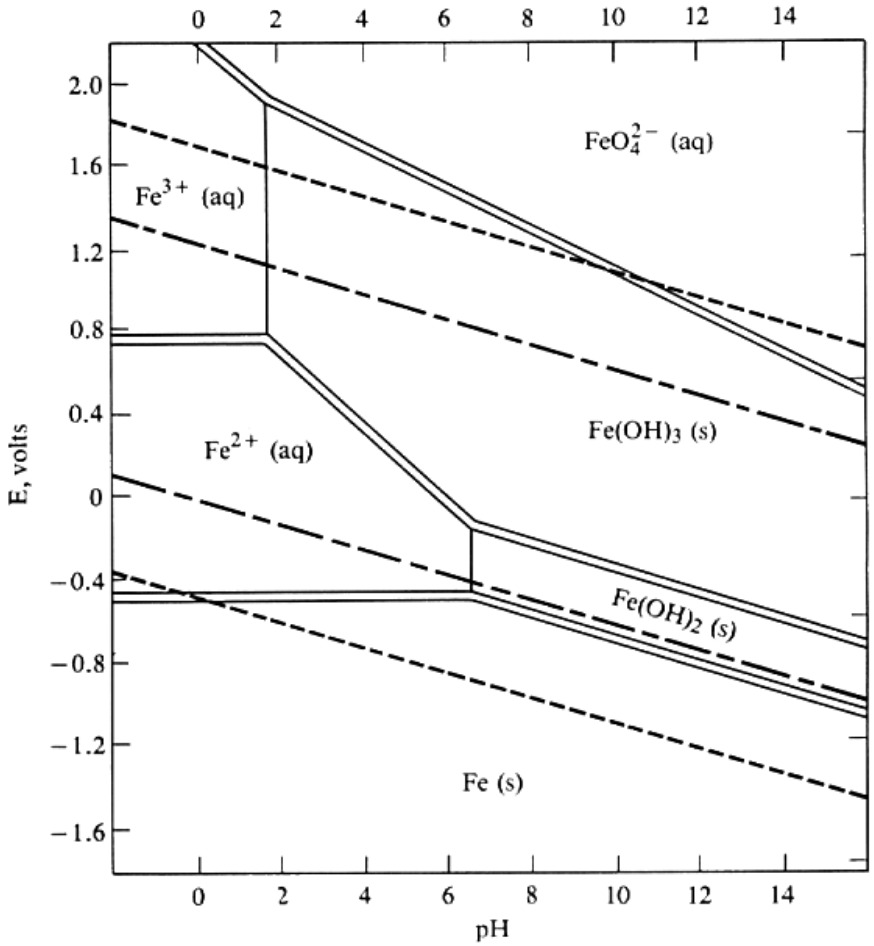

Figure 1-7 Pourbaix diagram for iron[26] Solid lines represent species related by acid-base equilibria. Solid double lines separate species related by redox equilibria. Longer dashed lines enclose the theoretical region of stability of the water to oxidation or reduction. Shorter dashed lines enclose the practical region of stability of the water

The passivation potentials and conditions for oxide film formation can be predicted by consideration of its Pourbaix diagram, see Figure 1-7 for the Pourbaix diagram for iron.[26] These give the thermodynamic stability of different species considered in electrochemical reactions as curves by plotting the pH against potential. However, the diagrams give no indication about the kinetics of dissolution. In addition, the values shown in the diagrams are for the bulk materials which may be different from those of the nanometer sized passive film. In forming the passive layers, one ionic species must diffuse or migrate through the oxide and hence the layer grows either at the inner or outer interface. Alternatively it is possible that cation or anion vacancies move through the film lattice.[27, 28]

It is known that passive films consisting of an iron oxide structure can form on pure iron. However, there are many disagreements over the nature of the oxide and whether it consists of a single or multiple layered structure. Earlier studies point towards a double layer structure consisting of an outer maghemite (γ-Fe_2O_3) and inner magnetite (Fe_3O_4)[29-31] using galvanostatic reduction experiments. Others authors using a similar technique conclude that it consists of a single Fe_2O_3 layer.[32-34] The discrepancies are reportedly due to different reduction mechanisms of the passive layer.[25] More recent studies indicate more complex behaviour than that expected for a homogeneous single layered structure.[35] Alternative theory suggest an inner oxide layer with an outer hydrated film although it is now known that the presence or absence of a hydrated films strongly depends on experimental conditions during passivation.[36] *In-situ* EXAFS studies now suggest that the film consists of a spinel structure.[37, 38] The passive films formed are highly dependant upon the metals used in the alloy.

1.4.2 Chromating

The incorporation of chromium is known to be good at forming protective layers, stainless steel contains at least 11% Cr which forms a $FeCr_2O_4$ passive layer.[39] Chromium is a powerful reductant and is easily oxidized to Cr_2O_3. Thus it forms a good self-protecting layer, however chromium metal is not used alone since it is very brittle, The addition of chromium to steel allows the formation of a passive film to take place at a lower potential and increases the protectiveness and stability of the layer. The composition of the protective coating has been the subject of much debate in the literature. A widely accepted view is that it contains an enriched number of oxidised chromium species, however the film formed depends strongly on the conditions used.[25]

Alternative methods of using chromium, involve the use of hexavalent chromium in passive coatings such as those found on zinc.[40] The first step of treatment involves dissolution of zinc and hydrogen atoms from the surface using acid. The hexavalent chromium is then reduced to the trivalent state and is precipitated into a Cr-O-Cr polymer. This gelatinous layer containing the trivalent chromium is then adsorbed into a topcoat of the hexavalent chromate. When the surface is chipped or cracked the hexavalent species is leached out of the surrounding layer and can repassivate the exposed surface. However, current environmental concerns and legislation means that use of hexavalent chromium is now no longer a viable option.[40, 41]

1.4.3 Cathodic protection

Cathodic protection changes the usual potential of the metal and makes the metal negatively charged with respect to its surroundings.[42] As a consequence it will act as a cathode and avoid oxidation. Cathodic protection can be carried out by a variety of methods.

Due to differences in oxidation potentials, attachment of sacrificial blocks of metal (nodes) which oxidise preferentially over the metal can be used to inhibit corrosion.[43, 44] These anodes have a lower oxidation potential than the metal and therefore the electrochemical circuit is set up such that the metal becomes the

cathode as desired. Unfortunately, these anodes need to be regularly replaced but this is a much cheaper option than rebuilding the structure. Some examples are magnesium stakes attached to steel power pylons or zinc anodes attached to boats as shown in Figure 1-8.

Figure 1-8 Sacrificial zinc anodes attached to the hull of a tug boat[45]

In the case of steel, a technique known as galvanizing can be used. The steel is coated with metallic zinc which acts in two fashions. Firstly, as a protective coating and secondly when the surface is scratched it will prevent oxidation of the steel because zinc has a lower oxidation potential and is oxidized preferentially. The use of galvanised steel is not recommended in situations where the presence of copper is likely. This is due to the copper-zinc bimetallic couple which can set up and ends up corroding the steel faster.[46]

1.4.4 Corrosive environment

To inhibit corrosion it may be possible to modify the metal's environment.[10] For example, in some industrial tanks it may be possible to remove CO_2 from the liquid by aerating the system to neutralise the pH. However this can cause some unwanted results, in this case it increases the oxygen concentration in the system. In addition to the unwanted problems it may cause, environmental modification is not usually viable for most metal applications where the metal has been used for outdoor structures.

1.4.5 Anodic inhibitors

A different form of corrosion inhibition aims to blanket the electrochemically active surface of the metal and suppress corrosion.[47] Anodic inhibitors which consist of inorganic anions such as carbonates, silicates, and phosphates with calcium or zinc produce films with the metal oxides and hydroxides on the anodic sites. A passive layer is then formed containing the anion with the metal in an insoluble salt. However a metal oxide layer must be present to demonstrate this passivation.

Although mixed corrosion protection is generally synergistic, these anodic inhibitors should not be used in conjunction with galvanized iron. The charges on the corrosion cell would be reversed and the iron would corrode faster.[10]

1.4.6 Paints and plastic resin coatings

Metals can also be coated with paints or plastic resins which act as a physical barrier between the metal surface and the corroding environment.[13] Surface coatings such as these consist of various layers for a variety of functions. Often the outermost coat is supplied for resistance to atmospheric weathering and to provide a largely aesthetic purpose.[10] Beneath this may be a layer which contains inhibitive properties and good adherence to the bottom layer which is often a chemical conversion coating of chromate or phosphate. The surface treatment required largely depends on the conditions which the metal are exposed to.

It has been said ‘that a poor coating applied to a well-prepared surface is better than a good coating to a poorly prepared surface’.[48] The pre-treatment of surfaces can vary depending on the extent of damage and length of time between manufacture and

coating. The Steel Structure Painting Council (SSPC) has published a series of surface preparation standards widely used in North America. Briefly, they range from solvent cleaning to remove oil, grease and salts, to blast cleaning which is capable of removing visible rust by blasting with sand or grit, to pickling which removes rust by chemical reaction or electrolyis.[49]

Similar to the other methods discussed above, paints and resins are not without their problems. They need to remain complete and in-tact to be most useful; as with passive films, scratches or chips on surface lead to localised forms of corrosion which may weaken the metal beneath.

1.5 Organic corrosion inhibitors

It is possible to use organic molecules to inhibit corrosion. One approach involves the use of organic conducting polymers (CP).[50] The structures of some CP are shown in Figure 1-9. They combine the properties of electrical conductivity with the flexible nature of organic polymers.[51] Alteration of their properties can be carried out by doping to improve conductivity or by use of appropriate monomers. These organic polymers can exhibit electroluminescent properties to form compounds known as organic light emitting diodes (OLEDs) that have been used in devises such as mobile phone screens.

For corrosion inhibition conducting polymers are laid as a primer and then followed by topcoats of conventional barrier polymers, such as epoxy, polyester or polyurethane.[52] Although known to be effective, there are many disagreements in the literature regarding their mode of action on ferrous alloys.[53] It is known they act as a physical barrier to the corrosive environment but it is their ability to protect against corrosion when the coating is chipped or scratched that is most intriguing. Many of the inconsistencies of experimental data within the literature are due to differences in the surface involved and its pre-treatment, conditions used for film formation and the environment for corrosive testing. However, it is likely that they act in a galvanic

fashion when the surface is broken, although unfortunately they do not retain the lifetimes observed using classic galvanisation techniques.[53]

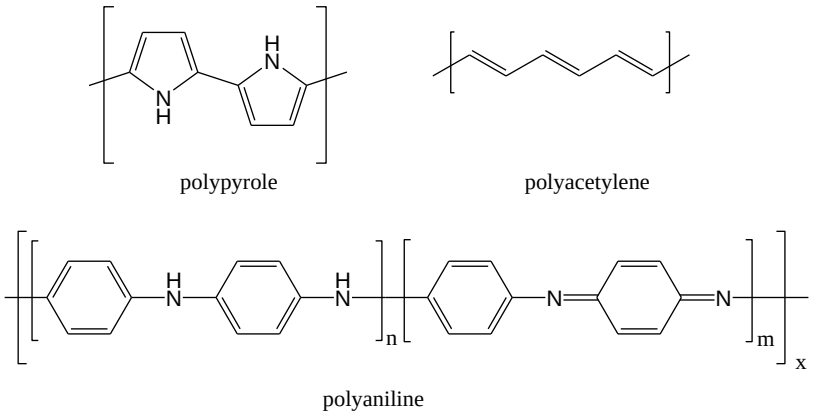

Figure 1-9 Structures some organic polymers[25]

Other organic molecules can act as corrosion inhibitors in different ways. Since a metal surface acts as an anode and is positively charged it is possible to cover the surface with negatively charged species. This can be done with organic inhibitors which act via an adsorption mechanism.[54] These are organic molecules which have an anionic head and an appropriate hydrophobic tail. The anionic heads of the molecules seek out positively charged anodic spots on the surface and the hydrophobic tail isolates it from the aqueous solutions.

However like all techniques there are limitations.[10] All anodic sites need to be eliminated so a reasonably high concentration of inhibitor needs to be used. This is unlike cathodic protection which can reduce corrosion at any concentration. In addition, it is useful if an excess of inhibitor is used so that in the case of chips or scratches any of the inhibitor that is leached from a surface coating binds to the exposed surface and prevents further corrosion similar to that found for chromating processes where inorganic sparingly soluble chromate pigments are incorporated into coatings.

Often, organic corrosion inhibitors are not used alone but in formulations containing many other components.[10] These mixtures contain compounds that act as binders, pigments and resins. Many coatings are applied as a liquid by spraying or brushing.

If they are applied as a solution or suspension it is preferable to use water as a solvent due to environmental concerns. The water-solubility of the ligands is therefore important and affects the type of molecules which can be used. In some cases surface pre-treatment measures may be difficult and it may be preferential to apply coating to surfaces which are already lightly corroded.

The rest of this thesis is concerned with the development of new ligands and methods of analysing their potential as candidates in organic corrosion inhibition. Chapter two considers the necessary requirements of a ligand to effectively inhibit corrosion. Adsorption isotherms and a quartz crystal microbalance are presented as possible methods to determine the binding characteristics of such ligands. The surface binding properties of the reaction products of phenolic oxime and succinic anhydrides derivates were used to rationalise an ICI patent, and is discussed in Chapter three. Inclusion of functional groups designed to generate ligand-ligand intermolecular interactions is the main focus of chapter four, and is illustrated using a series of benzoic acid and methionine derivates. Chapter five aims to establish the mode of binding of the dicarboxylic acid, phenyl malonic acid on iron(III) oxide surfaces.

1.6 References

1 W. F. McDonough and S. s. Sun, *Chemical Geology*, 1995, **120**, 223.

2 A. Imlay James, *Mol Microbiol FIELD Full Journal Title:Molecular microbiology*, 2006, **59**, 1073.

3 L. Host-Madsen and V. F. Buchwald, *Historical Metallurgy*, 1999, **33**, 57.

4 http://resourcescommittee.house.gov/subcommittees/emr/usgsweb/photogallery/

5 http://library.thinkquest.org/28209/egypt_mummy.htm.

6 http://eywire.diytrade.com/.

7 http://www.forthbridges.org.uk/railbridgemain.htm.

8 L. Maina, S. Benedetto, and M. Vitali, *Proceedings of the International Gas Research Conference*, 2001, TP03/1.

9 http://www.corrosionsource.com/technicallibrary/corrdoctors/index.htm.

10 D. A. Jones, 'Principles and Prevention of Corrosion', Prentice-Hall International (UK) Ltd, 1996.

11 http://www.corrosion-doctors.org/Forms-pitting/Pitting.htm.

12 R. P. Ryan, D. E. Williams, R. J. Chater, B. M. Hutton, and D. S. McPhall, *Nature (London, United Kingdom)*, 2002, **415**, 770.

13 H. Hadert, *Industrie Lackierbetrieb*, 1968, **36**, 184.

14 D. F. Bahr, A. L. Olson, K. R. Morasch, M. S. Kennedy, D. R. Marek, and A. Alamr, *Materials Research Society Symposium Proceedings*, 2004, **795**, 55.

15 C. O. A. Olsson, P. Agarwal, M. Frey, and D. Landolt, *Corrosion Science*, 2000, **42**, 1197.

16 D. C. Cook, *Corrosion Science*, 2005, **47**, 2550.

17 A. S. f. T. a. Materials, '199 Annual book of ASTM standards', American Society for Testing and Materials, 1999.

18 F. A. Champion, 'CORROSION TESTING PROCEDURES', Chapman and Hall, 1964.

19 T. J. Barlo, *Proceedings - Corrosion & Prevention*, 1999, 122.

20 http://www.laque.com/.

21 R. C. John, A. D. Pelton, A. L. Young, W. T. Thompson, I. G. Wright, and T. M. Besmann, *Materials Research (Sao Carlos, Brazil)*, 2004, **7**, 163.

22 T. M. Linjewile, J. Valentine, K. A. Davis, N. S. Harding, and W. M. Cox, *Materials at High Temperatures*, 2003, **20**, 175.

23 S. N. Smith, *Materials Performance*, 2003, **42**, 44.

24 C. W. Bennett and W. S. Burnham, *Journal of Physical Chemistry*, 1917, **21**, 107.

25 P. Schmuki, *Journal of Solid State Electrochemistry*, 2002, **6**, 145.

26 M. Pourbaix, 'Atlas of electrochemical equilibria in aqueous solutions', Pergamon, 1966.

27 C. Y. Chao, L. F. Lin, and D. D. Macdonald, *Journal of the Electrochemical Society*, 1981, **128**, 1187.

28 C. Y. Chao, L. F. Lin, and D. D. Macdonald, *Journal of the Electrochemical Society*, 1982, **129**, 1874.

29 M. Nagayama and M. Cohen, *Journal of the Electrochemical Society*, 1962, **109**, 781.

30 C. L. Foley, J. Kruger, and C. J. Bechtoldt, *Journal of the Electrochemical Society*, 1967, **114**, 994.

[31] J. L. Ord and D. J. De Smet, *Journal of the Electrochemical Society*, 1976, **123**, 1876.

[32] N. Sato, K. Kudo, and T. Noda, *Corrosion Science*, 1970, **10**, 785.

[33] K. Ogura and T. Majima, *Electrochimica Acta*, 1978, **23**, 1361.

[34] K. Ogura and K. Sato, *Electrochimica Acta*, 1980, **25**, 857.

[35] V. Schroeder and T. M. Devine, *Journal of the Electrochemical Society*, 1999, **146**, 4061.

[36] M. Buchler, P. Schmuki, and H. Bohni, *Journal of the Electrochemical Society*, 1998, **145**, 609.

[37] G. G. Long, J. Kruger, D. R. Black, and M. Kuriyama, *Journal of the Electrochemical Society*, 1983, **130**, 240.

[38] A. J. Davenport and M. Sansone, *Journal of the Electrochemical Society*, 1995, **142**, 725.

[39] W. R. Cieslak and D. J. Duquette, *Corrosion (Houston, TX, United States)*, 1984, **40**, 545.

[40] P. C. Wynn, B. Manager, and C. V. Bishop, *Products Finishing (Cincinnati)*, 2001, **65**, 55.

[41] D. E. Kimbrough, Y. Cohen, A. M. Winer, L. Creelman, and C. Mabuni, *Critical Reviews in Environmental Science and Technology*, 1999, **29**, 1.

[42] W. Green, F. Andrews-Phaedonos, G. Brewster, and D. McCormick, *Corrosion & Materials*, 2002, **27**, S/1.

[43] O. T. De Rincon, M. F. De Romero, A. R. De Carruyo, M. Sanchez, and J. Bravo, *International Corrosion Congress, Proceedings, 13th, Melbourne, Nov., 1996*, 1996, Paper 184/1.

[44] W. Wiederholt, *VDI Zeitschrift (1857-1968)*, 1970, **112**, 187.

[45] http://www.tis-gdv.de/tis_e/misc/elektro.htm.

[46] G. Wranglen, 'An Introduction to Corrosion and Protection of Metals', 1985.

[47] D. F. Stoye, 'Water-Borne Coatings', Carl Hasner Verlag, 1994.

[48] P. A. Schweitzer and Editor, 'Corrosion and Corrosion Protection Handbook. 2nd Ed', 1989.

[49] 'SSPC Handbook', ed. S. S. P. Council, Warendale.

[50] P. Zarras, N. Anderson, C. Webber, D. J. Irvin, J. A. Irvin, A. Guenthner, and J. D. Stenger-Smith, *Radiation Physics and Chemistry*, 2003, **68**, 387.

[51] J. Jang, *Advances in Polymer Science*, 2006, **199**, 189.

[52] E. W. Brooman, *Metal Finishing*, 2002, **100**, 104.

[53] G. M. Spinks, A. J. Dominis, G. G. Wallace, and D. E. Tallman, *Journal of Solid State Electrochemistry*, 2002, **6**, 85.

[54] Y. I. Kuznetsov, 'Organic Inhibitors of Corrosion of Metals', ed. J. G. N. Thomas, Plenium Press, 1996.

Contents

2 Methodologies used in ligand design and binding studies

2.1 Introduction

Chapter one mentioned some of the techniques used for testing corrosion inhibition. In many of these tests, extreme environments are used or the testing can take a long time to give meaningful data. For organic corrosion inhibitors, a strong correlation between good corrosion inhibition and high binding strength to metal (oxide) surfaces has been observed.[1] This thesis has therefore attempted to synthesise ligands that display strong binding to iron(III)oxide surfaces and have a high thermodynamic and kinetic stability. This chapter will introduce the concepts used in the design of ligands that will generate these properties and the analytical methods used to study their binding to iron(III) oxide surfaces.

2.2 Ligand Design

The large scale use of metals discussed in Chapter one and the widespread problems associated with their sensitivity to corrosion necessitates the design of ligands which are cheap and easy to produce. Avoidance of harmful functional groups, to produce ligands which are as benign as possible, is required as industrial procedures for controlling corrosion which involve the production of toxic by-products are being phased out and replaced by more environmentally friendly methods.[2] Finally, the ligands must have high efficiency. An understanding of the mechanisms which molecules use to produce effective corrosion inhibition is required in order to generate new and improved ligands. The important chemical functional requirements will be discussed in the sections that follow and are highlighted by an example of a commercially used corrosion inhibitor, Irgacor 419® previously studied at University of Edinburgh. [1]

2.3 Structure

Schematically the surface ligand can be considered to consist of three components as shown in Figure 2-1. The headgroup (red) binds to the surface, the tailgroup (blue) is used to provide the required surface property and the linker separates the two. Although each component carries out a different function, they are not necessarily independent of each other and can be multifunctional.

Strong binding can be achieved by providing a large number of strongly ligating atoms, as this is likely to generate several bonds between the ligand and the surface. Various functional groups can be used to ensure the ligating atoms are arranged such that they bind effectively to either metal and/ or oxide ions on the surface. The resulting complex should therefore be stable as this prearrangment of ligating atoms for surface coordination is similar to the binding of a chelating ligand with metal ions in solution, which have high stability constants due to the chelate effect.

Although use of a flexibile backbone could allow a ligand to arrange itself to maximise the number and strength of ligand-surface interactions, a rigid structure ensures the ligand remains bound to the surface. Ligands with greater flexibility may be able to meet the coordination sphere requirements of an isolated metal ion and would lead to sequestration and transfer of metal ions into a solution phase in contact with the surface, Scheme 2-1.

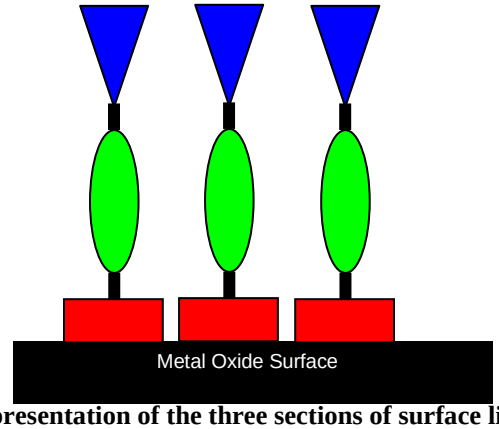

Figure 2-1 Schematic representation of the three sections of surface ligands: headgroups (red), linker (green), and tailgroup (blue)

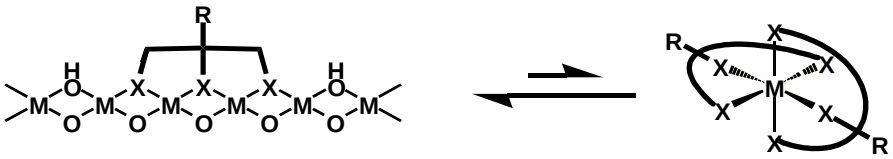

Scheme 2-1 Scheme showing equilibrium between ligand on surface and sequestration of ion into solution

2.3.1 Headgroups

Headgroups, shown in red in Figure 2-1, will preferably bind to the surface mainly by chemisorption processes although physiosorption using hydrogen bonding and van der Walls forces are possible. The choice of ligating atom will usually be dictated by the substrate used. Surfaces which contain hard metal ions such as iron(III) prefer hard ligating atoms such as oxygen.[3] For softer metal surfaces such as gold, sulfur would be more applicable.

In addition to the inclusion of appropriate ligating atoms the chemical viability of a group is also important. Therefore, for the examples above, carboxylic acids are much better than ester groups as protons are lost readily and similarly thiols are more suitable than thioethers. For example, chemisorption binding can involve the replacement of

surface hydroxyls or terminal water molecules depending on the nature of the metal oxide surfaces, consideration of charge balance is also therefore important. Factors such as the pK_a of a functional group could affect its ability to bind effectively.

2.3.2 Linker

The linker group, shown in green in Figure 2-1 which provides a connection between the headgroup and the tailgroup at first appears to have no major function apart from allowing efficient packing of ligands and the surface. However, in practice, such packing efficiency could contribute substantially to the stability of the complex, particularly kinetic stability. The design of a ligand should include appropriate functionality for generating additional ligand-ligand intermolecular interactions, via hydrogen bonding or other forms of secondary bonding, as discussed in Chapter 4. The linker could also be used to include an analytical label for detection at surfaces or in a solution phase in contact with the surface as discussed in Section 2.4.5. Finally, the structure of the linker is important for maintaining rigidity and can provide additional surface binding groups.

2.3.3 Tailgroup

The tailgroup of the ligand, in blue in Figure 2-1, provides the functionality to directly alter surface properties. The various choice of tailgroups can make surface ligands useful for many different applications such as adhesion promotion, friction modification and passivation.[4,5] The tail group of adhesion promoters usually contains monomers or other functional groups that can combine to a polymer based adhesive. Friction modifiers are used in engine oils to bind to metal surfaces and reduce the wear caused by two surfaces moving against each other. They allow lower viscosity oils to be used, lowering the overall friction. In organic corrosion inhibitors, the most obvious function of the tail is to provide hydrophobicity to generate a surface resistant to water-borne reagents.

2.3.4 Example: Irgacor 419

CM27-0419 known as Irgacor 419® is a commercially used corrosion inhibitor. A range of ligands, Figure 2-2, supplied by Ciba were investigated at the University of Edinburgh to rationalise the superior performance of CM27-0419 (Irg 419®), compared to the other ligands.[1] This ligand is referred to as **1** throughout the rest of the thesis. The headgroups for these ligands are carboxylic acids and in their deprotonated form bind strongly to an iron(III) oxide surface.

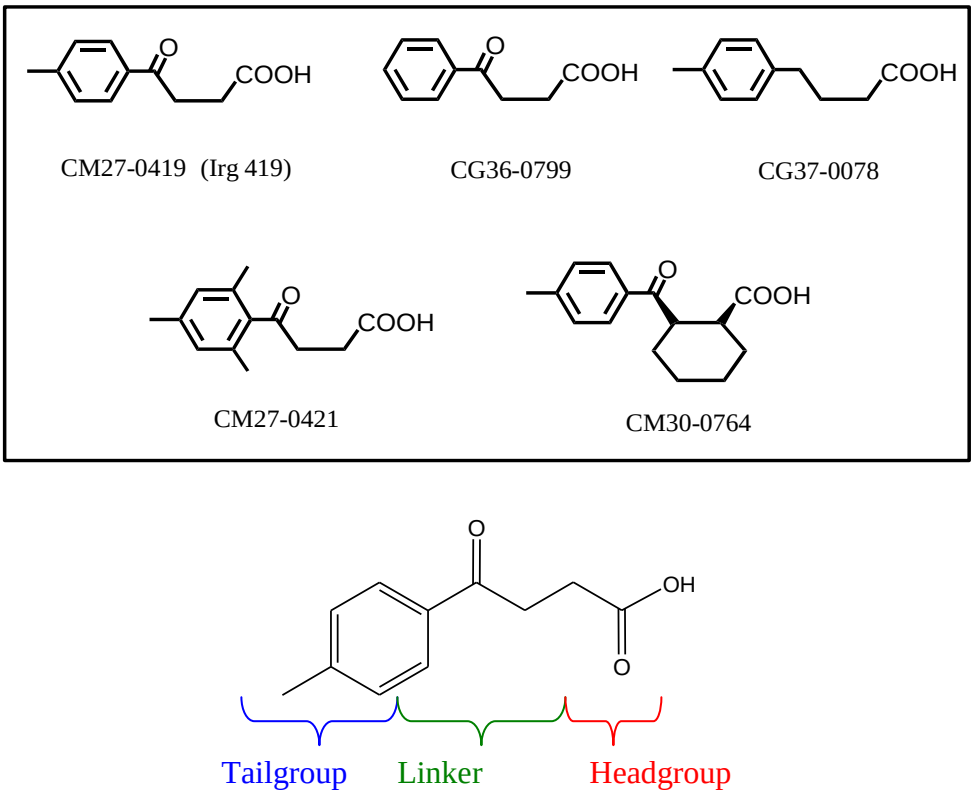

Figure 2-2 Structures of ligands supplied by Ciba and Irgacor 419® showing the headgroup, linker and tailgroup

A comparison of the binding strengths of the ligands by D Nation at University of Edinburgh revealed that the presence of a carbonyl, attached to a short, flexible alkyl

chain, resulted in stronger binding. The increased binding strength of the ligand was explained by the multisite attachment mode of binding generated by hydrogen bonding of the keto groups to surface hydroxyls as shown in Figure 2-3, a more detailed analysis is provided in Chapter 5. The linker group in this case is the short keto alkyl chain. It allows the ligand to have a degree of flexibility but does not favour sequestration of individual Fe(III) ions. CM27-0419 has a stronger binding strength than CM27-0421 because it can pack more efficiently on the surface as the bulkier mesitylene groups interfering with the surface-ligand packing in the latter case. CM30-0764 also has weaker binding compared to CM27-0419 as the linker group on is not flexible enough to provide the keto-hydoxyl secondary bonding interaction.

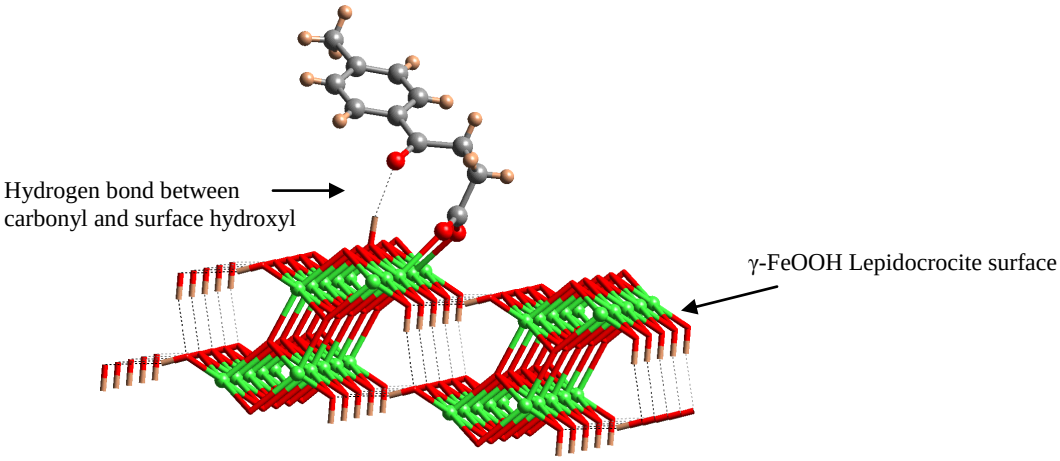

Figure 2-3 Multisite attachment of Irg 419 to γ-FeOOH lepidocrocite surface. Dotted line showing Hydrogen bond between keto group and surface hydroxyl. Atoms are colour coded as follows: Fe (green).[1]

A hydrophobic surface is produced from the π-π interactions that occur between the aromatic rings on the molecule. The tolyl tailgroup unit is important in generating the layer which protects the metal oxide from waterborne reagents, as shown in Figure 2-4. The aromatic tailgroup also provides an analytical label via UV-Vis spectroscopy for the determination of ligand concentrations in solution in adsorption isotherm experiments.

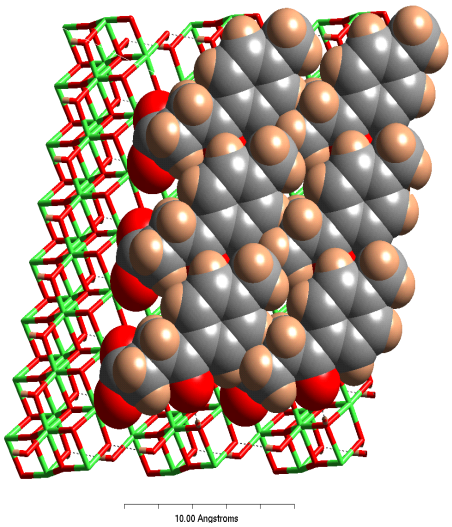

Figure 2-4 Hydrophobic layer generated by tolyl unit of Irg 419 bound to γ-FeOOH lepidocrocite surface[1]

Irgacor 419® is a very efficient ligand because many of the necessary requirements are fulfilled by the functional groups of a small molecule. For example, the presence of the aromatic group allows the residual ligand concentrations to be determined by UV-Vis spectroscopy and provides the ligand with the ability to generate intermolecular aromatic stacking interactions.

2.4 Adsorption Isotherms

The use of adsorption isotherms as a means of determining the thermodynamic stability of a surface complex is discussed in this section. Adsorption isotherms deal with the uptake of a small molecule (adsorbate), from the gas or liquid phase, onto a substrate (adsorbent). The data are usually presented in graphical form with the amount adsorbed plotted against the residual concentration of the adsorbate in solution.

2.4.1 Theory

The most favoured way to study the adsorption mechanism of small molecules onto surfaces is to determine the isotherm.[6] Some important aspects of isotherms include, the rate of adsorption, the shape of the isotherm, significance of any plateau region, extent of solvent adsorption, monomolecular or multilayering of adsorbate, effect of temperature and the nature of interactions between adsorbate and adsorbent.

When molecules bind to a surface, any bonding that occurs is due to a range of chemical or physical effects. Chemical adsorption (chemisorption) is the process by which chemical bonds are formed directly between the substrate and the adsorbent. This includes bonds such as thiolate bonds between thiols and gold or copper surfaces, or carboxylate bonds when deprotonated carboxylic acids bind with iron(III) oxide surfaces. Physical bonding effects, are typically much weaker but useful for providing secondary interactions, these include effects such as hydrogen bonding, hydrophobic bonding and van der Waals forces. The net or total interactions may include more than one type of the above.

Adsorption isotherms can be classed into four main classes, S, L, H and C, depending on the initial shape of the graph as defined by Giles *et al*. and shown in Figure 2-5. The behaviour observed at higher concentrations allows them to be classified into further sub groups.[7]

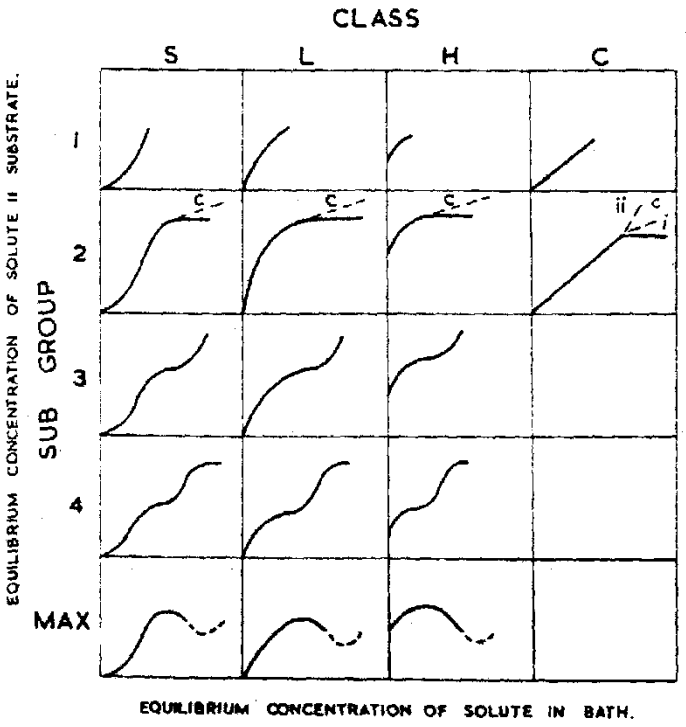

Figure 2-5 Groups and subgroups of isotherms[7]

The most common is the Langmuir, L, type. The curve is initially concave with the x-axis but then approaches a plateau. As the concentration is increased, binding sites are used up and it becomes progressively more difficult to find an appropriate site for attachment. The curve indicates no co-operative behaviour occurs and/or no competition exists from the solvent molecules.

The Langmuir model has been used in the determination of ligand binding strengths for most of the isotherms in this thesis. A derivation of the equation is given in Section 2.4.2. Alternative theories are described elsewhere, where relevant.

The High Affinity, H, group is a special case of the L group, where the binding of the absorbent is very high. The initial curve is almost vertical and low concentrations of adsorbate are completely adsorbed. The remainder of the curve behaves as in the L case when the availability of binding sites is reduced. Isotherms of the Constant Partition

class, C, have an initial linear portion. The binding does not change as the concentration increases because the ratio of adsorbent to adsorbate remains the same. This case is seen with microporous adsorbents.[7]

If the interaction between adsorbed molecules is negligible then the L or H case is usually observed. However, if the interaction between adsorbates is sufficiently large, then co-operative behaviour can be seen which gives rise to the S group. In the S group, initial adsorption is difficult but becomes easier as the concentration increases due to the nature of co-operative binding between the adsorbed molecules. This behaviour is usually observed when the solute is monofunctional with respect to headgroups, the solute has intermolecular interactions such that they pack vertically to the surface and the solvent or other adsorbed species compete for the binding sites.

2.4.2 Interpretation of Isotherms

The Langmuir model was originally derived for gas-solid adsorption processes but has been modified for use in liquid-solid systems. It is derived as follows.

If the equilibrium between an adsorbent(A) and a substrate(S) is:

(1)

$$S + A \rightleftharpoons SA$$

Then this gives an equilibrium constant of:

(2)

$$K_{ads} = \frac{[SA]}{[S][A]}$$

The maximum concentration of surface sites(S_M) is given by:

(3)

$$[S_M] = [S] + [S_A]$$

Where S_A is the concentration of surface sites with adsorbents. Therefore:

(4)

$$[S_A] = \frac{[S_M]K_{ads}[A]}{1 + K_{ads}[A]}$$

Which can be rearranged to the form:

(5)

$$K_{ads}[A] = \frac{\theta}{1-\theta} \quad \text{where} \quad \theta = \frac{[S_A]}{[S_M]}$$

The maximum surface coverage (S_M) and equilibrium adsorption constant (K_{ads}) are obtained directly from the Langmuir adsorption isotherm (5). The required surface area per molecule can be calculated using the surface area of the substrate defined in (6). This equation is based on the assumption that all binding sites are filled.

(6)

$$\text{Required surface area per molecule} = \frac{\text{Surface area of substrate}}{S_M}$$

The assumptions made in deriving the equation can limit its use and the model breaks down and can not be used effectively when no maximum surface is reached or very weak binding is displayed.

For adsorbents that can form second layers, a double Langmuir model is required to fit the data (7). Each adsorption process can result in different binding constants and surface coverages. This equation is also required where more than one adsorption site exists and is used by the adsorbent. These different sites can occur due to the morphology of the surface.

(7)

$$SA = S_1 \frac{K_1[A]}{1 + K_1[A]} + S_2 \frac{K_2[A]}{1 + K_2[A]}$$

Although useful for studying adsorption properties the nature of the technique is limited by several factors. These include the substrate or adsorbent chosen, the solvent system used, the binding of the ligand. This is a thermodynamic technique and kinetic interpretations are not possible.

2.4.3 Choice of substrate or absorbent

In order to determine the binding capabilities of a ligand it is necessary to obtain a detectable change in ligand concentration in the solution or gas in contact with the surface. This means that significant amounts of ligand must be absorbed and removed from the solvent phase and thus a high surface area material is required. Other issues associated with the substrate include, reproducibility of solid, possible contamination of surface and potential need for surface pre-treatment.

Few solids have completely reproducible surfaces unless great care is taken to ensure a high level of consistency. Consequently it is unsurprising that materials can differ from batch to batch. This is also complicated by the fact that some materials can be seen in a variety of forms, in particular iron oxide/hydroxides have several polymorphs. These FeO(OH) structures include α-goethite,[8] β-akageneite,[9, 10] γ-lepidocrocite[11] and δ-feroxyhite.[11] The type and number of surface hydroxyl groups depends on the method of preparation and treatment given before adsorption experiments are carried out. [12]

These iron(III) hydroxides can interconvert and change their morphology.[13] It is therefore important that a comparison between ligands is made with the same substrate. α-FeO(OH) has been chosen as it is the most thermodynamically stable form of the iron(III) hydroxides.

2.4.4 Choice of Solvent

The solvent used in isotherm determination is also of importance. The ligand must have sufficient solubility to ensure that complete surface coverage does not require use of very large volumes of solution. This can restrict the types of ligand/ substrate binding systems for study. A good choice of solvent also allows analysis of the ligand to be sufficiently easy and ideally without changing the solvent. Important factors depend on the method of ligand concentration analysis, for this thesis UV-Vis spectroscopy has been used for quantative analysis and therefore the solvent should have very little or no absorbance at the wavelengths used for quantitative determination.

The effect of the solvent on the substrate is important. A compatibility issue exists to ensure the surface is not dissolved or the nature of the surface is changed. It is also preferable that little or no competition occurs with the ligand for binding sites. Finally, the decision should be made such that results obtained are comparable for industrial usage.

95:5 methanol:water was chosen as the solvent for adsorption isotherm determination in this thesis. Although water would be the first choice for industrial purposes the mixed solvent can dissolve a greater number of organic ligands than water alone. In addition, the activity of water in 95:5 methanol:water is quite similar to that of water in pure water and this solvent system is frequently used for the measurement of stability constants for metal complex formation in solution for complexes of organic ligands.[14] Also, there are no major peaks in the UV-Vis absorption spectra in the wavelength region for ligand analysis.

2.4.5 Determination of Residual Ligand concentration

It is necessary to quantify the ligand concentrations in solution to determine the isotherm. Quantitative methods based on interferometry,[15] titrimetric,[16] gravimetric[17, 18] and radiation analysis[19] have deficiencies associated and can be difficult if a very small change needs to be measured accurately. In addition, the analytical method used should be quick and easy to carry out on a large number of samples.

To assist in concentration determination, the ligand can incorporate benefical functionality, such as chromophores, as mentioned in Section 2.3.2. The inclusion of an appropriate group may not present problems synthetically and could result in low detection limits, but must not alter the intrinsic binding strength of the head group if the purpose of the determining the isotherm is to assess the efficacy of the ligand.

The spectroscopic techniques used for determination of ligand concentrations in this thesis are UV-Vis and ICP-OES.

2.4.6 UV-Vis spectroscopy

The UV-Vis spectrum of a compound can be used to quantitatively measure the amount of compound in solution.[20] In a typical spectrum, the intensity of light absorbed is plotted against the wavelength of light absorbed. The peaks correspond to absorption of energy and promotion of electrons to excited states. Functional groups which give rise to these peaks are known as chromophores. Overlap of rotational and vibrational levels with the electronic transitions results in continuous absorption bands.

The three main types of transitions involve σ, π, and n electrons, charge-transfer electrons,or d and f electrons. Only those using σ, π, and n electrons are considered here. Possible transitions are $n \rightarrow \pi^*$, $\pi \rightarrow \pi^*$, $n \rightarrow \sigma^*$.

$n \rightarrow \pi^*$; these transitions involve the excitation of an electron between a nonbonding orbital and an antibonding π^* orbital associated with an unsaturated centre in the molecule. These are typically found in molecules containing: C=O, C=S, N=O.

$\pi \rightarrow \pi^*$; excitation of an electron from a bonding π orbital to an antibonding π^* orbital occurs in molecules that contain double or triple bonds. An increase in conjugation usually moves the absorption to larger wavelengths.

$n \rightarrow \sigma^*$; here an electron is excited from a nonbonding orbital to an antibonding σ^* orbital. These are generally of less importance than the first two in generating peaks in the UV-Vis spectra used for analysis in this thesis.

The wavelength of absorption corresponds to the energy difference between the ground state and the excited state. Transition of electrons from filled lower energy levels to empty higher energy levels can occur between bonding, non-bonding and anti-bonding orbitals. In order for the transition to be *allowed* the energy levels must have the same spin states. Transitions between states with different spins are *forbidden*.

Electronic absorption spectra are highly solvent dependent.[20] The energy levels of the molecules can be lowered or increased depending on the polarity of the solvent. In general, upon increasing solvent polarity, peaks arising from $n \rightarrow \pi^*$ transitions are shifted to shorter wavelengths. This is due to increased solvation of the lone pair which lowers the energy of the n orbital. $\pi \rightarrow \pi^*$ absorptions are shifted to longer wavelengths in more polar solvents due to lowering of energy of both states but with a greater effect on the excited state therefore lowering the overall energy of the transition.

2.4.7 Beer Lambert Law

In electronic absorption spectroscopy the concentration of an absorbing species is related to the absorbance of incident radiation, Equation 8, known as the Beer Lambert Law.

(8) $$\log \frac{I}{I_0} = -\varepsilon [J] l$$

Where I_0 is the intensity of the incident radiation, I is the intensity after passage through the sample of length l, [J] is molar concentration of absorbing species J and ε is called the molar absorption coefficient (formally known as the extinction coefficient). The left hand side of the equation can also be written as the absorbance, A, to give equation 9.

(9) $$A = \varepsilon [J] l$$

This law can only be used when the absorbance lies between zero and one. Above this range, the ratio of concentration to absorbance is no longer linear.

2.4.8 Inductively Coupled Plasma – Optical Emission Spectroscopy

Inductively Coupled Plasma – Optical Emission Spectroscopy (ICP-OES) is a spectroscopic technique with moderate to low detection limits (0.2-100 ppb). Samples are introduced into the system through a nebuliser with argon gas and are dissociated into its constituent atoms and ions. These are then excited by the plasma and a characteristic radiation is emitted for each element as it falls back to the ground state. The intensity of the emission is proportional to the concentration of the element and quantitative analysis is carried out by reference to calibration curves.

The elements detected by ICP-OES in this thesis are shown below along with the characteristic wavelengths chosen for each element in Table 2-1.

Element	Wavelength for analysis/ nm
Fe	273.9
S	180.6

Table 2-1 Elements detected by ICP-OES in this thesis and their characteristic wavelengths.

2.4.9 Omission of Kinetic data

The graph obtained from an adsorption isotherm experiment gives information about the thermodynamic stability of the ligand-surface bound complex. However, the nature of the technique, with an equilibration time of two hours will give no indication of the kinetics of binding or the overall kinetic stability of the surface complex.

This could potentially result in a ligand which has a very large surface binding constant but acts as a very poor corrosion inhibitor since a high kinetic stability is often also required. Cases have been found of ligands which have very strong surface binding strengths but are very poor passivators on aluminium surfaces.[21] The lack of kinetic information is a major drawback in using adsorption isotherms to assess the potential efficacy of different ligands for surface engineering. Consequently some thought has been given to alternative methods which might provide such information. One of these was the application of a quartz crystal microbalance to the study of surface coordination chemistry.

2.5 Quartz Crystal Microbalance

Quartz Crystal Microbalance

The quartz crystal microbalance(QCM) is a highly sensitive piece of equipment capable of detecting very small mass changes with real-time data capture. As a change in mass is observed as a function of time, kinetic information can be obtained. The device operates due to the piezoelectric effect and functions as a gravimetric tool.

A brief description of the technique is given below and more information about the background and theory is given in the Appendix.

The Sauerbrey equation was developed as a means of using a quartz crystal oscillator as a sensing device for measuring the thickness of thin films.[22] The equation (10) shows the relationship between the oscillation frequency of the fundamental mode of the QCM (f_0), the overtone number (n), the density (ρ_q), the shear modulus of quartz (μ_q), the change in frequency (Δf) and the change in mass (Δm).

(10)

$$\Delta f = -\frac{2\Delta m n f_0^2}{A\sqrt{(\mu_q \rho_q)}}$$

For a given crystal of quartz the values of f_0, n, ρ_q, μ_q are constant and the frequency changes only with respect to mass per unit area. This means that the QCM is most effective when used to study processes that are uniform across the whole surface of the crystal.

For simple systems, such as the formation of a monolayer or a thin film that exhibits rigid-layer behaviour the relationship shown in equation 11, which is a simpler version of equation 10, can be used where m is the mass of the unloaded resonator.[23]

(11)

$$\frac{\Delta f}{f_0} = -\frac{\Delta m}{m}$$

It is this simple relationship between the frequency change and the mass on the surface of the crystal which provides the basis for our proposal to use the QCM for competitive binding studies of surface ligands. The sensitivity of the QCM depends on the fundamental frequency of the crystal which usually ranges between 2-20 MHz.[24] Such balances are commercially available but some custom built QCMs have been shown to be able to operate at 27MHz.[25] Thinner crystals have higher frequencies but are very fragile, crystals with fundamental frequencies at about 2MHz are very robust but much less sensitive. The trade off is therefore sensitivity against robustness and the standard compromise is usually 10 MHz.

Equation 11 can be simplified to Equation 12 as the resonant frequency and mass are constant for any given crystal. The sensitivity factor (C_f) for a 9MHz crystal supplied by Maxtec is 0.181 Hz ng $^{-1}$ cm^{-2} at 20^{o}C. For a change of 1 Hz this corresponds to a mass change of 5.5 ng cm^{-2}.

(12)

$$\Delta f = -C_f \Delta m$$

The QCM is set-up such that the results are captured in real-time by computer. This means that changes are measured in-situ as they happen rather than after reaction. The reaction vessel involved can vary depending on the experiment being measured, and include flow cells where reactants are continuously flowed around the cell and pass the surface of the quartz, or open containers where reactants can simply be injected or added to the solution as data capture occurs. Figure 2-6 shows a photograph and schematic of a quartz crystal that is sandwiched between two gold electrodes.

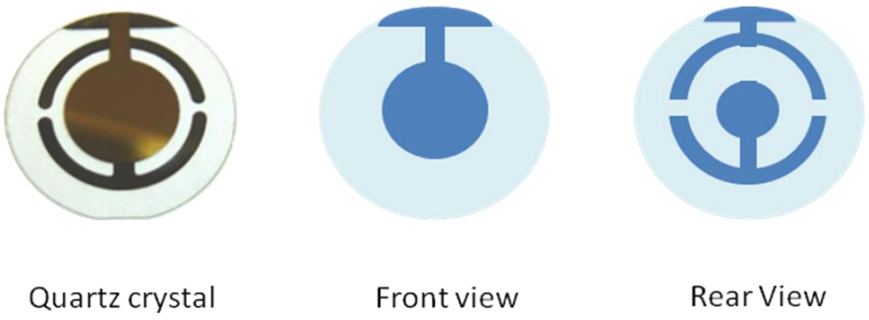

Figure 2-6 Picture of Quartz crystal showing schematic of the front and rear view of crystal surface. The darker blue shading indicates gold plating on the light blue quartz surface.

The QCM apparatus contains the crystal sandwiched between two O-rings. One side of the surface is exposed to the liquid being studied. The frequency of oscillation is continuously measured by computer and a change in frequency is converted to the change in mass. Since the change in mass depends only on the frequency change, resonant frequency and mass of unloaded resonator no calibration is required.

The QCM has also been combined with many in-situ surface analytical techniques including Surface Plasmon Resonance,[26] Auger Electron Spectroscopy,[27] X-ray Photoelectron Spectroscopy, Fourier-Transform IR[28] and contact angle grazing measurements.[29]

2.5.1 Potential Advantages over Adsorption Isotherms

In addition to the kinetic information obtained the QCM could also have the potential advantages over typical adsorption isotherm experiments. The high sensitivity reduces the requirement for high surface area substrates as a smaller change may be measured, this would also require less ligand. The gravimetric analysis removes the requirement for an analytical label on the ligand and could allow the study of a wider range of ligands. Electrochemical pre-treatment protocols can be used to generate and study different surfaces.

In addition, it may be possible to carry out competitive ligand binding studies between molecules with different molecular weights and could lead to experiments allowing an easy ranking of ligands.

2.6 Adsorption isotherm results

The binding of 3-(4-methylbenzoyl)-propionic acid, **1**, to goethite has been studied by Dr D Nation at the University of Edinburgh.[1] In order to provide a comparison with the work in this thesis, the adsorption isotherm was re-determined with a different batch of goethite which was then used for all other measurements in this thesis. The uptake of **1** on the new batch of goethite, surface area 22.65 m^2 g^{-1} as determined by the BET isotherm, is shown in Figure 2-7. The binding strengths and surface coverages obtained by analysing the data, using the Langmuir model, are shown in Table 2-2. The results are the same within experimental error. **2** differs from **1** in having a 4-bromo substituent compared with a 4-methyl substituent (see Figure 2-8). The larger molecular weight, but otherwise similar steric and electronic properties, was deemed to be useful in studies of competitive binding by the QCM. It was expected that the binding constants would be very similar and this is shown to be the case in Table 2-2.

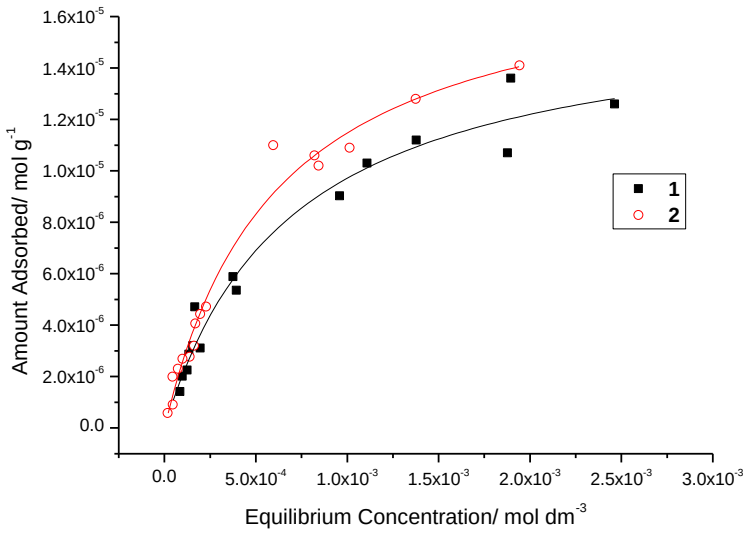

Figure 2-7 Uptake of 1 and 2 onto goethite from 95:5 MeOH/ H_2O

	New Goethite		Previous Studies[1]
	1	**2**	**1**
Equilibrium binding constant(10^{-3}) / k	1.5(2)	1.8(1)	1.26(2)
Surface coverage(10^5)/ mol g^{-1}	1.6(1)	1.6(2)	1.4(1)
Required surface area per molecule/ $Å^2$	238(15)	238(30)	273(20)

Table 2-2 Adsorption isotherm data for 1 and 2 onto goethite, (surface area 22.6 m^2 g^{-1})together with results determined previously[1] for the uptake of 1 on a different sample of goethite with surface area 18.8 m^2 g^{-1}(errors in parenthesis)

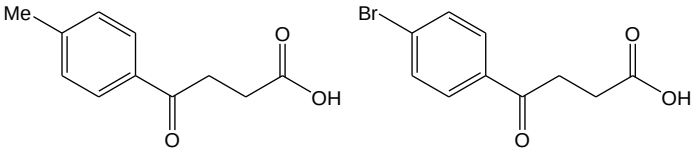

1 **2**

Figure 2-8 Structures of 1 and 2

2.7 QCM Studies

Initial studies were carried out in collaboration with Nick van Dyke at Loughborough University. Preliminary experiments were used to determine if the uptake of **2** onto an iron oxide substrate would produce a sufficient change in frequency as measured by an Electrochemical QCM.

An iron coated quartz crystal was used as a working electrode in a conventional three electrode design. An iron oxide layer was generated and held at 0 V vs SCE to generate a steady-state oxide layer. The ligand was added after 20 seconds. The mass response, Figure 2-9, shows that after the addition of the corrosion inhibitor there is a slight decrease in mass which corresponds to an initial restructuring of the solvent molecules. After a few seconds an increase in frequency was observed, indicating an increase in mass, which was proposed to correspond to the adsorption of **2**.

Due to this promising initial result, a 9 MHz Research QCM supplied by Maxtec was purchased and set-up in our laboratory. 1-inch diameter, gold coated 9 MHz quartz crystals were used in a Teflon coated holder as supplied. This was placed in a beaker of degassed, deionised water and left to reach equilibrium for two hours before any measurements were made. A stable frequency baseline is required for use of the QCM. Values of frequency drift claimed for the equipment are less than 3 Hz per hour.

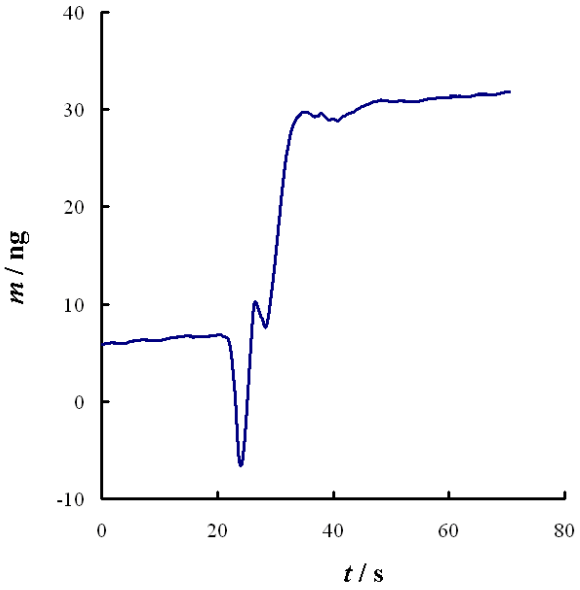

Figure 2-9 Mass change versus time for Fe passivated at 0 V vs Ag/AgCl/3 M NaCl. 1 was added after 20 seconds.

Monolayer coverage of **2** is observed at 1.8 x 10^{-5} mol g^{-1}, approximately equivalent to a mass of 3.4 x 10^{-3} g. This corresponds to the mass adsorbed on 22.5 m^2 of goethite. Therefore, 1 cm^2 is covered with 150 ng. However, this value refers to how much ligand is adsorbed onto a single square centimetre, in practice the surface area of an electrode coated with goethite could be larger. It should therefore be possible to measure the fractional uptake of monolayers.

Figure 2-10 shows the frequency and change in frequency against time for an Au plated electrode in a beaker of deionised water over a period of two hours. The graph shows a drift in the frequency baseline. These drifts were not continuous, nor predictable. Erratic changes are observed with the frequency increasing and decreasing and the rate of change in frequency was also variable.

Figure 2-11 shows the frequency and change in frequency against time for a Au plated electrode in a beaker of deionised water over 24 hours. Changes in frequency greater than 10 Hz per hour occurred at times between 9am and 5pm. The system then stabilised

to give changes in frequency of less than five Hz per hour, for a few hours overnight and further drifting occurred in the morning. The timing of these instabilities suggests that these changes correspond to electrical interference or temperature dependence.

Figure 2-10 Frequency(purple) and change in frequency(red) versus time for Au plated RQCM crystal immersed in deionised water

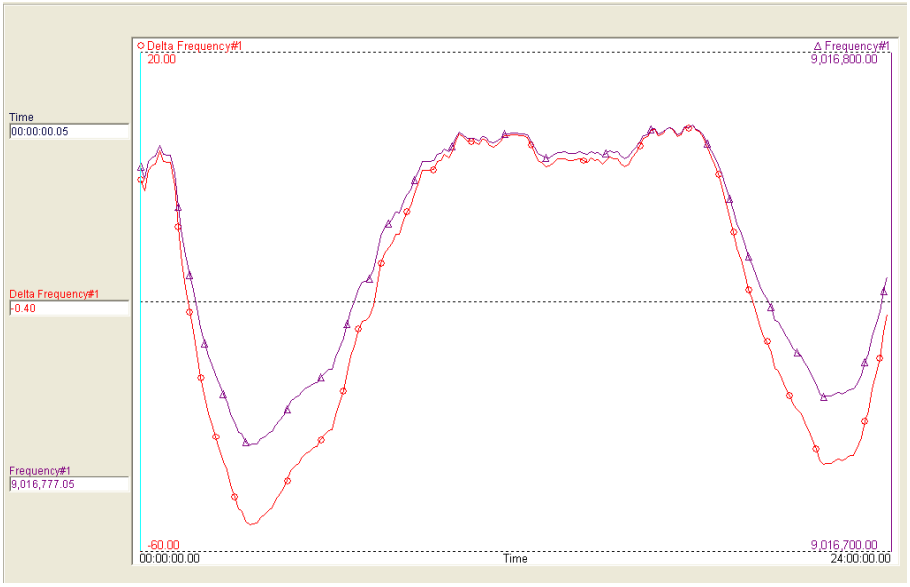

Figure 2-11 Frequency(purple) and change in frequency(red) versus time for Au plated RQCM crystal immersed in deionised water

Various attempts were made to reduce the background 'noise' affecting the frequency. To reduce effects of air circulation, the beaker was covered and sealed. To limit the effects of external electrical activity the quartz crystal assembly was enclosed in a Faraday cage. However, these measures proved ineffective.

The changes in frequency expected for small additions of ligand were of the order of a few Hertz. However, the RQCM purchased was overly sensitive to the surrounding environment and unfortunately this method of measuring ligand adsorption could not be carried out.

2.8 Conclusions

Reviewing the chemical literature (see also Chapter one) provides confidence that small organic ligands can be used to inhibit corrosive processes. The use of appropriate ligating groups which could form coordinative bonds to metal ions in surface oxides

along with the inclusion of simple secondary functionality is effective in generating a multisite attachment mode of binding. To function as a corrosion inhibitor the ligand-surface complex should be both thermodynamically and kinetically stable and provide "barrier properties" to limit attack by waterborne reagents.

Adsorption isotherms can be used to determine the binding strengths and surface coverages of ligands onto a high surface area substrate. Adsorption from a 95:5 MeOH/H_2O solvent mixture onto goethite can be carried out easily and have been shown to provide information on how strongly candidate corrosion inhibitors bind to metal oxide surfaces. As these provide information only on thermodynamic stability alternative techniques to assess kinetic stability were considered. The QCM is a gravimetric tool capable of detecting very small mass changes, its ability to obtain in-situ, real time-data capture suggested it would be ideal to obtain information on rates of ligand exchange on surfaces. Unfortunately, the RQCM purchased was found to be overly sensitive to the surrounding environments and could not be used in these studies.

Adsorption isotherms are used throughout the rest of this thesis to evaluate the relative binding strengths of different classes of benign organic molecules which could function as corrosion inhibitors. The various ligand types studied were outlined at the end of Chapter 1.

2.9 Experimental

2.9.1 Adsorption Isotherm measurements

All adsorption isotherms in this thesis were carried out by determination of ligand adsorption from 95:5 MeOH/H_2O onto a single batch of goethite. Accurately weighed amounts of goethite (*ca.* 400 mg) were stirred with a solution (10 dm^{-3}) of known concentration of ligand at 25 ^{0}C for two hours in polycarbonate centrifuge tubes. These

were then centrifuged and the supernatant solution was filtered through glass microfibre filter paper under pressure (N_2).

Known volume of the supernatant were diluted and the concentrations determined by UV-Vis spectroscopy using the Beer-Lambert Equation, $A=\varepsilon cl$, and the predetermined molar adsorption coefficient. For analysis by ICP-OES, the solvent was removed under reduced pressure and made up to volume using deionised water. The concentration of S in the solution was then calculated with reference to calibration curves.The amount of ligand adsorbed per gram of goethite was then calculated and this was plotted against the residual equilibrium concentration of ligand in solution. Binding constants and surface coverages were calculated by fitting the data to rectangular or double rectangular hyperbola functions. These equations are discussed in Section 2.4.2. All adsorption isotherm data are included in the Appendix.

2.9.2 Quartz Crystal Microbalance measurements

Initial QCM studies were carried out at Loughborough University in Professor Stephen Fletcher's laboratory using a 10 MHz EQCM as supplied by Elchema. The iron oxide surface was created on an iron coated electrode using previously determined literature procedure which give a known iron oxide surface as determined by X-ray diffraction.[30-32]

The electrochemical cell used was a conventional three electrode design, and included a silver/silver chloride (3 M NaCl) reference half cell and a platinum gauze counter electrode. The working electrode was a 5 mm diameter iron disk deposited on the quartz crystal. The pretreatment solution was a 0.136M borate buffer (7.07g/L H_3BO_3 + 8.17g/L $Na_2B_4O_7.10H_2O$) prepared in organic-free deionised water (18.2 MΩ cm) at pH 8.4.

Further studies were carried out on a 9MHz RQCM as supplied by Maxtec Inc on gold coated quartz crystals in organic-free deionised water (16.6 MΩ cm).

2.10 References

1 M. Frey, S. G. Harris, J. M. Holmes, D. A. Nation, S. Parsons, P. A. Tasker, and R. E. P. Winpenny, *Chemistry--A European Journal*, 2000, **6**, 1407.
2 D. A. Jones, 'Principles and Prevention of Corrosion', Prentice-Hall International (UK) Ltd, 1996.
3 L. Pauling, *Journal of the American Chemical Society*, 1929, **51**, 1010.
4 J. Cognard, *Comptes Rendus Chimie*, 2006, **9**, 13.
5 J. M. Herdan, *Lubrication Science*, 2000, **12**, 265.
6 G. D. Parfitt, Rochester, C. H., 'Adsorption for Solution at the Solid/ Liquid Interface', Academic Press, 1983.
7 C. H. Giles, T. H. MacEwan, S. N. Nakhwa, and D. Smith, *Journal of the Chemical Society, Abstracts*, 1960, 3973.
8 J. Bohm, *Zeitschrift fuer Kristallographie, Kristallgeometrie, Kristallphysik, Kristallchemie*, 1928, **68**, 567.
9 J. D. Bernal, D. R. Dasgupta, and A. L. Mackay, *Clay Minerals Bull.*, 1959, **4**, 15.
10 A. L. Mackay, *Mineral. Mag.*, 1960, **32**, 545.
11 O. Glemser and E. Gwinner, *Z. anorg. allgem. Chem.*, 1939, **240**, 161.
12 M. Villalobos, M. A. Trotz, and J. O. Leckie, *Journal of Colloid and Interface Science*, 2003, **268**, 273.
13 F. A. Cotton and G. Wilkinson, 'Advanced Inorganic Chemistry', Wiley, 1972.
14 L. F. Lindoy, 'The Chemistry of Macrocyclic Ligand Complexes', Cambridge University Press, 1989.
15 D. C. Jones and G. S. Mill, *Journal of the Chemical Society*, 1957, 213.
16 H. R. Kruyt and C. F. van Duin, *Recueil des Travaux Chimiques des Pays-Bas et de la Belgique*, 1920, **39**, 679.
17 H. W. Foote and J. K. Dixon, *Journal of the American Chemical Society*, 1930, **52**, 2170.
18 J. J. Kipling, 'Adsorption from Solutions of Non-Electrolytes', Academic Press, 1965.
19 J. K. Dixon, A. J. Weith, Jr., A. A. Argyle, and D. J. Salley, *Nature (London, United Kingdom)*, 1949, **163**, 845.
20 J. B. Lambert, H. F. Shurvell, D. A. Lightner, and R. G. Cooks, 'Organic structural spectroscopy', Prentice-Hall, Inc, 1998.
21 R. J. Cooper, P. J. Camp, D. K. Henderson, P. A. Lovatt, D. A. Nation, S. Richards, and P. A. Tasker, *Dalton Transactions*, 2007, 1300.
22 G. Z. Sauerbrey, *Z. Phys.*, 1959, **115**, 206.
23 M. R. Deakin and D. A. Buttry, *Analytical Chemistry*, 1989, **61**, 1147A.
24 C. K. O'Sullivan and G. G. Guilbault, *Biosensors & Bioelectronics*, 1999, **14**, 663.
25 Y. Okahata, K. Niikura, Y. Sugiura, M. Sawada, and T. Morii, *Biochemistry*, 1998, **37**, 5666.

[26] M. Minunni, M. Mascini, G. G. Guilbault, and B. Hock, *Analytical Letters*, 1995, **28**, 749.

[27] J. Onsgaard and O. Ellegaard, *Nuclear Instruments & Methods in Physics Research, Section B: Beam Interactions with Materials and Atoms*, 1984, **230**, 666.

[28] T. T. Dao, C. A. Spence, and D. W. Hess, *Proceedings of SPIE-The International Society for Optical Engineering*, 1991, **1466**, 257.

[29] E. Occhiello, M. Morra, F. Garbassi, and J. Bargon, *Applied Surface Science*, 1989, **36**, 285.

[30] M. F. D. Toney, A. J. Oblonsky, L. J.. Ryan, M. P, Vitus,C. M, *Physical Review Letters*, 1997, **79**, 4282.

[31] A. J. O. Davenport, L. J. Ryan, M. P. and Toney M. F., *J. Electrochem. Soc.*, 2000, **147**, 2162.

[32] L. J. D. Oblonsky, A. J.Ryan, M. P. Isaacs, H. S.and Newman, R. C., *J. Electrochem. Soc.*, 1997, **144**, 2398.

Contents

3 Binding studies of phenolic oxime esters and related compounds

3.1 Introduction

The importance of corrosion prevention has already been discussed in Chapter 1. Many companies are involved in this area and speciality chemical companies are particularly interested in designing organic corrosion inhibitors. Some are already in use and it is important for the design of new actives to understand the mechanisms and functionality that lead to strong surface binding and good corrosion protection.

This chapter deals with the synthesis and binding of a series of ligands which are structurally related to two commercial corrosion inhibitors, "P50 oxime" and "PIBSA", in Scheme 3-1. Studies at ICI showed that these had a synergistic effect on corrosion inhibition, the performance being better than that of the components.[1] Subsequently it was claimed that the improved corrosion protection was afforded by a product of the reaction between P50 oxime and PIBSA as shown in Scheme 3-1.[2]

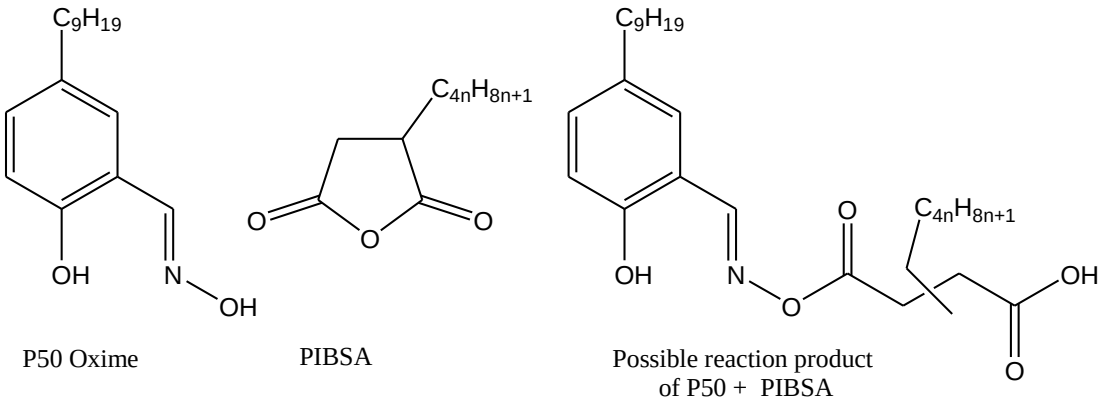

Scheme 3-1 Structures of P50 oxime, PIBSA and reaction product

"P50 oxime", 5-nonylsalicylaldoxime, is one of several phenolic oximes which were originally developed as solvent extractants for copper[3] and are now responsible for approximately one third of the world's production.[4] They were later shown to be

good corrosion inhibitors for mild steel particularly when present in conventional alkyol and acrylate paints.[5]

3.2 Phenolic oximes

Phenols act as hard Lewis acids and have long been known to be good ligands for iron(III). They usually form highly coloured complexes with very high binding constants.[6]

Oximes consist of a carbon doubly bonded to a nitrogen which is in turn attached to a hydroxyl group. The groups are planar and aldoximes are usually arranged in the E (trans) form as shown in Figure 3-1. In the case of ketoximes the isomer is defined by which substituent R^1 or R^2 has the higher priority.

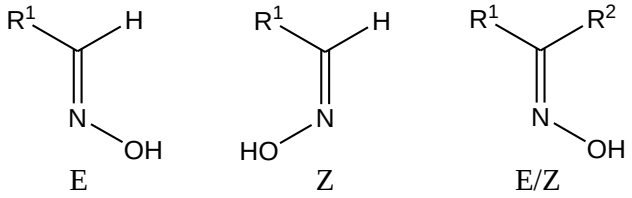

Figure 3-1 Structures of aldoximes and ketoximes showing configurations

Isomerisation of oximes is possible and is important since the conformation can affect the properties for example drug activity.[7] It is commonly thought that isomerisation and hydrolysis take place via a tetrahedral carbonolamino intermediate, Scheme 3-2. This mechanism was first investigated by Rosenberg.[8]

Recent DFT studies by Nsikabaka and co-workers have suggested that for acetaldoxime, isomerisation in aqueous acidic media, takes place via a concerted mechanism, Scheme 3-3.[7] Water behaves as a nucleophilic catalyst and the formation of a carbon(oxime)-oxygen(water) bond stabilises the system thus allowing rotation around the CN oxime bond. Interconversion of E/Z isomers at metal oxide surfaces might be important to the process of surface complex formation and a mechanism similar to that in which a metal cation, rather than a proton is bonded to the imine nitrogen atom is possible.

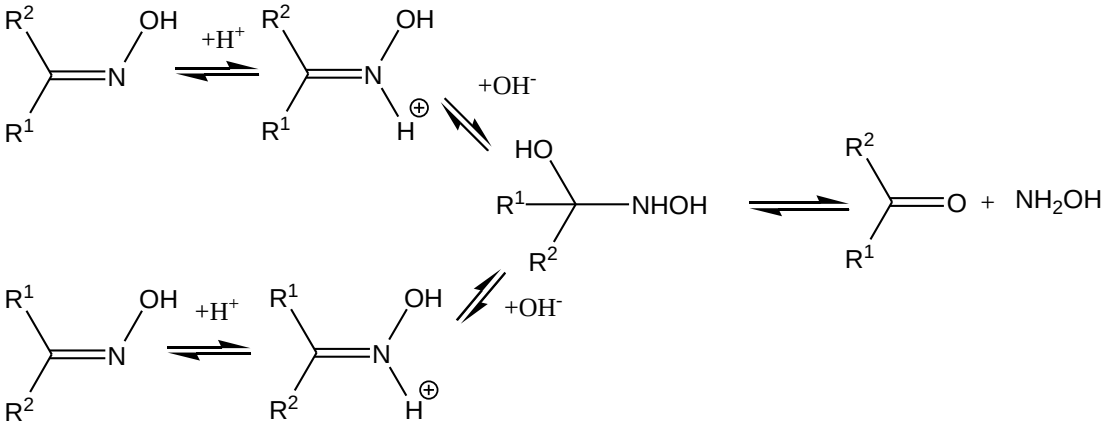

Scheme 3-2 Isomerisation and hydrolysis mechanism in acidic solution via tetrahedral protonated carbonolamine intermediate

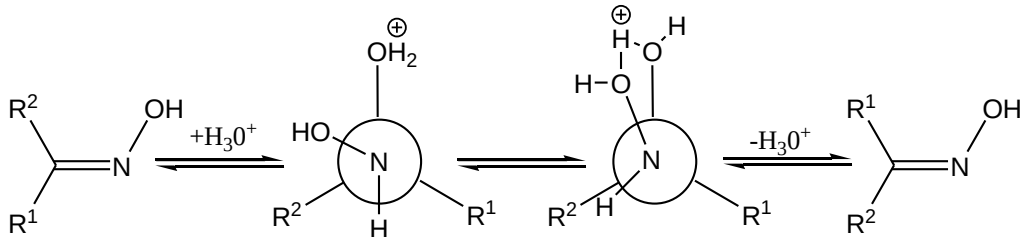

Scheme 3-3 Concerted reaction mechanism for oxime isomerisation suggested by Nsikabaka and co-workers

Oximes have been found to be able to coordinate to a number of different metals and binding can occur using either or both the oxygen and nitrogen atoms. [9] The mode of coordination depends on the hardness/softness of the metal cation. Hard metals prefer to be bound to the hard oxygen and soft metals to the softer nitrogen.[10]

Oximes can also bind to iron and electrochemical studies have shown that absorption of oximes onto an iron surface has an inhibitor effect on the corrosion potential.[11] It was also suggested that oximes are better corrosion inhibitors than analogous amines although no full investigation was made to determine if it was due to stronger surface binding or larger surface coverage.

The combination of the hydroxyl and oxime groups in phenolic oximes, particularly in salicylaldoximes, leads to strong metal complexation. These free ligands have a

number of hydrogen bond donors and acceptors and under ambient pressure often dimerise in the solid state as shown in Figure 3-2, **A**. [12] In the dimer arrangement two ligands hydrogen-bond to each other forming a 14-membered *pseudo*-macrocyclic ring.

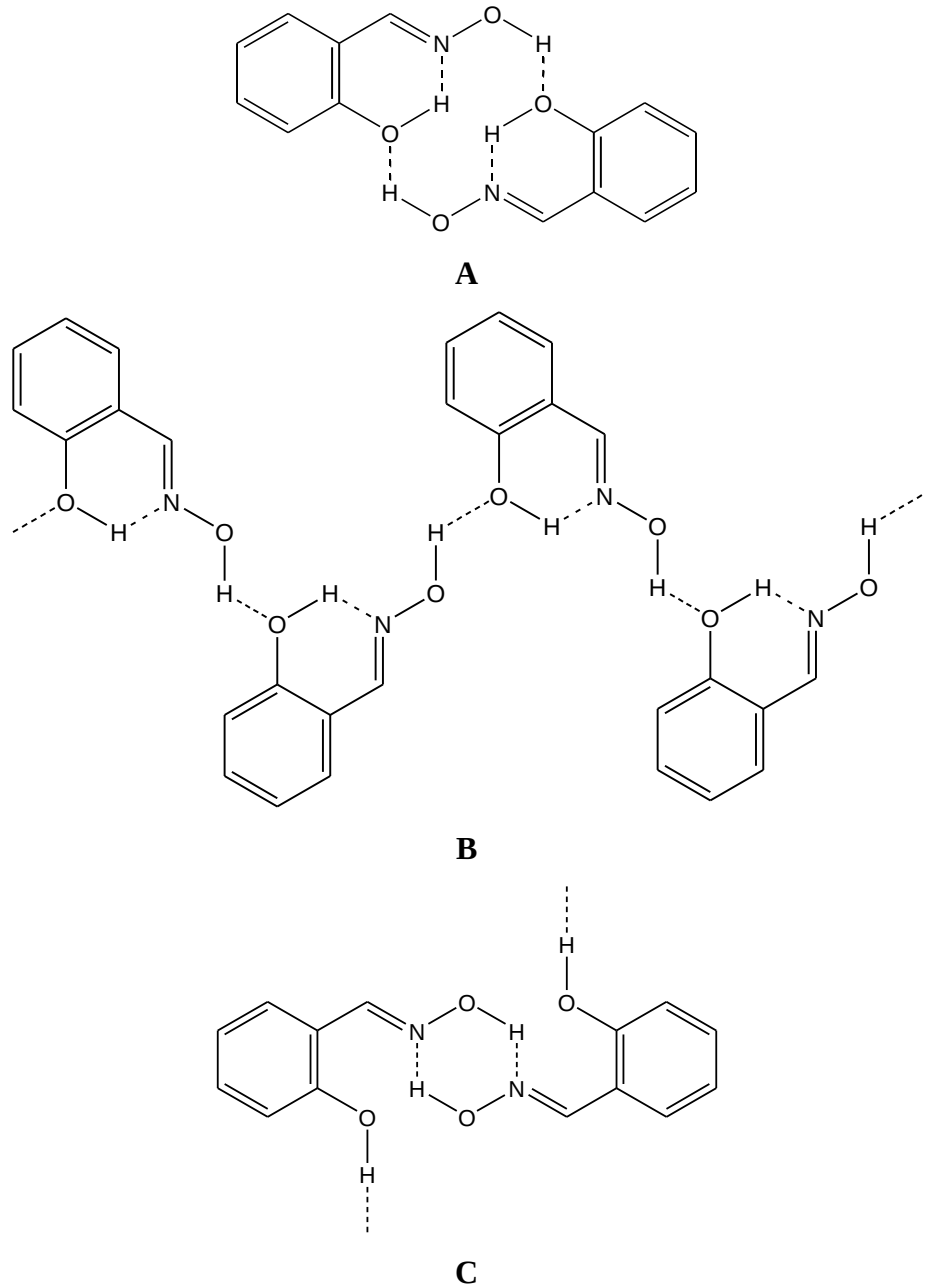

Figure 3-2 Structures of salicylaldoximes: the *pseudo*-macrocyclic dimer, A, and polymeric structures involving oxime to phenol H bonding, B, and a combination of oxime-oxime and phenol-phenol H-bonding, C.

The preferred arrangement appears to be affected by the presence of bulky groups that can interfere with packing leading to a second structure in which the ligand forms extended polymer chains, **B**, which also contain oxime to phenol hydrogen bonding. High pressure studies have found that there is a third structure for salicylaldoxime in which the intramolecular hydrogen bonding from the phenol to the oxime nitrogen changes to intermolecular phenol to phenol bonding bonding. The oxime groups also form intermolecular hydrogen bonded units via the six memebered rings to give the polymeric chains shown in **C**.[13]

In the case of the oxime dimer (**A** in Figure 3-2), metal ions which can be square planar, such as Cu^{2+}, can replace two phenolic protons whilst keeping the hydrogen bonded *pseudo*macrocyle intact, see Figure 3-3. In the case of P50 oxime, this preorganisation of the donor set along with the fast kinetics of copper complexation make the ligand useful for the recovery of copper by solvent extraction.

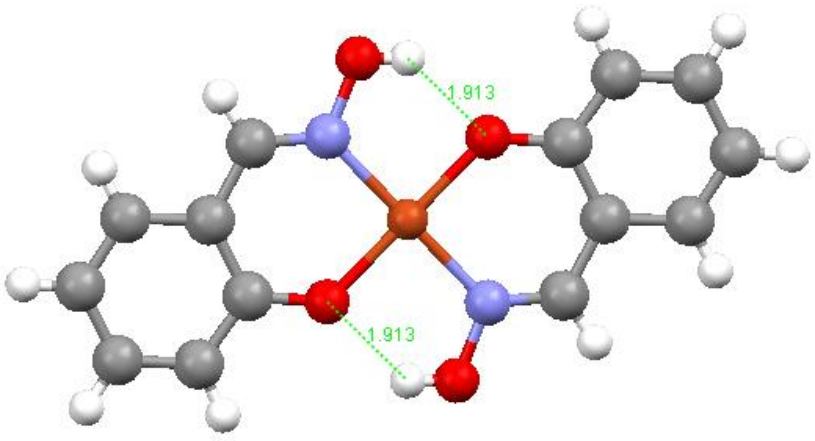

Figure 3-3 Crystal structure of $Cu(salox)_2$

Phenolic oximes have also been found to be good ligands for a number of metals other than copper. Complexes with about a third of the transition metals and some group three and four metal cations have been reported. [14, 15].

3.3 Binding modes of Salicylaldoxime systems

Salicylaldoximes can bind with a range of nuclearities and form mixed metal complexes. The following discussion highlights the variety of binding modes that can occur and provides background information on how salicylaldoxime ligands could bind to arrays of metal ions in oxide surfaces. Of the 19 possible binding modes, ranging from mono to trinucleating, shown in Figure 3-6, 10 are found to occur in 2007, Version 5.28 of the Cambridge Structural Database (CSD). Searching was carried out on version 1.8 of Conquest using the search fragment shown, the core can be modified with substituents on the aromatic ring or at the oxime carbon atom.[16] The notation describing the binding modes is an extension of that devised by Harris (see SectionSection 5.5).[17] The system defines the total number of metal atoms bonded to the unit, (digit preceeding the dot) and (left to right) the number of metal atoms bonded to the phenol oxygen, the oxime nitrogen and the oxime oxygen atoms respectively. As a fully deprotonated phenolic oxime has a total of five lone pairs [phenolate (2), oxime nitrogen (1) and oximato oxygen (2)] it is possible that tetra and pentanuclear structures could also be formed. However no occurrences of such complexes are recorded in the CSD.

The nomenclature used to describe the salicylaldoxime ligands in the complexes is that used by Smith *et. al*.(see Figure 3-7); *sal* is used as an abbreviation for the general form of the ligand and can be modified with additional substituents on the aldehydic hydrogen and/ or on the aromatic ring.[15] The positions and types of ring substituents (R_1) are given first, followed by the degree of ligand protonation, ('H_2' for free ligand, 'H' for monodeprotonated and nothing for the dianion). The substitution (R_2) at the oxime carbon atom is given last.

Some commonly used nomenclature of bonding modes between metals and ligands in coordination chemistry are shown in Figure 3-4. Where ligands contain many donor atoms and binding types, the terminology can become confusing. Harris

notation is particularly useful, since it states in an unambiguous manner the location of bonds between metal atoms and ligating atoms as described below.[17]

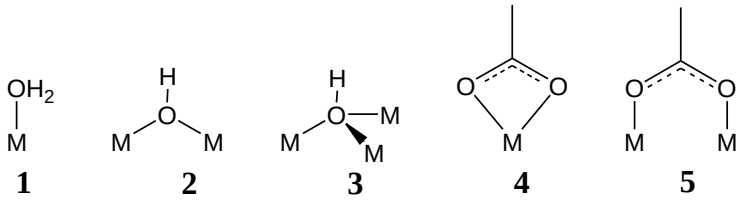

Figure 3-4 Commonly used nomenclature used to describe various ligand to metal modes in coordination chemistry. 1-terminal water, 2-μ hydroxide, 3-μ_3 hydroxide, 4-μ acetate, 5-η^2 acetate

For a ligand containing *n* donor atoms D_1, D_2, D_n bound to a number of metal atoms, *X*, the binding mode is referred to as ***[X . Y_1 Y_2 Y_n]***. Each value of *Y* refers to the number of metal atoms bonded to each donor atom *D*. In cases where no metal atom is coordinated to a donor atom the number is stated as zero. The order of donor atoms should be presented as logically as possible, and where heteronuclear atoms are present the priority is given to that with the highest atomic number. Some examples are shown in Figure 3-5 including those for **4, 5** in .

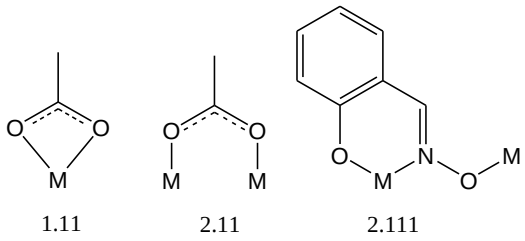

Figure 3-5 Examples of ligand to metal coordination modes showing Harris notation

It is possible for ligands to coordinate to atoms other than metals, e.g. in hydrogen bonds. Oxygen and nitrogen atoms can acts as hydrogen bond acceptors, and in their protonated form as hydrogen bond donor and acceptors. In order to differentiate, the nomenclature can be extended to include subscripts of a or d depending on whether the atom acts as acceptor or donor respectively. In some cases, it is possible that an atom has more than one such contact, in which case more than one subscript is added.

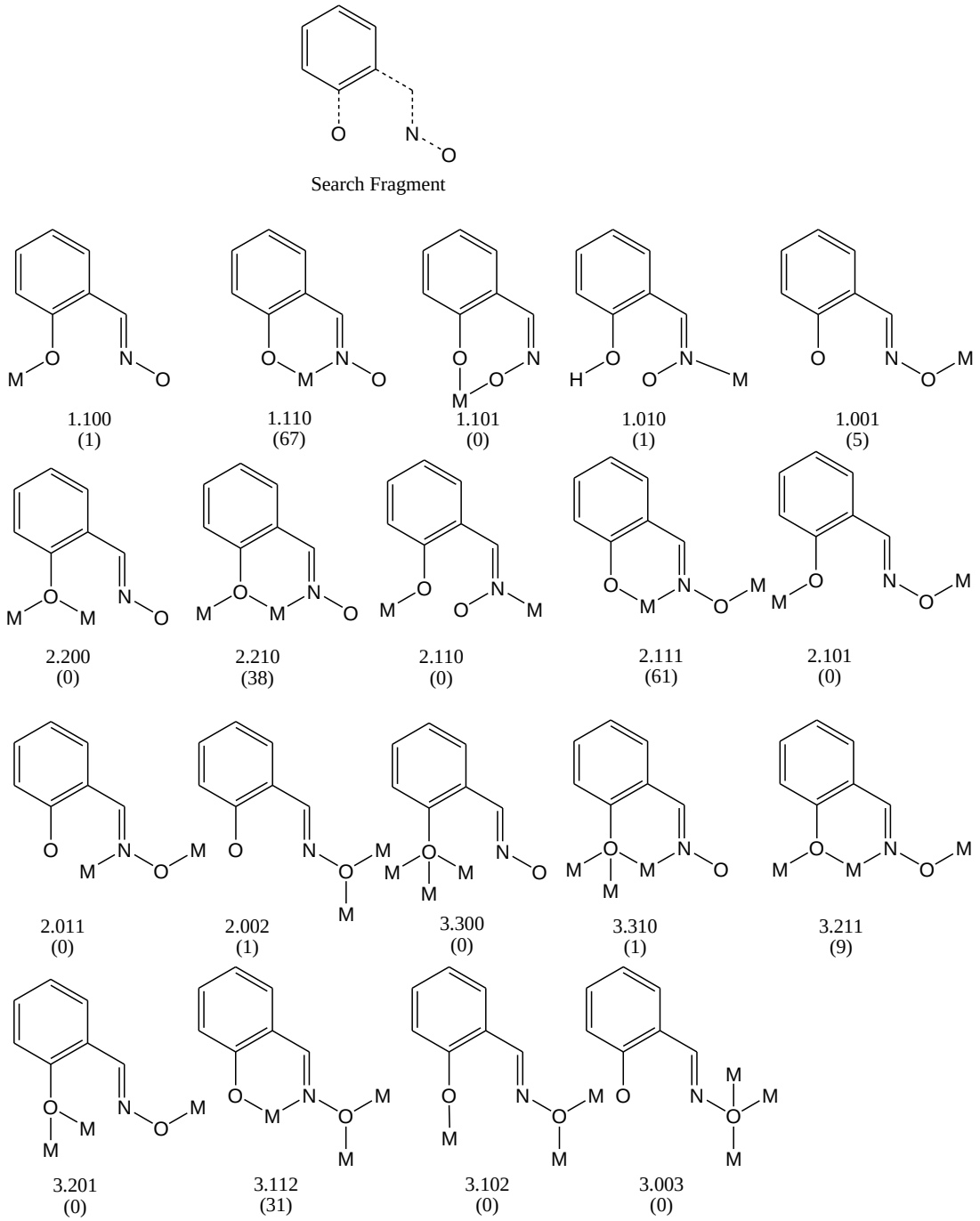

Figure 3-6 The search fragment used to interrogate the CSD, dotted lines represent any bond, and the sixteen possible binding modes of phenolic oximes with Harris notation stating total number of metals bound (first digit) and number of metals bound to each ligating atom (left to right).[17] The number of occurrences in the CSD of each type is given in patenthesis.

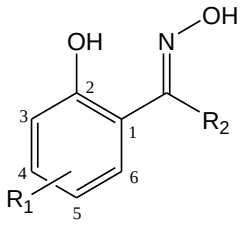

n-(R_1)-$H_x$sal(R2)

Figure 3-7 Scheme for naming ligands based on the salicylaldoxime framework

1.100 Binding Mode

A single example of the 1.100 mode was found. The mixed ligating ability of salicylaldoxime has been exploited by van Veggel *et. al.* in the design of hetero-dinuclear complexes.[18]. A crown ether adjacent to the phenol of a salicylaldoxime unit in the macrocyclic ligand L, Figure 3-8, provides a strong O_6^{2-} donor set for a Ba(II) ion. Each metal centre is 9 coordinate, the three other sites are occupied by a terminal $CF_3SO_3^-$ and two bridging $CF_3SO_3^-$ ligands.

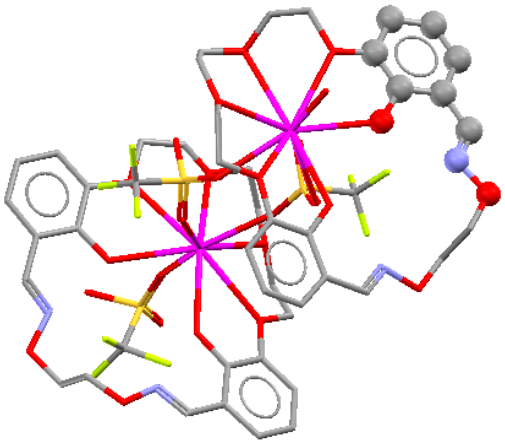

L=

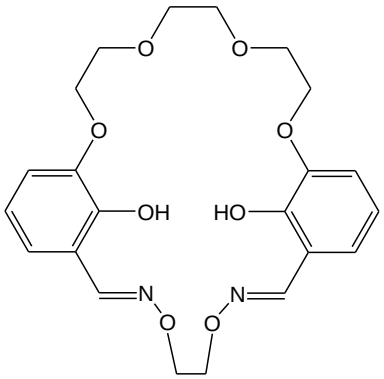

Figure 3-8 Example of the 1.100 binding mode. The crystal structure of $[Ba_2L_2(CF_3SO_3)_4]$. Atoms are colour coded; Ba (purple), S (yellow), F (green). The hydrogen atoms have been omitted for clarity.[18]

1.110 Binding Mode

The most common motif is the 1.110 mode with a total of 67 hits in the CSD. Binding involves deprotonation of the phenol and insertion of the metal cation between it and the nitrogen atom, the phenol oxime cavity, see Figure 3-3. This simple chelating motif has been found for a number of different metals spanning the periodic table.[19]

1.010 Binding Mode

Of the other mononucleating binding modes, a single example was found of the 1.010 type and involves a Pt(IV) centre shown in Figure 3-9. This was formed from reaction of a Pt(II) complex with molecular chlorine. [20] The structure displays two different binding modes of salicylaldoxime, the common 1.110 mode and an unusual, 1.010, monodentate coordination using only the oxime nitrogen.

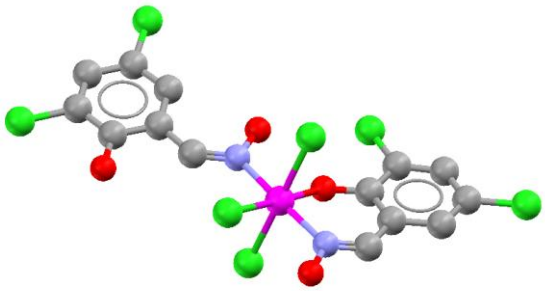

Figure 3-9 Example of the 1.010 binding mode. The crystal structure of [$PtCl_3$(3,5-dichloro-H_2salH)(3,5-dichloro-HsalH)]. Atoms are colour coded: Pt (purple), Cl (green). The hydrogen atoms have been omitted for clarity.[20]

1.001 Binding Mode

The remaining motif containing just a single metal atom is the 1.001 mode with a total of 5 occurrences.[19] An example is shown in Figure 3-10 of a complex consisting of a Sb(V) centre in a 5-coordinate distorted trigonal bypyramidal arrangement with three phenyl groups and two *trans*-coordinated salicylaldoximate ligands binding using only the oximato oxygen atom.[21]

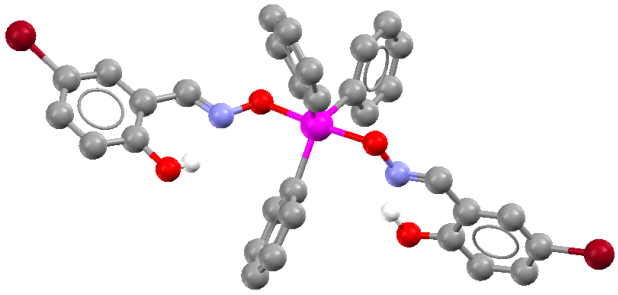

Figure 3-10 Example of the 1.001 binding mode. The crystal structure of [Ph_3Sb(5-bromo-HsalH)$_2$]. Atoms are colour coded: Sb (purple), Br (dark red). The hydrogen atoms have been omitted for clarity.[21]

2.210 Binding Mode

Another common dinucleating motif is the 2.210 mode which has 38 occurrences.[19] A Sn complex, formed by reaction of di-n-butyltin oxide with salicylaldoxime in a 3:2 ratio, shows two coordination modes, the 2.210 type along with the 2.111 mode. [22] A hydrogen-bond exists between the uncoordinated oximate oxygen atom and the phenolate oxygen atom of the salicylaldoxime showing the 2.111 mode.

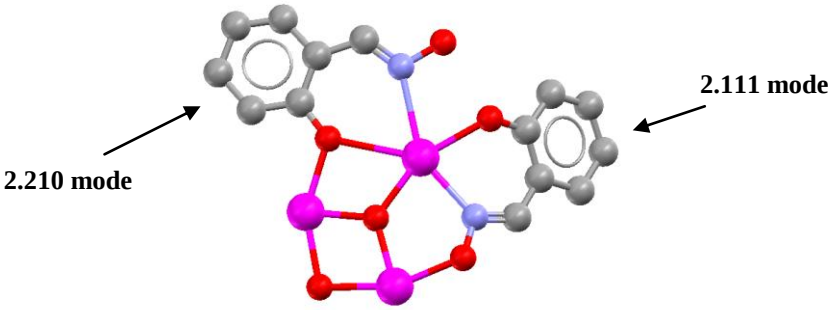

Figure 3-11 Examples of the 2.210 and 2.111 binding modes. Part of the crystal structure of [Sn_3Bu_6O(OH)(HsalH)(salH)]. Atoms are colour coded: Sn (purple). The hydrogen atoms and n-butyl groups have been omitted for clarity.[22]

In the 2.210 mode in Figure 3-11 the phenolate oxygen atoms bridge two metal centres. The M-O-M bonds lie close to the plane of the aromatic ring. This arises when the oxygen is sp^2-hybridised and the configuration has an unused p orbital

perpendicular to the benzene ring maintaining the conjugation, as shown in Figure 3-12. This occurs in almost all cases where the phenolate oxygen is bound to more than one metal. An exception is discussedSection for the 3.310 mode.

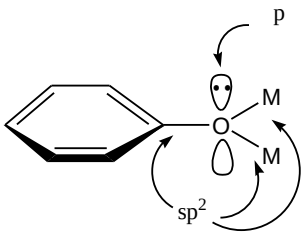

Figure 3-12 sp^2 Orbital configuration of Oxygen atomshowing filled p orbital

2.111 Binding Mode

The second most commonly found binding mode is the dinucleating 2.111 type with 61 occurrences in the CSD.[19] An example is shown in Figure 3-13.[23] The complex contains a tris salicylaldoximato Fe(III) unit with a *fac*-octahedral structure. Each of the oximate oxygen atoms bonds to a second Fe(III) ion, also in a *fac* arrangement, which is capped with a 1,4,7-trimethyl-1,4,7-triazacyclononane (tmtacn) ligand.

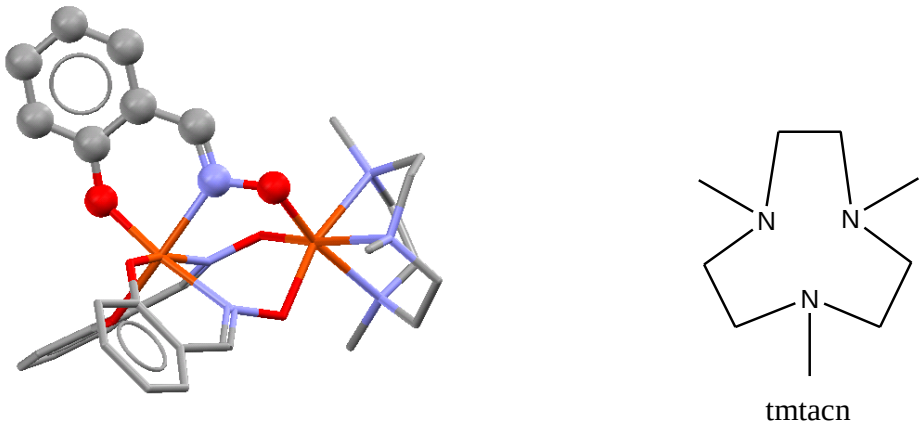

Figure 3-13 Example of the 2.111 binding mode. The crystal structure of $[Fe_2(salH)_3(tmtacn)]$. Atoms are colour coded: Fe (orange). The hydrogen atoms have been omitted for clarity.[23]

2.002 Binding Mode

A single example of the 2.002 type is found in the Sn(IV) trimer reported by Mercier *et. al.*.[24] This was crystallised under total darkness and moisture-free conditions. The

2.002 mode ligand is orientated approximately perpendicularly with respect to the Sn_3 plane (see Figure 3-14). One Sn(IV) atom has pentagonal bipyrimidal configuration and the other two have trigonal bipyrimadal geometries. The structure contains two intramolecular hydrogen bonds, one is found within the oxime-hydroxyl cavity and the other is between the oxime hydroxyl and a phenolate oxygen atom. The complex also contains two other salicylaldoxime units which bind using the 2.111 and 2.210 type.

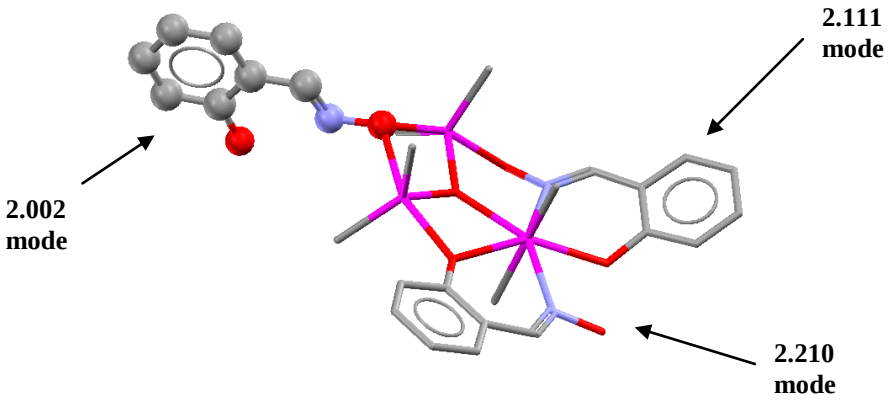

Figure 3-14 Examples of the 2.002, 2.111 and 2.210 modes. Crystal structure of $[Sn_3O(H_2salH)(HsalH)(salH)Me_6]$. Atoms are colour coded: Sn (purple). The hydrogen atoms have been omitted for clarity.[24]

3.310 Binding Mode

The 3.310 type trinucleating mode has only a single occurence in the CSD. Nakasbayshi *et. al*. synthesised the complex shown in Figure 3-15.[25] The Ba(II) ligating unit (LH_2 in Figure 3-15) is analogous to that shown earlier in Figure 3-8. This structure contains phenolate oxygen atoms which no longer bind in a planar fashion. The mixed metal cluster uses two different regions of the polydentate ligand for metal binding, a crown ether for a Ba(II) centre and two salicylaldoximes for a Ni(II) centre. Conversion of the oximato hydroxyl to an oxime ether reduces the ligating ability of the salicylaldoxime unit since the oximato oxygen atom is no longer involved in coordination. Ba(II) ions are 8 coordinate with an approximately hexagonal bipyramidal structure. The plane consists of 4 sites provided by crown ether oxygen atoms and two phenolate oxygen atoms. The remaining ligands are

monodentate $CF_3SO_3^-$ and H_2O groups. The octahedral Ni(II) lies within two co-planar *cis*-phenolate oxime cavities. The axial sites are defined by phenolate and water oxygen atoms. In this arrangement the phenolate adopts the μ_3 mode rather than the more common μ_2 mode and is involved in a Ni_2O_2 square at the centre of the complex. This again highlights the possibility for metal oxide surface binding.

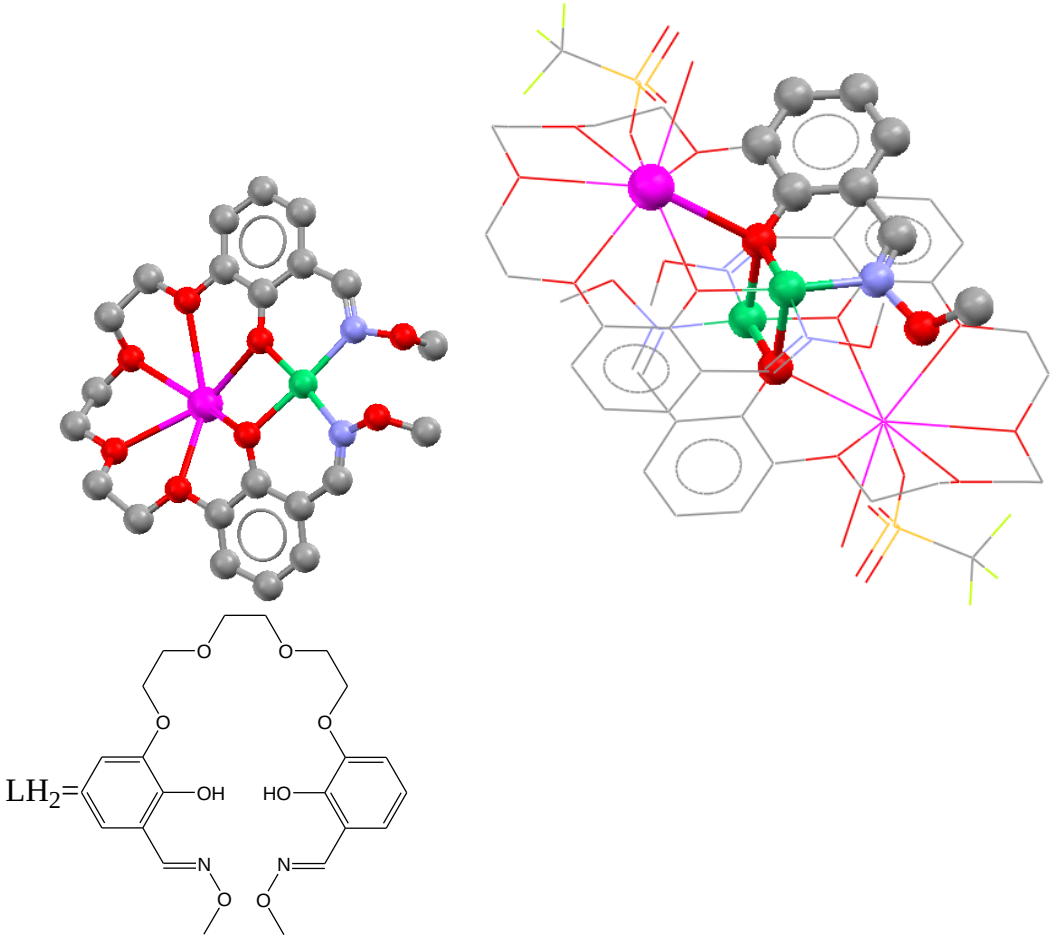

Figure 3-15 Example of the 3.310 binding mode. The crystal structure of $[Ba_2L_2Ni_2(SO_3CF_3)_2]$. Atoms are colour coded: Ba (purple), Ni (green). The hydrogen atoms and a terminal SO_3CF_3 group have been omitted for clarity [25]

3.211 Binding Mode

Less common trinucleating binding modes include the 3.211 type with a total of 8 hits. This is found in larger polynuclear complexes containing Zn, Ni, or mixed metal systems such as Cu + Fe, Ni + Cu and Ni + Fe.[19] An example of such a mixed metal metal cluster is shown in Figure 3-16.[23] The ligand (LH_4) in this system is composed

of two salicylaldoxime units linked together by a diimine bridge formed from an aldehyde substituent in the 3-position of the parent salicylaldehyde. A Ni(II) ion is bound in a *pseudo*-octahedral environment between the two nitrogen atoms of these additional imine groups and the two phenolate oxygen atoms with axial methanol molecules. The extended superstructure of the ligand leads to an unusual *cis*-arrangement of the two salox units about a square-pyramidal Cu(II) ion with an axially coordinated methanol molecule. The terminal oximato oxygen atoms bind *cis* to an octahedral Fe(III) ion which is capped with a *fac*-1,4,7-trimethyl-1,4,7-triazacyclononane ligand and a chloride ion completes the coodination sphere.

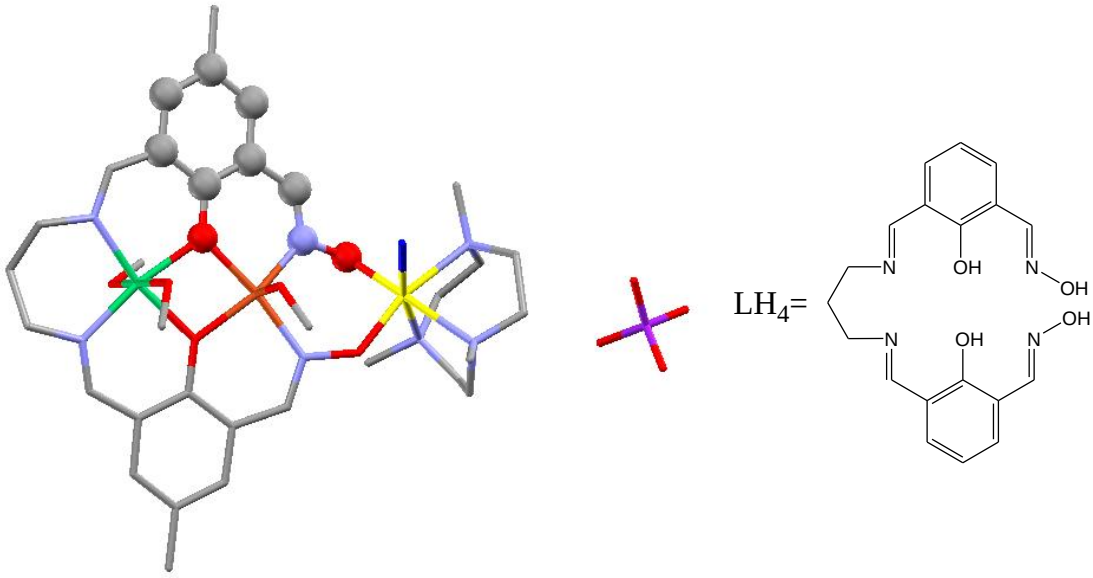

Figure 3-16 Example of the 3.211 binding mode. The crystal structure of $[NiCuFe(CH_3OH)_3L(tmtacn)Cl]SO_4$. Atoms are colour coded: Ni (green), Cu (orange), Fe (yellow), Cl (dark blue), S (purple). The hydrogen atoms have been omitted for clarity. [23]

3.112 Binding Mode

There are 31 reported structures containing the 3.112 mode.[19] An example is shown in Figure 3-17 in which salicylaldoximes are bound to a V_3O_3 trimer.[26] The complex has two doubly deprotonated salicylaldoximato units which present all three ligating atoms. A V(V) atom is bound in each of the phenolic oxime cavities and each oximato oxygen atom bridges two metal centres. The remaining sites on the V(V) are

coordinated by ethoxide and oxo ligands. This complex has a metal oxo core (M_3O_3) similar to that found in metal oxides and highlights the potential effectiveness of using salicylaldoximes for surface binding.

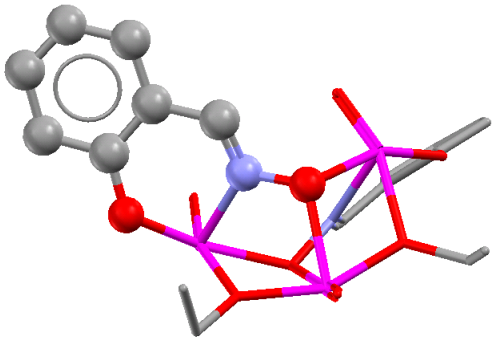

Figure 3-17 Example of the 3.112 binding mode. The crystal structure of $[V_3O_3(saHl)_2(OEt)_5]$. Atoms are colour coded: V (purple). The hydrogen atoms have been omitted for clarity.[26]

The oximato M-O-M unit it not coplanar with the oxime group and the oxygen atom is best described as sp^3 hybridised, similar to those found in metal alkoxides as shown in Figure 3-18. Although a delocalised system similar to that for phenols is possible because conjugation could occur with the oxime CH=N unit, this is not found to be the case.

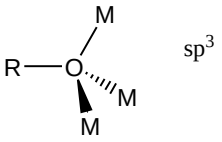

Figure 3-18 The sp^3 configuration of oxygen atoms in μ_3 alkoxide complexes

Salicylaldoxime ether binding

The survey of the CSD shows that chemisorption of salicylaldoxime onto metal oxide surfaces could involve a variety of polynucleating modes of attachment. The arrangement of the phenolic oxygen with the nitrogen atom suggests the most likely coordination of the ligand with the surface will use both these groups. In addition, further surface attachment by the loss of the oxime hydroxyl proton generates

structures which can form a larger number of ligand-surface bonds. In the context of the corrosion inhibitors, it is important to define how replacement of the oxime proton with a carbon atom influences coordination properties. The CSD was searched using the structure shown in Figure 3-19, restricting the oxime to be an ether. 18 cases were found where this ligand binds a metal. None use the oximato oxygen to form bonds to metal centres. This is important for rationalising the weakly binding characteristics of a salicylaldoxime ether in Section 3.9

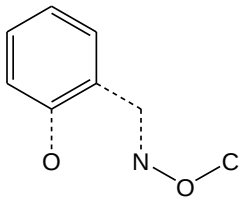

Figure 3-19 Structure of salicylaldoxime ether, dotted lines represent any bond

Salicylaldoximes have also found their way into the synthesis of single molecular magnets containing polynuclear transition metal clusters. Iit is worth noting that the variety of coordination modes which have been described above and the ability to bridge metal centres demonstrated by salicylaldoxime is important in the synthesis of this family of compounds.[27], [28]

3.4 Succinic anhydride

The succinic anhydride headgroup of PIBSA has been widely studied due to its availability. Structurally related compounds are shown in Figure 3-20.

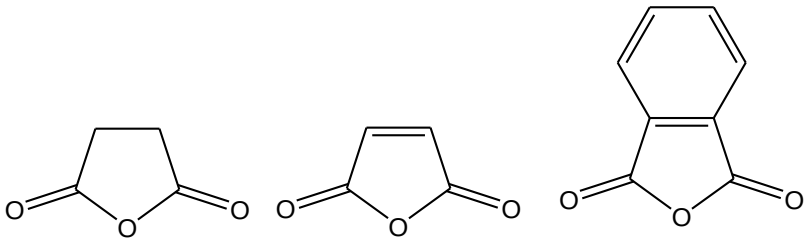

Figure 3-20 Structures of succinic, maleic and phthalic anhyrdides

Succinic anhydride derivatives are commonly used in polymer chemistry since it is reactive and effectively difunctional. Yoshimura *et. al.* have synthesised bio-degradable hydrogels reacting succinic anhydride with starch. [29] The gels are hydrophilic networks that can easily absorb large amounts of water and are made by esterification of the anhydride with the hydroxyl group on the starch molecules using 4-dimethylaminopyridine as a catalyst according to Scheme 3-4. The water absorbency of these polymers is dependant on the degree of crosslinking and hydrophilicity of the pendant group.

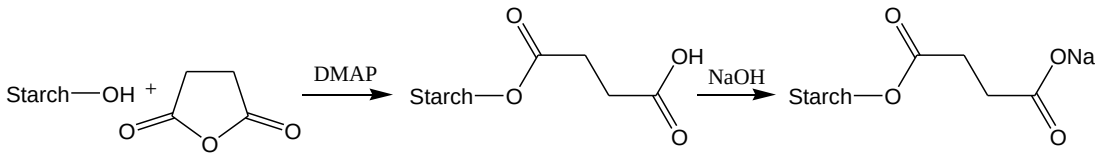

Scheme 3-4 Synthesis of succinic anhydride-starch hydrogel polymer

By appropriate design of monomers, hydrogel polymers can be sensitive to the H^+ ion concentration in surrounding media. Mandracchia *et. al* have found that cross linking of (polyhydroxyethylaspartamidemethylacrylatesuccinic anhydride) forms an anionic hydrogel that swells at high pH.[30] The pH dependence of swelling results from ionisation of the carboxylic acid groups which repel each other.

Alkenylsuccinic anhydrides have been used to alter the surface activity of gelatin derivatives. Introduction of hydrophobic chains into gelatin molecules or its hydrolyzates has been shown to improve surface activity, wetting ability, emulsifying power and foaming properties.[31] Reactions of the gelatin hydrolyzates and alkenylsuccinic anhydrides of various lengths are shown in Scheme 3-5. Longer alkyl chain lengths on the succinic anhydride molecules were found to be more effective than shorter chain lengths at enhancing stated surface properties.

Alkyl succinic anhydrides have found uses in many industries as surfactants,[32], [33]and as lubricant and engine additivies.[34] Succinimide derivatives of show good detergent-dispersant properties in lubricants. [35]

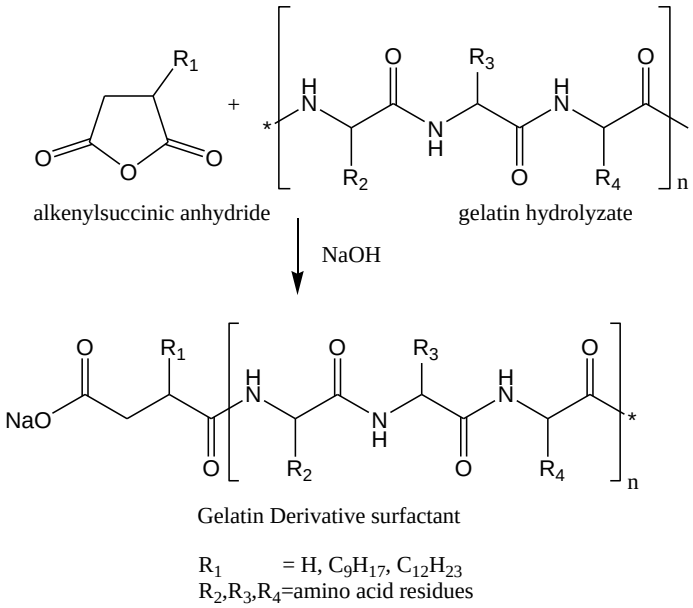

Scheme 3-5 Synthesis of succinic anhydride-gelatin hydrolyzates surfactants

3.5 Overview of the Chapter

In the rest of this chapter the observations that a blend of P50 and PIBSA is synergistic in corrosion inhibition is discussed.[1] We are particularly interested in whether the ring-opening reaction between P50 and PIBSA which generates potentially polynucleating ligands containing both the functionality of the phenolic oxime and that of the keto propionic acid component in Irgacor 419 will provide more interactions with a surface oxide and thus give stronger binding.

3.6 Ligands synthesis

Ligands studied in this chapter are listed in Table 3-1.

Ligand	Structural formula	Name
1	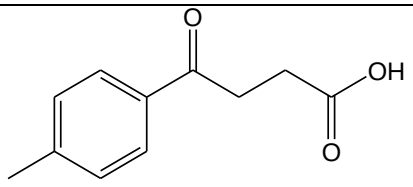	3-(4-methylbenzoyl)-propionic acid

3	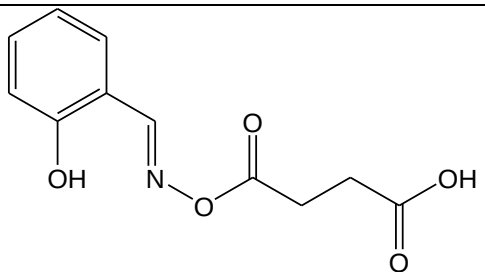	salicylaldehyde-*O*-(4-carboxypropanoyl) oxime
4	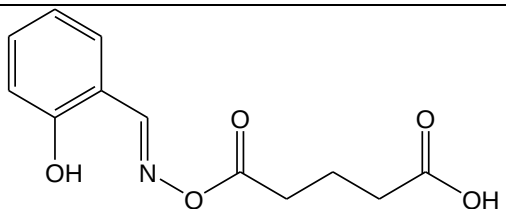	salicylaldehyde-*O*-(5-carboxybutanoyl) oxime
5	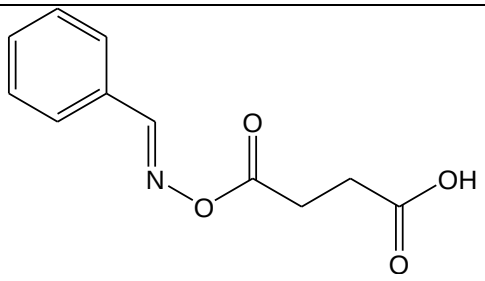	benzaldehyde-*O*-(4-carboxypropanoyl) oxime
6	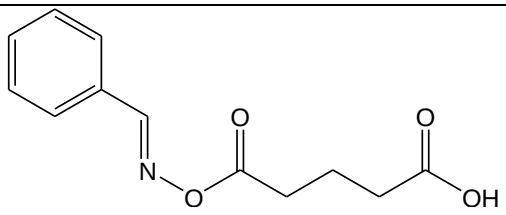	benzaldehyde-*O*-(5-carboxybutanoyl) oxime
7	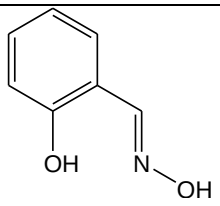	salicylaldoxime
8	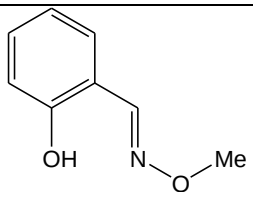	salicylaldehyde-*O*-methyl-oxime
9	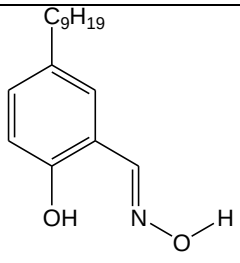	5-nonyl salicylaldoxime (P50 oxime)

Table 3-1 Structural formulae and names of ligands

1 was supplied by Ciba Speciality Chemicals. **9** is a commercial sample provided by Cytec Industries Ltd. **3**-**6** were prepared by reacting an oxime and a succinic or glutaric anhydride in the ring-opening reaction as shown in Scheme 3-6.

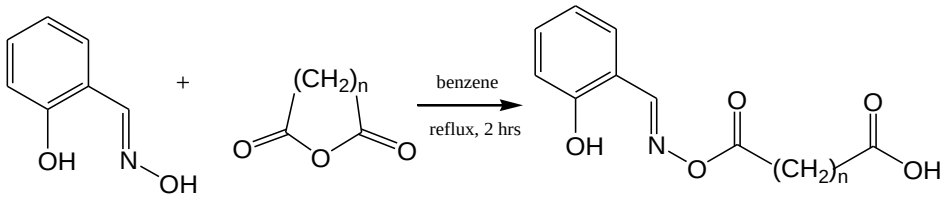

Scheme 3-6 Reaction of salicylaldoxime with succinnic or glutaric anhydride

The ring-opening reactions are likely to involve the attack of the oxime hydroxyl group at one of the carbonyl positions on the anhydride as shown in Scheme 3-7.

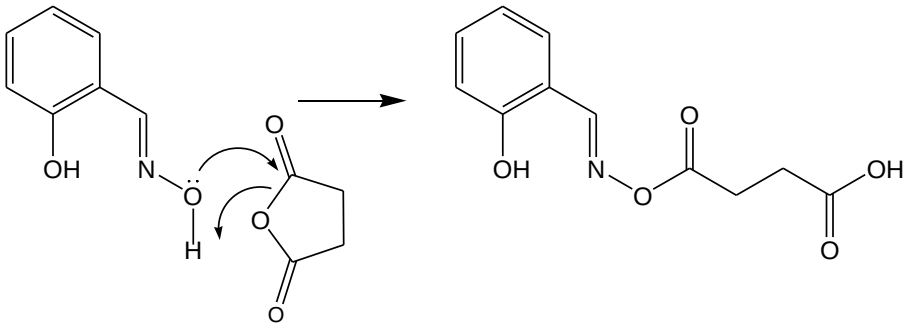

Scheme 3-7 Possible mechanism of reaction between oxime and anhydride

The synthesis of a ligand similar to **3** but with a multibranched nonyl subsitituent in the 5-position of the benzene ring and the keto acid functionality derived from succinic anhydride was attempted (see top of Scheme 3-8). The NMR and mass spectra gave evidence for the formation of the ligands, but purification by chromatography proved impossible. A similar reaction was carried out using (2-nonen-1-yl) succinic anhydride as a PIBSA analogue with salicylaldoxime (see bottom of Scheme 3-8). Again, however, this also proved impossible to purify by chromatography. Whilst such complex mixtures may be useful in industrial corrosion inhibition they cannot by used in quantitative binding studies (*vide infra*).

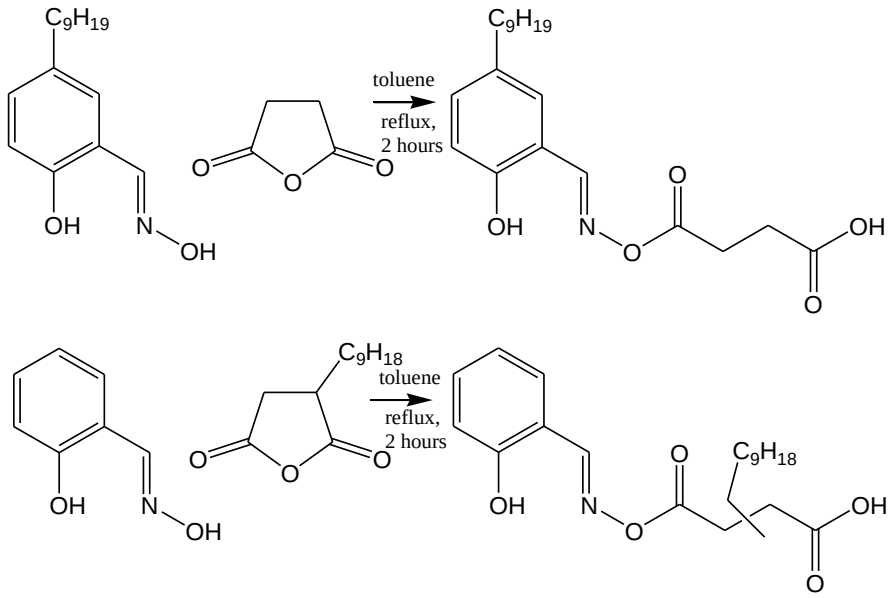

Scheme 3-8 Attempted syntheses of ligands containing large alkyl groups similar to those found in P50 oxime and PIBSA

8 was prepared by the oximation of salicylaldehyde using methoxylamine hydrochloride as shown in Scheme 3-9.

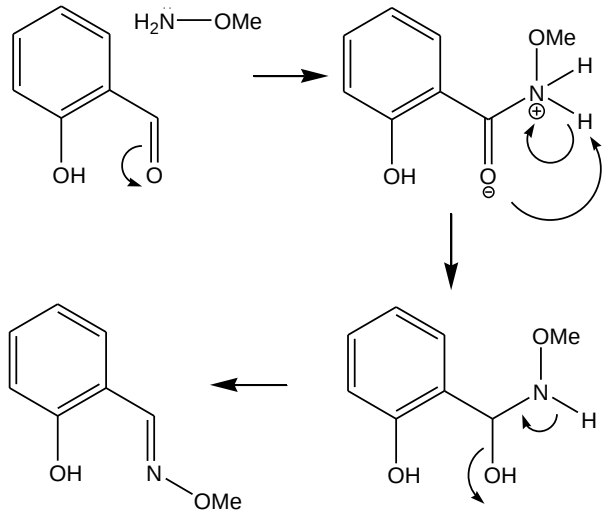

Scheme 3-9 Oximation of aldehyde using methoxylamine

3.7 Ligand characterisation

The oxime/keto acid ligands, **3**-**6**, have comparable NMR spectra. That of ligand **4** has been chosen as representative and Figure 3-21 shows the labelling scheme for the

protons used for assignment of ^{1}H NMR signals. The lowest field signal, at δ 9.63, is assigned to the phenolic proton. This appears as a broad singlet due to rapid exchange of protons between molecules. The next low field signal is due to the proton in the azomethine unit, f, occuring as a sharp singlet. No coupling can occur since it is attached to a quaternary carbon and a nitrogen with no protons attached. The aromatic protons at positions b-e, seen at δ 7.23-6.77, are not equivalent but overlap such that the coupling constants could not be measured on the instrument used. The multiplet around δ 2.4 is due to the methylene protons g and i. These are not equivalent, g are in a methylene linked to an oxime ester and i are close to the free carboxylic acid, and the overlap makes it impossible to define the coupling constants using a 250 MHz machine. The signal at δ 1.94 arises from the methylene protons h. These are shifted compared to protons at g/i since they are shielded from the carboxylate groups.

Table 3-2 compares the ^{13}C NMR signals for ligand **4** and salicylaldoxime using the numbering scheme shown in Scheme 3-10. The benzene ring signals have very similar shifts. In contrast, the azomethine carbon (7) shifts to higher field on reaction with the anhydride suggesting that ring opening to generate an ester involves the oxime hydroxyl group rather than the phenol.

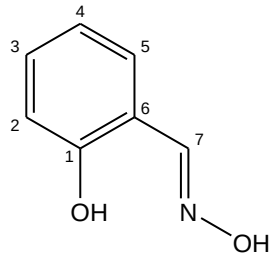

salicylaldoxime

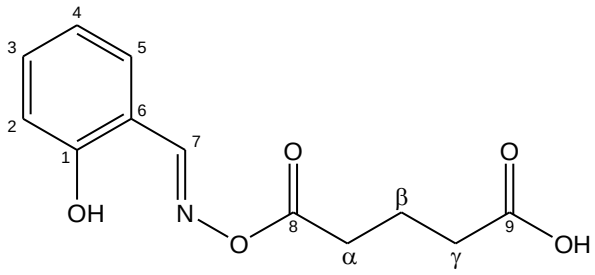

4

Scheme 3-10 Assignment of ^{13}C NMR signals for salicylaldoxime and 4

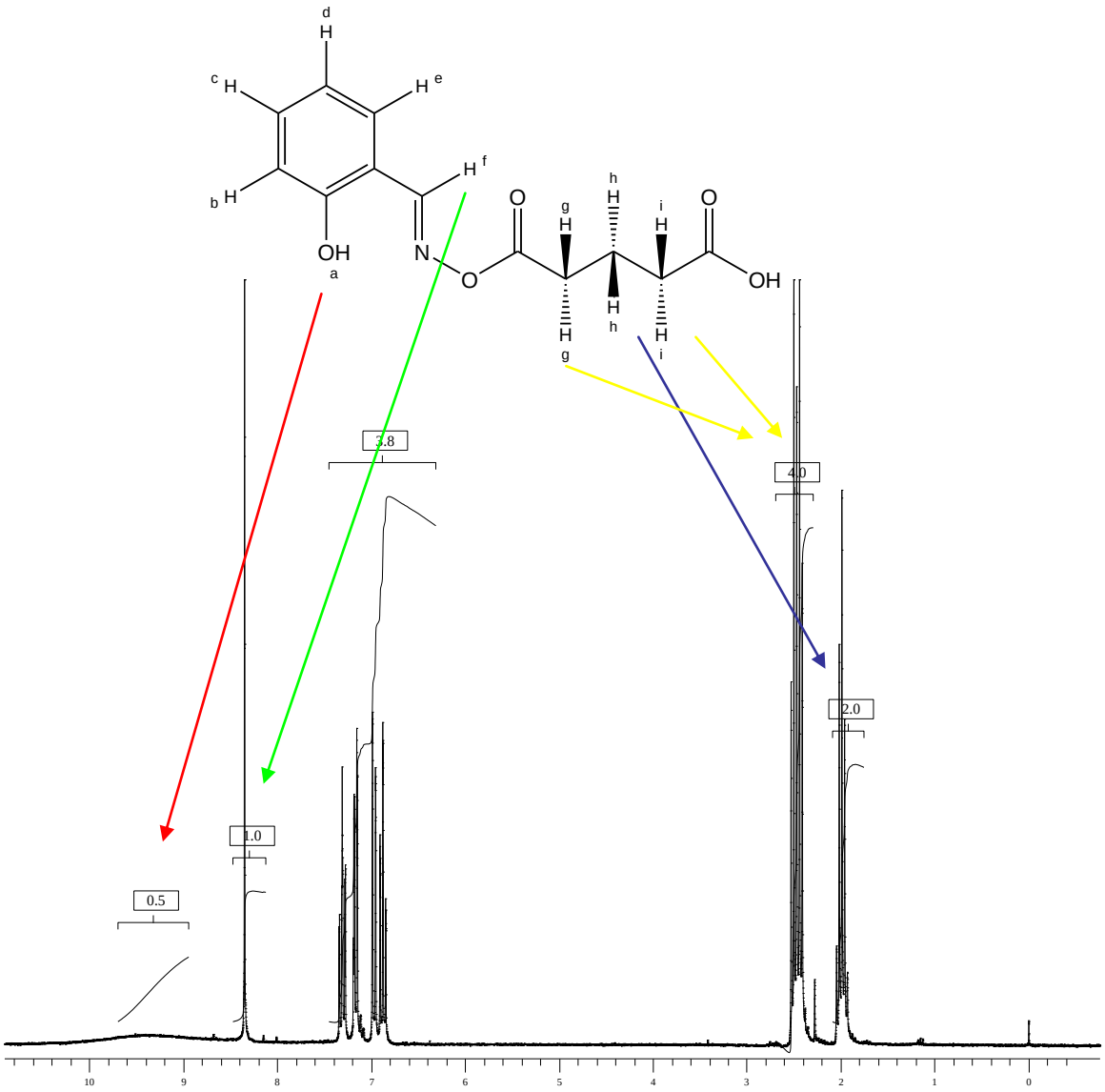

Figure 3-21 Assignment of ^{1}H NMR for 4 showing lettering scheme for ligand. The phenolic proton of 4 is shifted downfield from the value in salicylaldoxime. The ^{1}H signals in the anhydride are also changed upon ring opening as the protons are no longer chemically equivalent.

Characterisation of **5** is supported by the crystal structure shown in Figure 3-22. The asymmetric unit contain a single molecule in which the carboxylic acid group approaches that of a neighbouring molecule about an invesion centre to form the classic H-bonded dimer structure. The phenol group is intramolecularly hydrogen bonded to the oxime nitrogen with a OH…N distance of 1.83 Å. This is commonly seen in many phenolic oxime systems, see Section 3.1.

Atom number	Salicylaldoxime/ $\delta^{13}C$	**4** / $\delta^{13}C$
1	156.8	158.7
2	131.1	133.6
3	130.6	132.4
4	119.7	120.2
5	116.5	117.8
6	116.3	115.2
7	152.8	157.9
8		179.1
α		33.1
β		31.6
γ		19.9
9		167.4

Table 3-2 ^{13}C NMR δ values for salicylaldoxime and 4

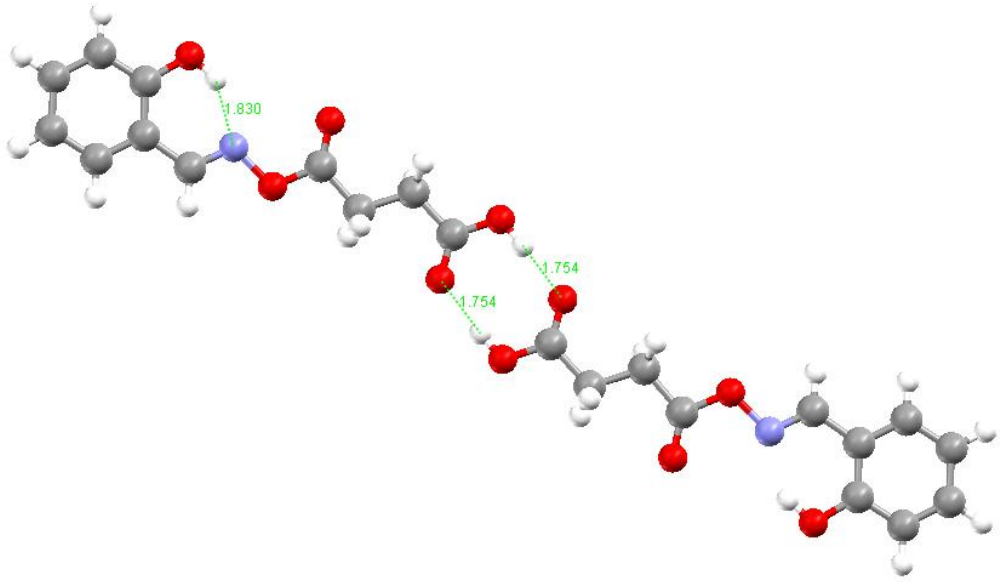

Figure 3-22 The dimeric structure of 3 in the solid state

The molecule is approximately planar with torsion angles of 170.83^{O} and 173.52^{O} about the central bonds of the oxime O, C8 , Cα, Cβ and C8 , Cα, Cβ, C9 units respectively. The planarity (and linearity) of these hydrogen-bonded dimers units results in the unusual packing arrangement shown in Figure 3-23.

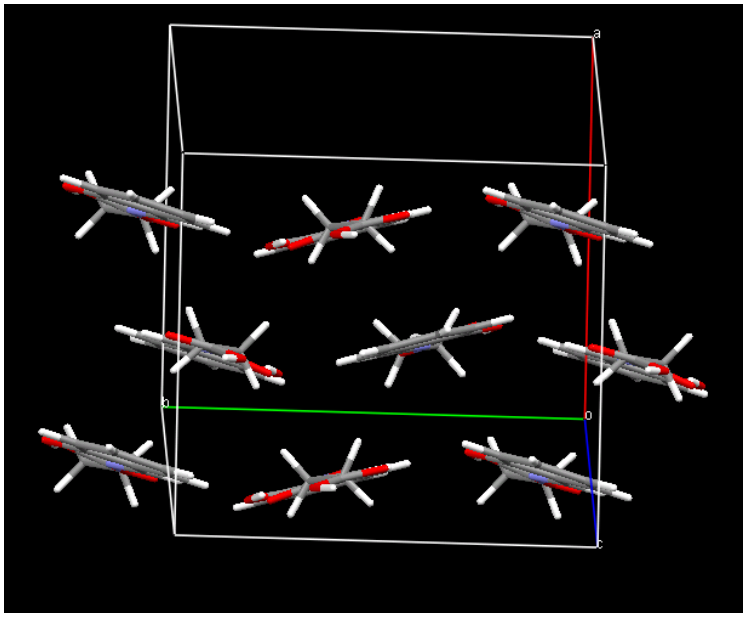

Figure 3-23 Crystal structure of 3 showing parallel stacking

3.8 Electronic absorption

3.8.1 Absorption Spectra

Ligands **3**-**6** have similar electronic spectra. **3** is chosen as an example and its spectrum is shown in Figure 3-24.

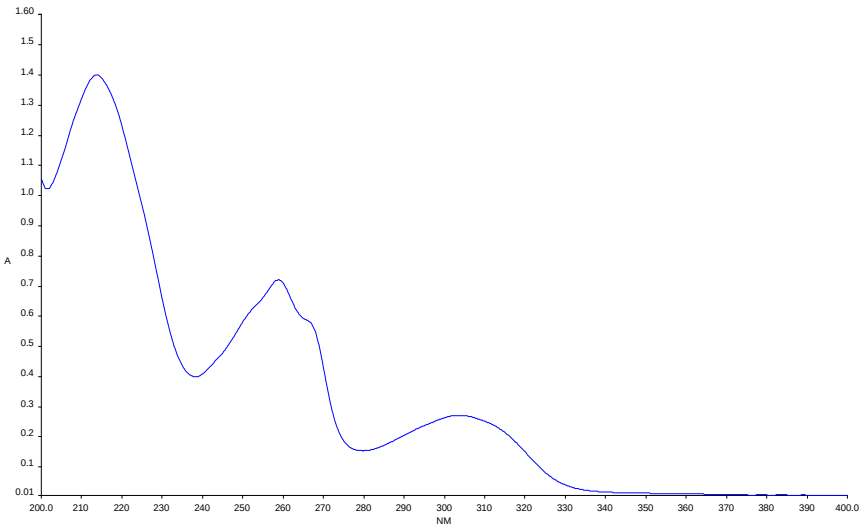

Figure 3-24 UV-Vis Spectrum for 3 in 95% MeOH/ H_2O

Table 3-3 lists the wavelengths of the major peaks for each ligand and assigns electronic transitions, these features are discussed in Chapter 2, Section 2.4.6.

Electronic transition	Absorbance maxima/ nm			
	3	**4**	**5**	**6**
Carboxylic acid n→π*	214	214	205	205
Aromatic π→π*	258	258	254	254
Oxime π→π*	303	303	330	330

Table 3-3 Absorbance maxima for electronic transitions for ligand 3-6 in 95% MeOH/ H_2O

An investigation was carried out to determine the solvent dependence on the position of the maxima for **3**. Table 3-4 shows the values obtained for solvent ratios from 93% MeOH/ H_2O to 100 % MeOH. No differences are observed except for the slight shift in pure methanol for the oxime π→π* transition from 304 to 312nm.

Solvent Ratio (MeOH: H_2O)	λ of Maxima/ nm	
93: 7	258	304
95:5	258	304
97: 3	258	304
100: 0	259	312

Table 3-4 Absorption maxima for 3 in different solvent ratios of MeOH: H_2O

3.8.2 Molar Absorption coefficients

The extinction coefficients for each λ_{max} were calculated using the Beer Lambert Law (Chapter 2, Section 2.4.7) and Table 3-5 lists the λ_{max} values and molar absorption coefficients for peaks used in determinations of the isotherms.

Ligand	λ_{max} / nm	Molar Absorption coefficient
1	252	15200
3	258	15200
4	258	15800
5	254	16100

6	254	17700
7	259	12500
8	259	14400
9	259	11600

Table 3-5 Extinction coefficients for ligands 1 and 2 to 9 in 95% MeOH/ H_20

3.9 Adsorption isotherm results

The new ligands, **3**-**6**, were studied to determine the effects on surface binding of systematic changes in structure. Ligating groups in addition to the keto-acid unit of **1** are present in **5** and **6** (an imino ester unit) and in **3** and **4** (a combination of an imino ether unit and a phenolic OH). The effect of increasing the chain length between the keto and carboxylic acid groups was studied by comparing **3** with **5** and **4** with **6**. The binding properties of the salicylaldoxime derivatives **7**-**8** were also investigated to see how these compared with analogues containing a keto acid unit. **5** and **6**, which have no phenolic substituent gave isotherms that display Langmuir behaviour, see Figure 3-25. The isotherm for **1** from Chapter 2 is included for comparison. The surface coverages, binding constants and required surface areas per molecule are stated in Table 3-6.

The surface coverages reached are approximately the same in all cases. This appears reasonable since all molecules are of an almost equivalent size and can bind using a similar mechanism. The binding constants for **1** and **5** are the same within experimental error based on fitting to the Langmuir form (Table 3-6) suggesting that they bind by a similar mechanism and that the 4-ketoacid unit is primarily responsible for surface attachment. Ligand **6** has a lower binding constant than **5** signifying that the 4-ketoacid unit is better than the 5-ketoacid unit for surface binding.

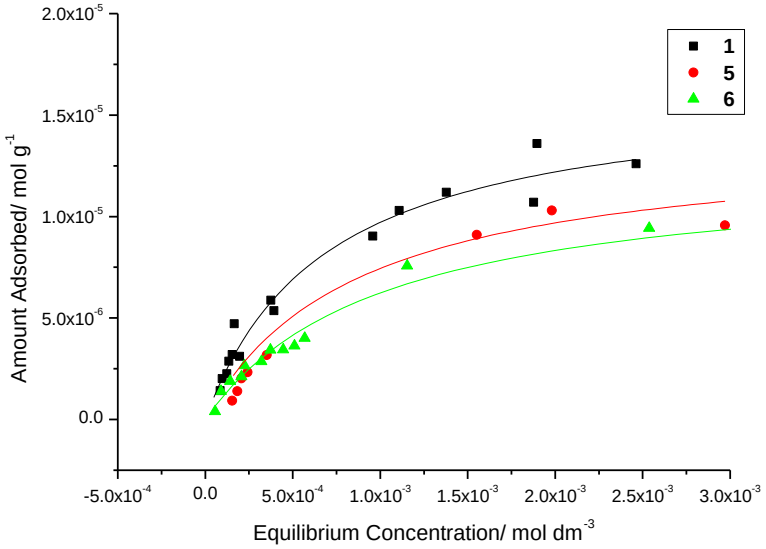

Figure 3-25 Uptake of 1, 5 and 6 on goethite from 95% MeOH/ H_2O

	1	5	6
Equilibrium binding constant(10^{-3}) / k	1.5(2)	1.5(5)	0.60(9)
Surface coverage(10^{5})/ mol g^{-1}	1.6(1)	1.4(2)	1.3(1)
Required surface area per molecule/ $Å^2$	238	275	294

Table 3-6 Adsorption isotherm data for ligand 1, 5 and 6 (errors in parentheses)

The isotherms of ligands **3** and **4** (Figure 3-26), have an approximately linear dependence of uptake on residual ligand concentration in solution with no evidence for surface saturation and do not fit classic Langmuir behaviour. Consequently curve fitting using a Langmuir model was unsuccessful.

Plotting the residual ligand concentration on a $\log_{10}$ scale allows isotherms to be compared in a different manner, Figure 3-27 compares results for **3** and **5**. Monolayer coverage can be assumed to occur at 1.4(2)x10^{-5} mol g^{-1} (Table 3-6) for **5** and is seen as the plateau in the plot. A similar saturation is not observed for **3** and coverage extends to greater than 2.5x10^{-5} mol g^{-1}. This value is approximately twice the maximum coverage shown by **5** and leads to a required surface area per molecule of

140 Å^2 for **3**, approximately half that calculated for **5**. This appears unreasonable if they show similar modes of surface binding because they have a similar size. This implies some other effect is occurring. A similar trend is observed when comparing **4** with **6**.

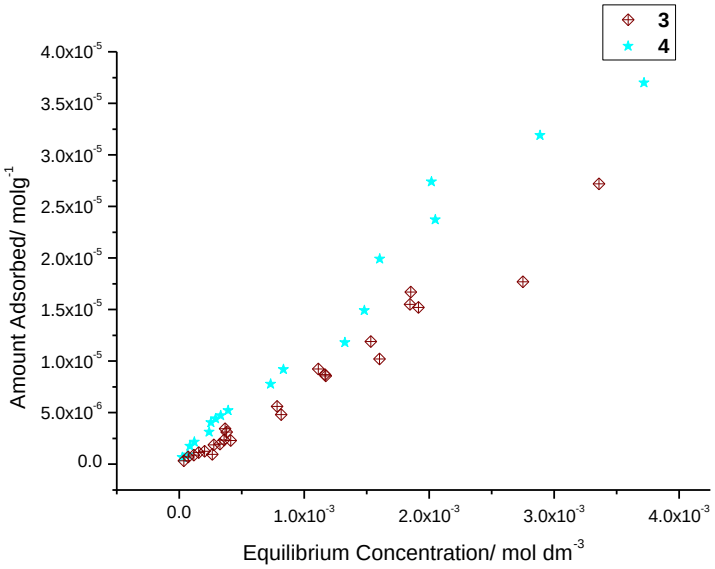

Figure 3-26 Uptake of 3 and 4 on goethite from 95% MeOH/ H_2O demonstrating lack of plateau region

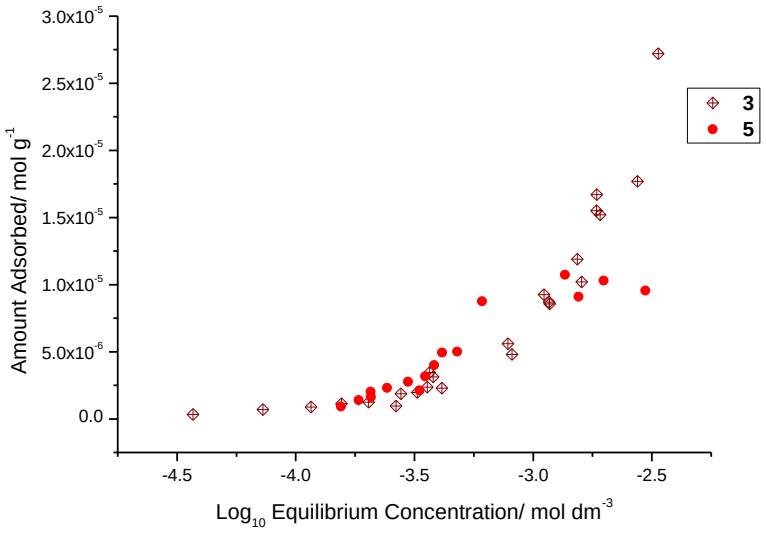

Figure 3-27 Uptake of 3 and 5 on goethite from 95% MeOH/ H_2O. Residual concentration plotted on a Log10 scale

At low residual ligand concentration in solution a multisite attachment binding mode may operate in which most of the ligating atoms (phenol O, imine N, keto O and carboxylate O atom), form primary or secondary bonding to the surface. When the ratio of surface binding sites to ligand is high there is enough space on the surface for several groups to bind. Two possible binding schemes for **3** are shown in Figure 3-28. The 4-ketocarboxylate component of **3** has sufficient flexibility to align ligating atoms with surface iron atoms and/or oxy/hydroxyl groups.

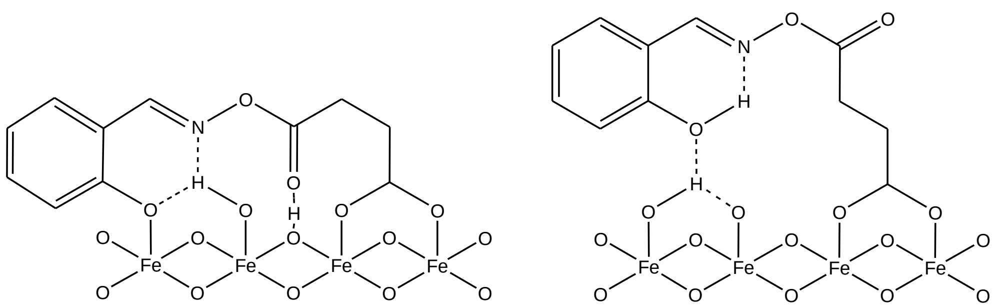

Figure 3-28 Two possible binding modes of 3 at low ligand concentration. The dashed lines represent hydrogen bonding

As the concentration of ligand increases it will be expected that competition for binding sites on the surface increases and if the isotherm behaves in a Langmuir fashion, it becomes progressively more difficult to find unused sites. Once a critical concentration is reached, it is possible that the mode of ligand binding changes. This second mode of binding to the oxide is most likely to involve the carboxylate group because **5** and **6**, which contain this but no phenolic unit, bind strongly to the iron(III) oxide surface, see Table 3-6. Also the phenol ligands **7** and **8** which contain no keto-carboxylate unit show much weaker binding (*vide infra*).

.

If the second mode of surface binding does not involve the phenolic oxime part of the molecule this could be orientated towards the solution phase as in Figure 3-29 and could be used for secondary bonding to other ligands. As the isotherms for **3** and **4** show the characteristics of multilayering, it is possible that this could be provided by pendant oxime:carboxylic acid or oxime:oxime associations.

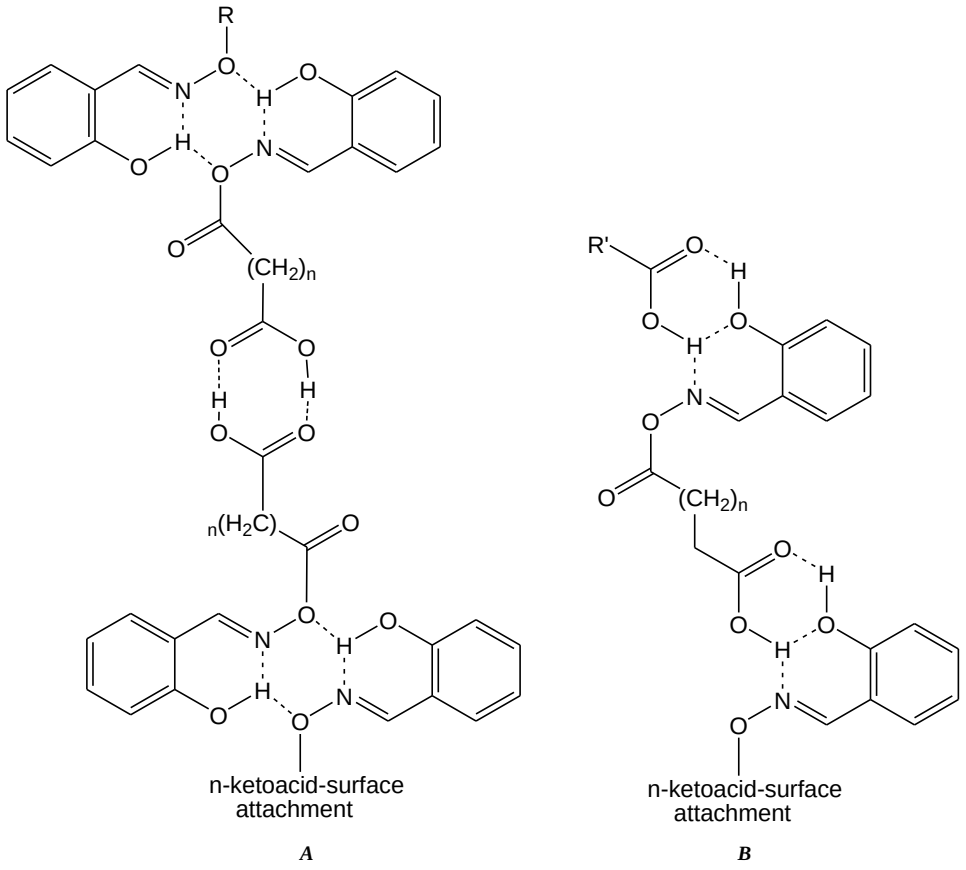

A ***B***

Figure 3-29 Possible binding mechanisms at high residual ligand concentration showing potential for multilayering effects using an oxime:oxime and carboxylic acid:carboxylic acid sequence (A), or an oxime:carboxylic acid sequence(B). Hydrogen bonding interactions are represented by dashed bonds. R and R' indicate continuation of the ligand structure

There are many possibilities for intermolecular hydrogen bonding to assemble multilayers on the oxide surfaces. Two are shown in Figure 3-29. Modelling is complicated by the flexibility of the 4-ketopropanoate and 5-ketobutanoate units, in the $(CH_2)_n$ component shown in Figure 3-29, and by the option of building up of layers involving either a sequence of alternating oxime:oxime and carboxylic

acid:carboxylic acid (A) or oxime:carboxylic acid (B) assemblies. Multilayering by the former is supported by the solid state structure of **3** which forms classic carboxylic acid dimer units (Figure 3-22); the oxime:oxime unit is similar to that found in a polymorph of salicylaldoxime (see Section 3.2).

Surface attachment using just the carboxylate functionality without coordination of the keto group has been considered but deemed unlikely. Such single site attachment could also explain why no maximum surface coverage is reached. The ligand would require less space on the surface and therefore more ligand could be adsorbed at monolayer coverage. However, a weaker binding strength would be expected since the ligand would be attached using only the acid and this is not found to be the case. It is also possible that intermolecular hydrogen bonding between ligands could contribute to the reasonably strong binding that is observed. Effects of intermolecular hydrogen bonding on the adsorption characteristics of a ligand are discussed in more detail in Chapter 4. The phenolic oxime unit would then be already used in intermolecular bonding at the monolayer level. Multilayering would then not be possible and thus a surface coverage maximum would be expected.

By determining the surface coverage at greater residual ligand concentrations it is possible that a maximum could be found. This has proved impossible experimentally for the reasons discussed in Chapter 2 which are inherent to the technique.

The implication from the discussion above is that the phenolic oxime ether unit does not compete effectively with the keto acid units in **3** and **4** for the goethite surface. The uptakes of **7**-**8**, which have no keto-acid functionality, are shown in Figure 3-30.

The isotherm of **8** is very poorly defined and confirms that the phenolic oxime ether shows no detectable uptake at a goethite surface, Figure 3-30. This was unsurprising since the CSD search discussed in Section 3.3 resulted in very few hits using salicylaldoxime ethers, of which none used the oximic oxygen atom in coordination. Unlike **3** and **4**, **7** and **9** have the oximic hydroxyl group present in addition to the

phenolic hydroxyl group. Consequently, in theory, they could form polynuclear complexes of the types found in the literature, and reasonably strong surface binding is possible.

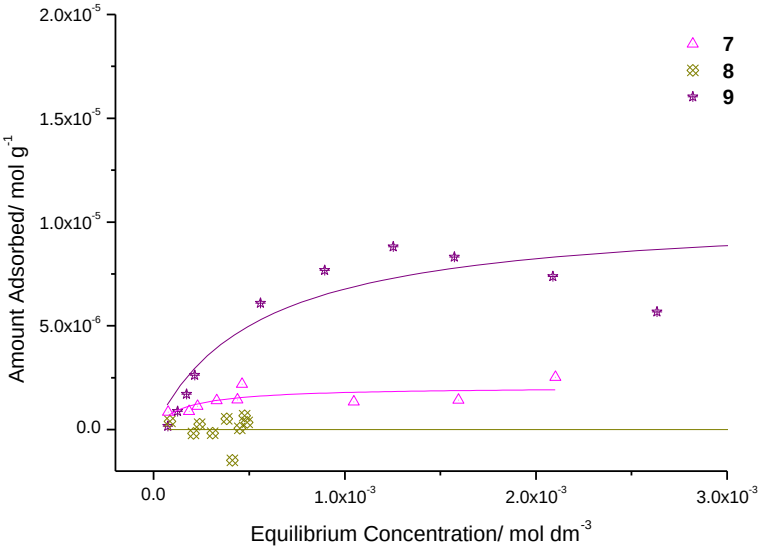

Figure 3-30 Adsorption isotherms for Ligands 7, 9 and 8

	9
Equilibrium binding constant(10^{-3})/ k	1.4(4)
Surface coverage(10^{5})/ mol g^{-1}	1.2(1)
Required surface area per molecule/ $Å^2$	311

Table 3-7 Adsorption isotherm data for 9 (errors in parentheses)

The shape of the isotherm in Figure 3-30 shows that **9** displays a significant increase in binding compared to **7**. This was surprising since no more surface coordinating groups are present in the former. This result is attributed to the hydrophobic effect displayed by the bulky alkyl chain. A correlation between binding strength and length of alkyl chain is also presented in Chapter four.

3.10 Conclusions

This chapter has investigated the chemistry described in the ICI patent which claims that a blend of P50 oxime and PIBSA is synergistic by the formation of a new compound. The hypothesis that a larger number of surface ligating groups results in greater binding strength by an increase in multisite attachment was found not to be the case.

Ligands containing 4-ketoacid units were found to be more effective than analogous 5-ketoacid units. The ketoacid ligands, **5** and **6**, which do not contain phenolic hydroxyl groups display classic Langmuir behaviour forming well defined monolayers; those that do contain phenolic hydroxyls, **3** and **4**, display non-Langmuir behaviour and do not approach a maximum surface coverage. The phenolic oxime unit does not compete with the ketoacid functionality for surface binding sites and are involved in forming multilayers on the metal oxide.

The multilayering effects shown by the phenolic ligands **3** and **4** can be attributed to hydrogen bonding. These intermolecular forces could occur between the uncoordinated phenolic oximes and either other phenolic oxime units or carboxylic acid units in the neighbouring layer.

In the case of the ICI patented molecule, the reaction product of P50 oxime with PIBSA contains a strongly binding 4-ketoacid group and the functionality required for multilayering, the phenolic oxime unit. In addition, pendant alkyl chains are present which could provide a facility for good adhesion to an acrylate or alkyd polymer coating by incorporation of the pendant nonyl or polyisobutylene groups into the resin structure.

The determined binding characteristics of some simple salicylaldoxime derivates suggest that ligands which contain oximic ethers displays virtually no affinity for goethite, since the oximic oxygen atom is not free for coordination . The weak surface binding of **7** was a bit surprising as the literature shows a wealth of

polynucleating coordination chemistry and P50 oxime (**9**) is known to be a good corrosion inhibitor for mild steel and shows strong binding in adsorption isotherm studies. The hydrophobic effect is therefore probably important for creating stable surface bound complexes.

3.11 Experimental

All reagents were used as obtained from Aldrich, Acros without further purification. ^{1}H and ^{13}C NMR were recordered on a DPX Bruker 360 MHz spectrometer. Fast atom bombardment (FAB) mass spectra were recorded on a Kratos MS50TC spectrometer. Infra-red (IR) spectra were obtained on a JABCO FTIR-460 spectrometer as potassium bromide discs. Electronic absorption measurements were made on a Unicam UV-2 Spectrophotometer.

3-(4-methylbenzoyl)-propionic acid (1)

Was obtained from Ciba Speciality Chemicals and used as received.

salicylaldehyde-O-(4-carboxypropanoyl) oxime (3)

A solution of salicylaldoxime (2.37 g, 0.02 mol) in toluene (5 ml) was added dropwise whilst stirring to a hot solution of succinic anhydride (1.97 g, 0.02 mol) in toluene (25 ml). The solution was stirred under reflux for 2 hours. The solid formed on cooling was filtered and recrystallised from a hot THF/ hexane mixture to give a white crystalline material. (Found C, 55.56; H, 4.44, N, 5.83 $C_{11}H_{13}NO_5$ Requires C, 55.23; H 5.48, N, 5.86.) λ_{max} (95:5 MeOH/ H_2O)/ nm 303, (ε/ dm^3 mol^{-1} cm^{-1} 3500) 258, (15, 200), 214, (19, 000), ^{1}H NMR (d-acetone): δ 10.11 (s, 1H, O*H*), 8.83 (s, 1H, C*H*=N), 7.64-7.46 (m, 2H, Ar-*H*), 7.09 (m, 2H, J 3Hz, Ar-*H*), 2.81 (m, 4H, $CH_2CH_2CO_2H$). ^{13}C: Carbons are identified according to numbering scheme given on Scheme 3-9 in Section 3.7. δ 171.7 (C8), 168.2 (C9), 157.2 (C1) , 156.2 (C7), 132.3 (C2), 130.8 (C3), 119.0 (C4), 115.9 (C5) , 114.6 (C6), 27.1 (Cα), 26.2 (Cβ). FAB-MS m/z 238 (100%, M^+).

salicylaldehyde-O-(5-carboxybutanoyl) oxime (4)

A solution of 2-hydroxybenzaldehyde oxime (2.36 g, 0.02 mol) in hot benzene (20 ml) was added dropwise to a hot solution of glutaric anhydride (2.28 g, 0.02 mol) in benzene (20 ml). The solution was stirred under reflux for 2 hours. The yellow precipitate formed on cooling was collected and recrystallised from hot benzene to give a very pale yellow powder (3.07 g, 82 %). λ_{max} (95:5 MeOH/ H_2O)/ nm 313 (ε/ dm^3 mol^{-1} cm^{-1} 5, 200), 258, (15, 800). IR (cm^{-1}, KBr disc): υ 3050, 2974 (CH), 1772, 1713 (C=O) 1196 CO. ^{1}H NMR ($CDCl_3$): δ 9.63 (bs, 1H, OH), 8.27 (s, 1H, C*H*=N), 7.23-6.77 (m, 4H, Ar-H), 2.40 (m, 4H, OC(O)CH_2CH_2CH_2COOH,) 1.94 (m, 2H, OC(O)CH_2CH_2CH_2COOH). ^{13}C: δ 179.1 (C8), 167.4 (C9), 158.7 (C1), 157.9 (C7), 133.6 (C2), 128.7 (C3), 120.2 (C4), 117.8 (C5), 115.2 (C6) , 33.1 (Cα), 31.6 (Cγ), 19.9(Cβ). FAB-MS m/z 252 (83.7%, M^+).

benzaldehyde-O-(4-carboxypropanoyl) oxime (5)

A solution of benzaldehyde oxime (2.43 g, 0.02 mol) in hot benzene (20 ml) was added dropwise whilst stirring to a hot solution of succinic anhydride (2.01 g, 0.02 mol) in benzene (20 ml). The solution was stirred under reflux for 2 hours. The product obtained was recrystallised from hot benzene to yield a white powder (3.69 g, 83%). (Found C, 59.60; H, 4.98; N, 6.21. $C_{11}H_{13}NO_4$ Requires C, 59.19; H 5.87; N, 6.27) λ_{max} (95:5 MeOH/ H_2O)/ nm 313, (ε/ dm^3 mol^{-1} cm^{-1} 5, 200), 254, (16, 100). IR (cm^{-1}, KBr Disc): υ 3276 (OH), 2938 (CH), 1757 (C=O), 1138 (CO). ^{1}H NMR (d-DMSO): δ 8.71 (s, 1H, C*H*=N), 7.80-7.74 (d,d, 2H, J 2.0, 8 Hz, Ar-H) 7.54-7.50 (m, 3H, Ar-H), 2.80-2.54, (m, 4H, CH_2C$H_2$$CO_2$H).^{13}C: δ 173.2 (C8), 170.2 (C9), 156.7 (C7), 131.4 (C3), 130.3 (C6), 129.2 (C1), (C5), 128.1 (C2), (C4), 28.6 (Cα), 27.5 (Cβ). FAB-MS m/z 222 (89.2%, M^+).

benzaldehyde-O-(5-carboxybutanoyl) oxime (6)

A solution of benzaldehyde oxime (3.05 g, 0.02 mol) in hot benzene (10 ml) was added dropwise whilst stirring to a hot solution of glutaric anhydride (2.24 g, 0.02 mol) in benzene (25 ml). The solution was stirred under reflux for 2 hours. The

product obtained was recrystallised from hot benzene to give a white solid (3.01 g, 65 %). λ_{max} (95:5 MeOH/ H_2O)/ nm 254 (ε/ dm^3 mol^{-1} cm^{-1} 17, 700). IR (KBr disc): υ 3495 (OH), 2946 (CH), 1769 (C=O), 1127 (C-O). ^{1}H NMR ($CDCl_3$): δ 8.27 (s, 1H, C*H*=N), 7.65 (d, 2H, Ar-H), 7.45-7.30 (m, 3H, Ar-H), 2.60-2.40 (m, 4H, C*H*$_2$CH$_2$C*H*$_2$CO$_2$H), 2.05-1.95 (m, 2H, CH$_2$C*H*$_2$CH$_2$CO$_2$H). ^{13}C: δ 173.5 (C8), 170.0 (C9), 156.8 (C7), 131.7 (C3), 130.4 (C6), 129.5 (C1), (C5), 127.9 (C2), (C4), 33.0 (Cα), 31.3 (Cγ), 20.1 (Cβ). FAB-MS m/z 236 (92.2%, M^+).

Salicylaldoxime (7)

Was used as received from Aldrich

Salicylaldehyde-O-methyl-oxime(8)

Methoxyl amine hydrocholoride (2.44 g, 2.93 mmol) was dissolved in hot ethanol (150 ml) and stirred with potassium hydroxide (1.641 g, 2.93 mmol) for 2 minutes. This was then cooled over ice and filtered directly into a flask containing salicylaldehyde (3.58g, 2.93 mmol) and refluxed for two hours. The solvent was then removed under reduced pressure to give a pink oil. Water (100 ml) and chloroform (150 ml) were then added. The layers were separated and the aqueous layer was extracted with further chloroform (2 * 100 ml). The organic extracts were combined, dried over magnesium sulphate and the solvent removed. This was purified by column chromatography using 10% Ethyl acetate in hexane to yield a pale yellow oil (Rf=0.56) (3.0g, 68%). λ_{max} (95:5 MeOH/ H_2O)/ nm 259 (ε/ dm^3 mol^{-1} cm^{-1} 14, 400) ^{1}H NMR ($CDCl_3$): δ 9.87 (s, 1H, O*H*), 8.15 (s, 1H, C*H*=N), 7.30 (d,d, 1H, J 7, 2 Hz, Ar-H), 7.26 (d, 1H, J 7 Hz, Ar-H), 7.00 (d, 1H, J 7 Hz, Ar-H) 6.90 (d,d, 1H, J 7,2, Ar-H) 3.98 (s, 3H, C*H*$_3$). ^{13}C: δ 157.3 (C1), 151.3 (C7), 131.0 (C2), 130.6 (C3), 119.4 (C5), 116.6 (C5), 116.1 (C4), 62.4 (CH_3). FAB-MS m/z 151 (7.3 %, M^+).

5-Nonyl salicylaldoxime(9)

Was used as received from Avecia

3.12 References

1 B. Tury, in 'Anticorrosion coatings containing poly(oxyalkylene) glycol derivatives and long-chain carboxylic acid anhydrides', Application: EP EP, 1991.

2 B. Tury, in 'Lubricating oil and grease compositions and use', Application: WO WO, 1994.

3 P. A. Tasker, P. G. Plieger, and L. C. West, *Comprehensive Coordination Chemistry II*, 2004, **9**, 759.

4 G. A. Kordosky, *International Solvent Extraction Conference, Cape Town, South Africa, Mar. 17-21, 2002*, 2002, 853.

5 J. A. Milner and R. M. Turner, in 'Ore treatment process', Application: GB GB, 1979.

6 R. M. Milburn, *Journal of the American Chemical Society*, 1955, **77**, 2064.

7 S. Nsikabaka, W. Harb, and M. F. Ruiz-Lopez, *Theochem*, 2006, **764**, 161.

8 S. Rosenberg, S. M. Silver, J. M. Sayer, and W. P. Jencks, *Journal of the American Chemical Society*, 1974, **96**, 7986.

9 P. Chaudhuri, *Coordination Chemistry Reviews*, 2003, **243**, 143.

10 R. G. Pearson, *Journal of the American Chemical Society*, 1963, **85**, 3533.

11 E. Laengle and N. Hackerman, *Journal of the Electrochemical Society*, 1971, **118**, 1273.

12 C. E. Pfluger and R. L. Harlow, *Acta Crystallographica, Section B: Structural Crystallography and Crystal Chemistry*, 1973, **29**, 2608.

13 P. A. Wood, R. S. Forgan, S. Parsons, E. Pidcock, and P. A. Tasker, *Acta Crystallographica, Section E: Structure Reports Online*, 2006, **E62**, o3944.

14 M. E. Keeney, K. Osseo-Asare, and K. A. Woode, *Coordination Chemistry Reviews*, 1984, **59**, 141.

15 A. G. Smith, P. A. Tasker, and D. J. White, *Coordination Chemistry Reviews*, 2003, **241**, 61.

16 J. C. C. I.J.Bruno, P.R.Edgington,M.Kessler,C.F.Macrae,P.McCabe,J.Pearson, R.Taylor, *Acta Cryst.*, 2002, **B58**, 389.

17 S. G. Harris, 'Crystallographic and modelling studies of organic ligands on metal surfaces', Edinburgh University, Edinburgh, 1999.

18 F. C. J. M. v. Veggel, S.Harkema, M.Bos, W.Verboom, G.K.Woolthuis, and D.N.Reinhoudt, *J.Org.Chem.*, 1989, **54**, 2351.

19 F. H. Allen, *Acta. Crystallogr.*, 2002, **B58**, 380.

20 S. F. Kaplan, V. Y. Kukushkin, S. Shova, K. Suwinska, G. Wagner, and A. J. L. Pombeiro, *European Journal of Inorganic Chemistry*, 2001, 1031.

21 V. V. Sharutin, O. V. Molokova, O. K. Sharutina, A. V. Gerasimenko, and M. A. Pushilin, *Russian Journal of General Chemistry*, 2004, **74**, 1485.

22 F.Kayser, M.Biesemans, M.Boualam, E.R.T.Tiekink, A. E. Khloufi, J.Meunier-Piret, A.Bouhdid, K.Jurkschat, M.Gielen, and R.Willem, *Organometallics*, 1994, **13**, 1098.

[23] C. N. Verani, E. Rentschler, T. Weyhermuller, E. Bill, and P. Chaudhuri, *Dalton*, 2000, 251.
[24] F.A.G.Mercier, A.Meddour, M.Gielen, M.Biesemans, R.Willem, and E.R.T.Tiekink, *Organometallics*, 1998, **17**, 5933.
[25] T. Nakabayashi, T. Ishida, and T. Nogami, *Inorganic Chemistry Communications*, 2004, **7**, 1221.
[26] V.Zerbib, F.Robert, and P.Gouzerh, *Chem.Commun.*, 1994, 2179.
[27] C. P. Raptopoulou, A. K. Boudalis, Y. Sanakis, V. Psycharis, J. M. Clemente-Juan, M. Fardis, G. Diamantopoulos, and G. Papavassiliou, *Inorganic Chemistry*, 2006, **45**, 2317.
[28] I. A. Gass, C. J. Milios, A. G. Whittaker, F. P. A. Fabiani, S. Parsons, M. Murrie, S. P. Perlepes, and E. K. Brechin, *Inorganic Chemistry*, 2006, **45**, 5281.
[29] T. Yoshimura, R. Yoshimura, C. Seki, and R. Fujioka, *Carbohydrate Polymers*, 2006, **64**, 345.
[30] D. Mandracchia, G. Pitarresi, S. Palumbo Fabio, B. Carlisi, and G. Giammona, *Biomacromolecules FIELD Full Journal Title:Biomacromolecules*, 2004, **5**, 1973.
[31] O. Toledano and S. Magdassi, *Journal of Colloid and Interface Science*, 1997, **193**, 172.
[32] K. Kubo, C. Itoh, S. Ohhashi, T. Yasukohchi, Y. Ohkawa, H. Kikuchi, N. Suzuki, M. Kurosawa, and H. Yamauchi, in 'Phospholipid derivatives used for surfactants, solubilizers, dispersants in cosmetics and lipid membranes and their preparation', Application: WO
WO, 2004.
[33] V. Nardello, N. Chailloux, G. Joly, and J.-M. Aubry, *Colloids and Surfaces, A: Physicochemical and Engineering Aspects*, 2006, **288**, 86.
[34] R. Hartley, in 'Lubricating oil additive concentrates', Application: EP
EP, 2006.
[35] J. Hancsok, L. Bartha, J. Baladincz, J. Auer, and Z. Kocsis, *Petroleum and Coal*, 1997, **39**, 21.

Contents

4 Interligand bonding

This chapter has two main aims, to assess the feasibility of using ICP-OES as an analytical tool to determine ligand concentration in adsorption isotherm experiments of the types described in Chapter 2, and to explore the benefits of adding functionality to simple carboxylic acids to allow intermolecular bonding and thus enhance the stability of complex formation at metal (oxide) surfaces.

Ligands designed to form intermolecular bonds extends the concept of "multisite attachment" [1] whereby the free energy of the complex formation at the surface is favoured by a combination of:

- metal-ligand primary bonds (inner sphere of metal complex),
- surface-ligand secondary bonds (equivalent to favourable interactions between atoms in outer coordination sphere), and
- ligand-ligand secondary bonding (equivalent again to favourable interactions in outer coordination sphere)

As part of this, it is necessary to consider how the entropy of complex formation changes as a result of multisite attachment, e.g. by restructure of movement of the ligand "tails" and changes in level of solvation of the ligands and the surface.

The aim of generating a very favourable assembly can be likened to supramolecular chemistry where the incorporation of a significant number of non-covalent intermolecular bonds can make a major contribution to the thermodynamic stability of an assembly.

4.1 Introduction

Interactions between molecules govern many of the physical and chemical properties of a substance such as melting/boiling points, solubility, viscosity and surface tension. From van der Waals forces to hydrogen bonding, the strength, directionality

and types of interaction are all dependent upon the size of the molecule, the atoms involved and the charge distributions that can result.

Supramolecular chemists have at their disposal a wide range of interactions including dipole-dipole, donor-acceptor and hydrogen bonding interactions, or metal ion coordination. However, the types of functionality that can be used are limited as benign molecules are required. Although capable of providing useful donor-acceptor functionality it is preferable not to use heteroaromatic rings due to potential toxicity.

The sections below consider some of the forms of non-covalent bonding relevant to the ligands discussed in this chapter.

4.2 van der Waals Interactions

van der Waals, or London forces occur in all molecular systems but due to their weak nature they are usually only observed between non-polar molecules as they are usually masked by polar effects in polar molecules. These forces arise when the electron density surrounding nuclei moves around, creating temporary dipoles that can generate attractive forces between neighbouring atoms or molecules. They are very weak, typically 1 kJ mol^{-1}, and are always attractive in nature.

Although individually weak, combining a number of van der Waal forces allows geckos to stick to a wide variety of surfaces.[2] Geckos feet are covered with approximately 500,000 tiny hairs called 'setae'. Each setae is covered with between 100 and 1000 spatulae. The adhesive interactions between the spatulae and the surface are caused by van der Waals and allow the gecko to stick. Recent research is attempting to use this concept to develop new synthetic material.[3]

Van der Waal forces are used to rationalise the properties displayed by hydrocarbons. The strength of the interactions depends on a number of factors such as the number of electrons, shape and distance between molecules. A molecule with a greater number of electrons is more polarisable than a smaller one with fewer electrons and

gives stronger van der Waal forces *vide infra* boiling point methane(-161.6^{0}C), pentane(36.1^{0}C). The same trend is also observed when comparing straight chained molecules to those which are branched and is due to the packing efficiency, b.p. pentane (36^{0}C) and 2,2-dimethylpropane (10^{0}C). The ligands discussed in this chapter all contain linear alkyl chains and a comparison is made with shorter and longer alkyl chains

4.3 Electrostatics

Molecules other than hydrocarbons which contain at least two heteroatoms, can have a permanent dipole due to the differences in electronegativity. The more electronegative atom retains a slightly negative charge leaving the less electronegative atom with a partial positive charge. Unlike van der Waal forces which occur due to temporary dipoles, electrostatic interactions can occur in systems where molecules have permanent dipoles. These forces are based on the attractions between opposite charges and include ion-dipole, dipole-dipole and non-directional ion-ion interactions as shown in Figure 4-1.

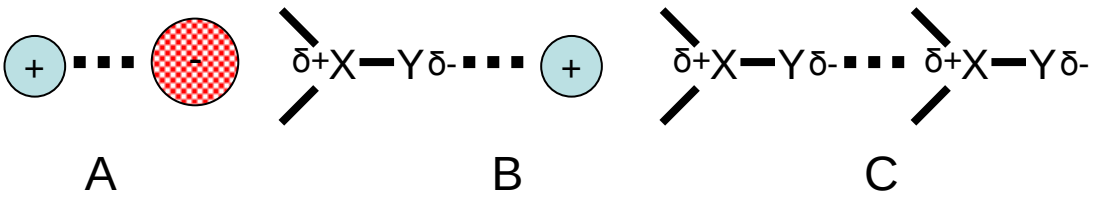

Figure 4-1 Electrostatic Interactions: A ion-ion, B dipole-ion, C-dipole-dipole

4.4 Hydrogen bonding

The attractions between dipoles can vary in strength[2] from 10 to 40 kJ mol^{-1}. Some of the strongest are due to a particular type of dipole interactions known as hydrogen bonding. Since Latimer and Rodebush proposed the idea that "a free pair of electrons on one water molecule might be able to exert sufficient force on a hydrogen held by a pair of electrons on another water molecule to bind the two molecules together" in

1920, hydrogen bonding has become a concept used to rationalise and understand many aspects in chemistry.[4]

Hydrogen bonding occurs when a hydrogen atom lies between two small, strongly electronegative atoms such as oxygen, nitrogen or fluorine. The electronegative heteroatom attached to the hydrogen pulls the electron density away from the hydrogen nucleus leaving it exposed with a partial positive charge. Electron density from the third atom is attracted to the hydrogen forming a very strong interaction.

Hydrogen bonds are directional and can vary in strength depending on a number of factors.[2] These include the heteroatoms involved and the temperature and pressure of the surrounding environment. In solutions, the hydrogen bonding that forms is highly dependent upon the solvent system used. In polar solvents, the partially charged atoms which form the hydrogen bonds will be solvated. An unfavourable enthalpy will then be required for desolvation, however, this will be countered with a favourable change in entropy as an increase in disorder occurs upon release of solvent.

The theory explains the unique properties of the low molecular weight molecule, water, and a wide variety of effects in biological systems, including the action of many drugs on the human body.[5] Hydrogen bonded systems and functional groups used in this chapter are discussed below.

4.4.1 Amides

An amide consists of an amine attached to a carbonyl as shown in Figure 4-2. The hydrogen bond exists between a NH and C=O on neighbouring molecules. The donor is provided by the hydrogen atom attached to an electronegative nitrogen atom. The lone pairs of the oxygen in the carbonyl group, acts as the acceptor. The electronegative atoms involved in the amide linkage results in the formation of very strong hydrogen bonds.[6]

The hydrogen bonding network can be extensive as each amide has both hydrogen bond donors and acceptors that are usually arranged in a *trans* arrangement along the (O)C-NH bond. Amides tend to have a rigid structure since the C=O consists of a sp^2 hydrid carbon atom although resonance structures similar to keto-enol forms are possible, forming amide-iminol pairs.[7] Examples of *cis* amide bonds however, can be found in cyclic structures.[8] Often these *cis* arrangements are stabilised by additional hydrogen bonding interactions.

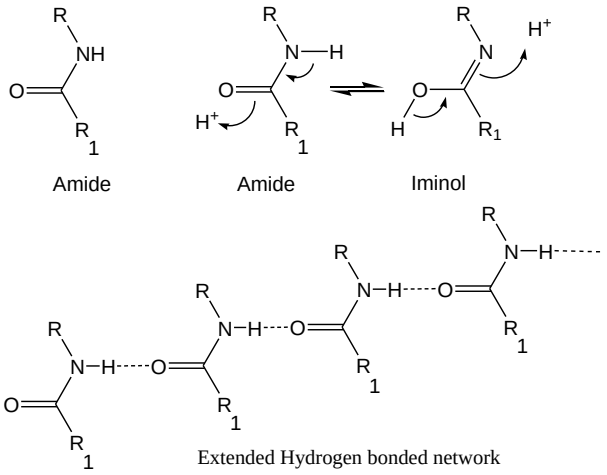

Figure 4-2 Structures of amide, tautomeric equilibrium between amide and iminol forms, and possible extended hydrogen bonded network

Amides have been shown to be useful in improving the thermal stability of Self Assembled Monolayers of thiol ligands on gold substrates.[10]

4.4.2 Thioamides

Thioamides are the S analogues of amides. The hydrogen bond donor is an NH group, and the hydrogen bond acceptor is now a C=S rather than C=O, Figure 4-3. As sulfur is a less electronegative atom than oxygen, the strength of the hydrogen bond is weaker in thioamides compared to those containing a carbonyl.[11] Thioamide compounds also have a tautomeric equilibrium and the thioiminol has a much higher tendency to form than for the corresponding iminol as proved by the C=N and C-S stretching frequencies often found in IR spectra.[11]

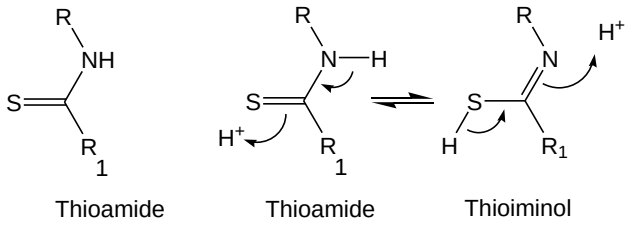

Figure 4-3 Structure of a thioamide and tautomeric equilibrium between thioamide and thioiminol forms

4.4.3 Urea

The urea group consists of two amine groups separated by a carbonyl group as shown in Figure 4-4. The presence of the additional hydrogen bond donor increases the likelihood that hydrogen bonding will exist between neighbouring molecules which can result in an increased hydrogen bond strength.[12]

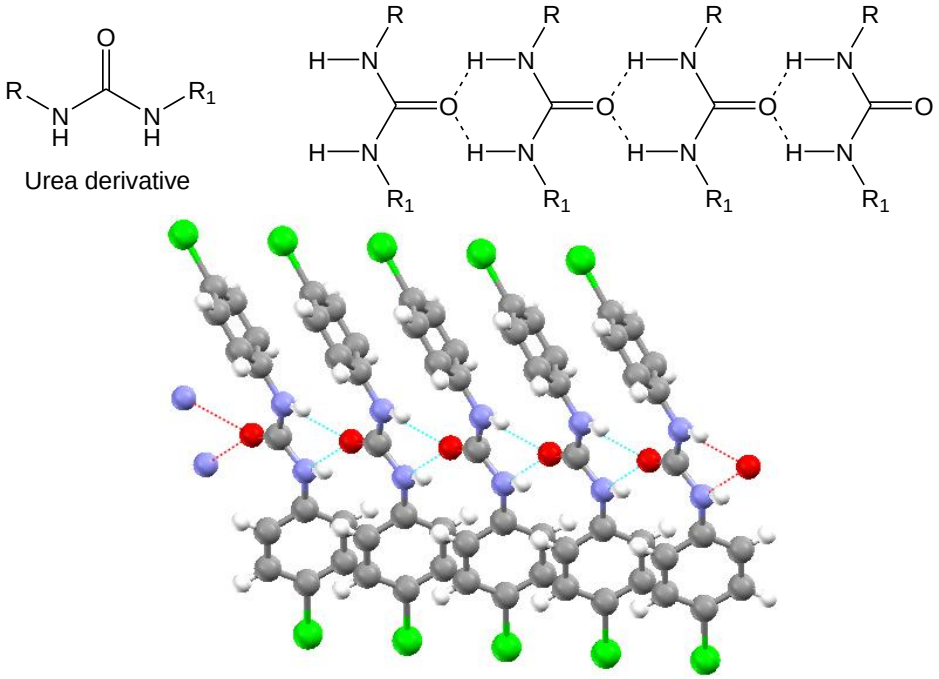

Figure 4-4 Top-Structure of urea derivative and possible hydrogen bonded network. Bottom-Crystal structure of ($BrC_6H_4NHCONHC_6H_4Br$) showing extended Hydrogen bonding network between NH and C=O. Bromine atoms are coloured green. [13]

4.4.4 Carboxylic acids

Carboxylic acids have the general formula shown in Figure 4-5. They are very useful as ligands in coordination chemistry and can bind to a wide variety of metals.[14] In particular, they are known to bind strongly to iron(III) ions and iron(III)oxide structures. In addition to this property, they contain electronegative oxygen atoms and have both hydrogen bond donor and acceptors.

Carboxylic acids are strongly associated in solutions and in the solid state, 8 membered dimers are often found demonstrating the likelihood that intermolecular hydrogen bonding will occur between ligands.[15] Crystal structures often show the hydrogen bonding network arranged such that the hydroxyl group is the donor and the carbonyl group is the acceptor as shown in Figure 4-5. Each pair forms two strong hydrogen bonds which often results in elongation of the single bond and a shortening of the double bond.

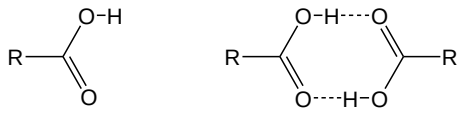

Carboxylic acid Acid-Acid dimer

Figure 4-5 Structure of carboxylic acid and dimers

Carboxylic acids are also known to form hydrogen bonded pairs with amides.[16] Both functional groups have the necessary hydrogen bond donor and acceptor pairs and can interact with each other as shown in Figure 4-6. The differences in electronegativity suggest that the acid-amide pair is bound together more weakly than a carboxylic acid dimer.

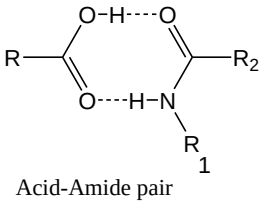

Acid-Amide pair

Figure 4-6 Structure of carboxylic acid- amide hydrogen bonded unit

4.4.5 Interactions with Aromatic systems

Hydrogen bonds can also form with aromatic groups. It has been shown by both experimental and theoretical methods that aromatic systems can also act as hydrogen bond acceptors, C-H … π,[17], N-H… π,[18] Studies carried out by Adams *et. al.* with a molecular zipper complex have used a double mutant principle to investigate the strength of a N-H--- π bond.[19, 20] The method involved the synthesis of four similar structures as shown in Figure 4-7. Complexes A and B differ mainly by the precence or absence of the pyrole N-H to aromatic-π interaction. Steric clashes are also present in complex A between the pyridine ring and the aromatic ring underneath. These are relieved in complex B which also affects the association constant. By generating the complex C, the effect of these steric clashes can be calculated. Therefore, by generating the double mutant complex D, the strength of the pyrole N-H to aromatic-π interaction can be measured. The overall free energy of binding is then calculated by comparison of the association constants of each pair as determined by ^{1}H NMR titration. This association constant can be related to the Gibbs free energy by Equation 13. A lower limit of -4.5 ± 0.5 kJ mol^{-1} was given for the NH-π interaction compared to -1.4 ± 0.8 kJ mol^{-1} previously measured for an edge CH -face π interaction.[19] This is expected if it is assumed the magnitude of the interaction is determined by electrostatics. The N-H bond dipole is much larger than the C-H bond dipole and interacts more strongly with the negatively charged π system[19,20].

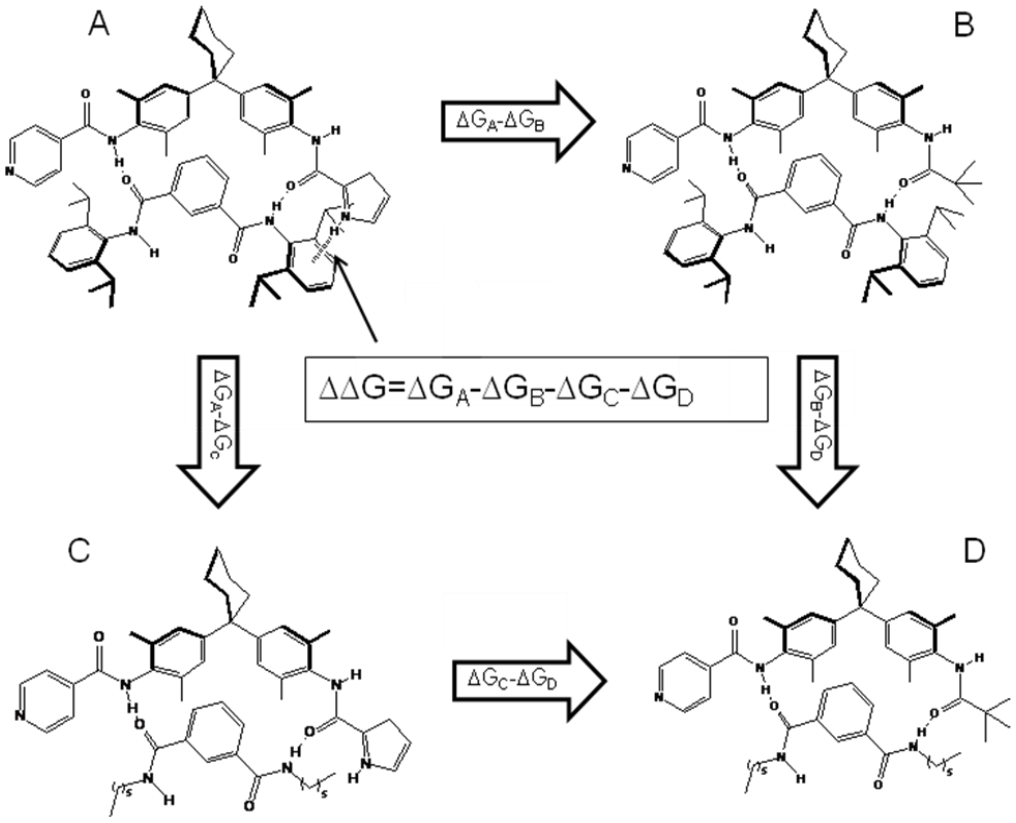

Figure 4-7 Chemical double mutant cycle for measuring the aromatic stacking interaction in complex A; X was varied to be = NMe_2, H, OMe, Cl, or NO_2.[20]

(13)

$$\Delta G = -RT \ln K$$

4.5 Aromatic interactions

The presence of aromatic rings creates the possibility for interactions in addition to those with hydrogen bond donors. A molecule is aromatic if it has a planar, monocyclic system of conjugation with a p orbital on each atom and only if the p orbital system contains $4n + 2\ \pi$ electrons, where n is an integer (n=0, 1, 2, 3 …).[21, 22] Three different types of interactions can occur between these rings, as shown in Figure 4-8. The most commonly observed types in crystal structures are the edge-face or offset face-face arrangements. Benzene itself crystallises in a herring bone

type structure using the edge-face structure as shown in Figure 4-9. The offset stacked arrangement observed in the crystal structure minimises π-electron repulsion and maximises attraction between σ-framework and π-electron on the ring below.

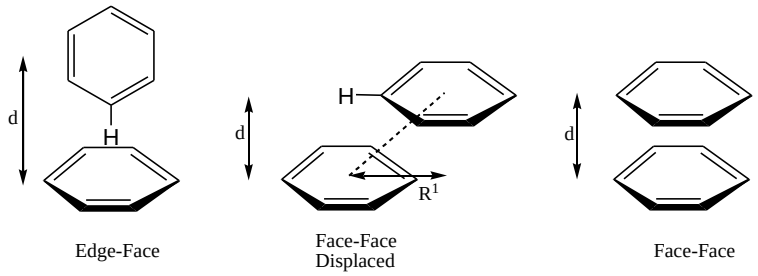

Figure 4-8 Structures of π Interactions showing edge-face, face-face(offset) and face-face arrangements, d=distance between planes, R^1=lateral offset

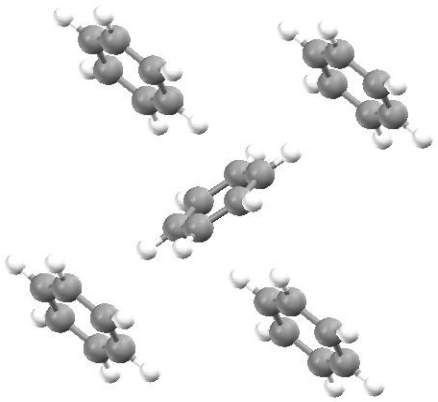

Figure 4-9 Crystal structure of benzene showing edge-face Herring bone packing

It has been suggested that the mode adopted depends on a number of factors in the system in question including: van der Waal forces, electrostatic interactions and desolvation. [23, 24,25] Since aromatic moieties have large planar surfaces, face stacked arrangements increase the van der Walls contacts. Solvophobic forces also favour face-face stacking arrangements since π electron surfaces are flat and non-polar.[26]

Hunter and Sanders proposed a model in 1990 that describes an aromatic ring as a positively charged σ-framework sandwiched between two regions of negatively charged π-electron density.[27] Substituents that alter the polarisation of the molecule

can affect the packing. Electron withdrawing groups decrease the electron density on the ring and therefore decrease the π electron repulsion.[28]

The double mutant method, mention earlier, has also been used to quantify the effects of aromatic substitutions on edge-face π interactions as shown in Figure 4-10.[28, 29] The electrostatic interaction between the positively charged CH groups with the negative aromatic rings is sensitive to local distributions of charge on the ring and depends on the nature of the group. In addition, the rings can be attracted or repulsed depending on the effects of X and Y on the global charge distribution. Attraction occurs when the groups have opposite effects and repulsion when the groups have the same effect. The authors identified a direct correlation between the strength of the aromatic interaction energies and the Hammett parameters of the substituent.[28, 29]

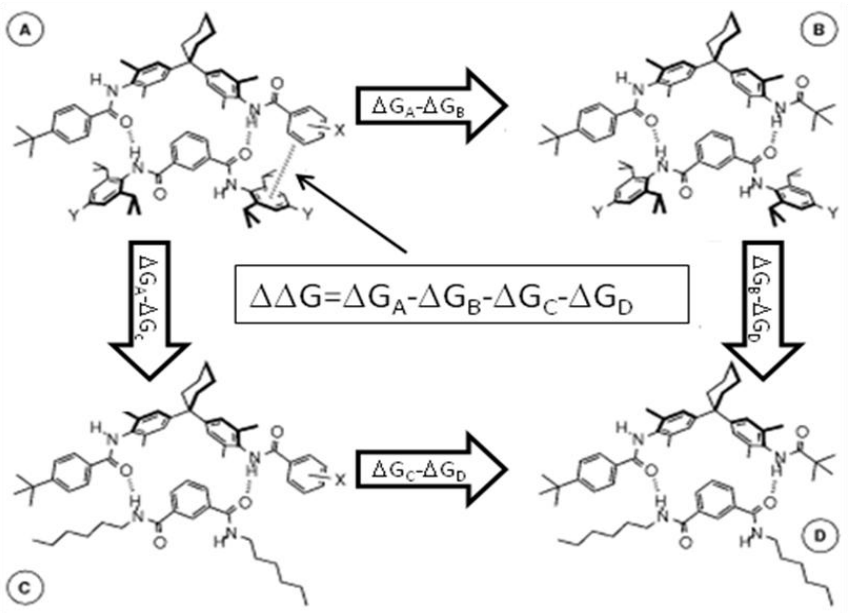

Figure 4-10 Chemical double mutant cycle for determining the magnitude of the terminal aromatic interaction in complex A. Y=NO_2, H, NMe_2. X=*p*-NO_2, *m*-NO_2, H, *p*-*t*Bu, *p*-NMe_2, *m*-NMe_2.[29]

There are also some cases in the literature where a lone pair is directly coordinated to an aromatic ring.[30, 31] For example, structural database mining of proteins along with Ab initio calculations carried out by Egli and Sarkhel suggest that interactions can occur between lone pairs of oxygen atoms and the π system of aromatic rings.[32]

4.6 Intermolecular Interactions with Sulfur

Sulfur is placed in group six of the periodic table under oxygen. It has a similar electronegativity to carbon although its chemistry can be quite different. Some functional groups containing sulfur are shown in Figure 4-11.

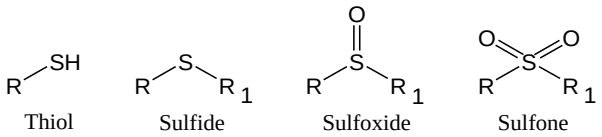

Figure 4-11 Structures of sulfur containing functional groups.

4.6.1 Sulfur-Aromatic interactions

Sulfur is an important element occuring in four of the 26 amino acids found within proteins; cysteine, cystine, taurine and methionine, the last of which is used in this chapter. The structures of proteins are a result of many different types of non-covalent bonding. Zauhar et.al have shown through statistical analysis of the Cambride Structural Database that interactions can occur between divalent sulfur (C-S-C) and aromatic rings.[33] They found that in the majority of cases, sulfur lies in the plane of the aromatic ring and approximately 5Å from the centre.

4.7 Hydrophobic effect

For its small size, water molecules have an unusually high number of hydrogen bond donors and acceptors which allows it to form well-ordered structures around non polar molecules. Often, these apolar groups will associate together and the corresponding desolvation which occurs, increases the entropy of the system. This is often matched with an increase in enthalpy due to the larger number of hydrogen bonds that then form between solvent molecules. The combination of these factors provides a driving force to generate the apolar assembles encouraging them to form.

4.8 Ligand Synthesis

Ligands 10-20 are shown in Table 4-1. Full details of the methods used for ligand synthesis and characterisation are given at the end of this chapter. Examples of typical reactions used are given below.

4.8.1 Benzoic acid ligands with pendant amide groups

Most of the ligands containing an amide group were prepared by reaction of the appropriate acyl chloride and amine. The acyl chloride was formed by heating a carboxylic acid with thionyl chloride to release HCl (g) and SO_2 (g) according to Scheme 4-1, which was then reacted with the amine to form the amide. The acid liberated is neutralised by NaOH(aq).

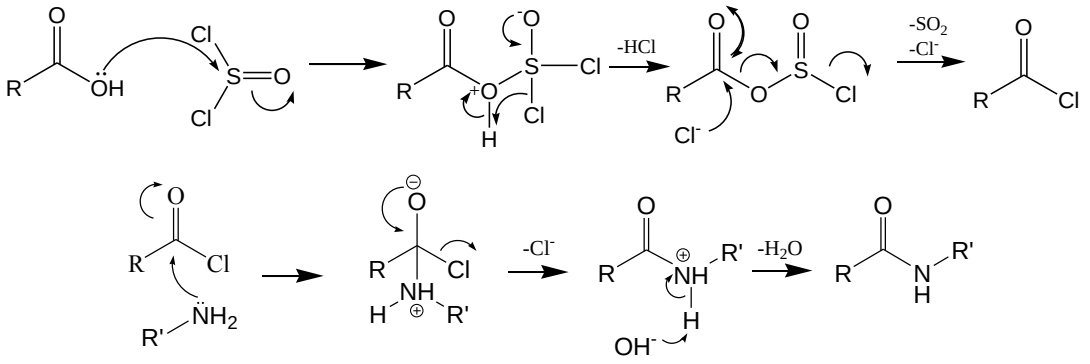

Scheme 4-1 Mechanism for acyl chloride formation from a carboxylic acid and thionyl chloride and for conversion to an amide by reaction with an amine

Ligand	Structure	Name
10	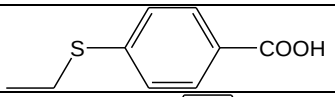	4-Ethylsulfanyl-benzoic acid
11	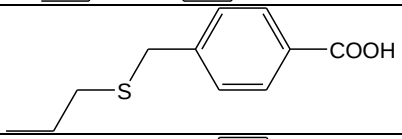	4-Propylsulfanylmethyl-benzoic acid
12	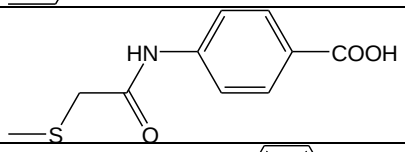	4-(2-Methylsulfanyl-acetylamino)-benzoic acid
13	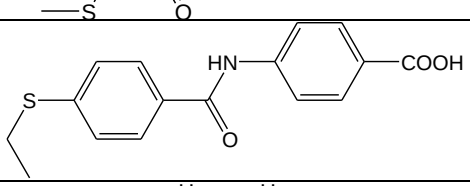	4-(4-Ethylsulfanyl-benzoylamino)-benzoic acid
14	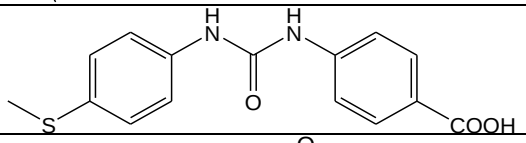	4-[3-(4-Methylsulfanyl-phenyl)-ureido]-benzoic acid
15	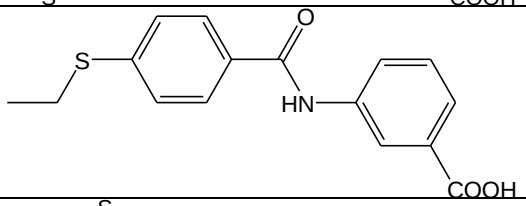	N-(4-ethylsulfanyl-phenyl)-isophthalamic acid
16	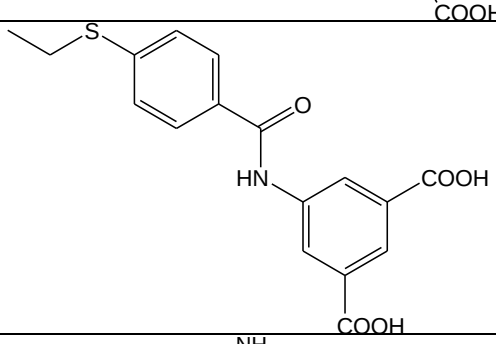	3-(4-Ethylsulfanyl-benzoylamino)-5-(1-hydroxy-vinyl)-benzoic acid
17	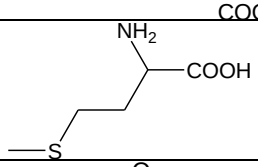	DL-methionine
18	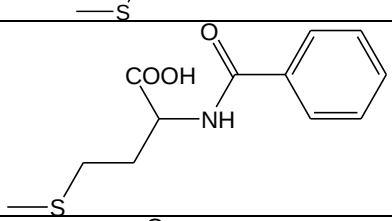	2-Benzoylamino-4-methylsulfanyl-butyric acid
19	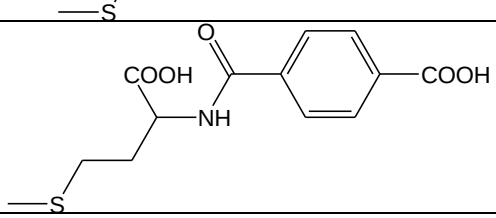	N-(1-Carboxy-3-methylsulfanyl-propyl)-terephthalamic acid

20	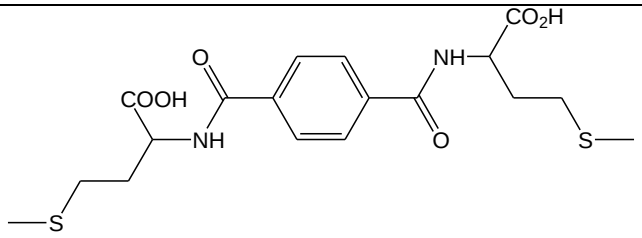	2-[4-(1-Carboxy-3-methylsulfanyl-propylcarbamoyl)-benzoylamino]-4-methylsulfanyl-butyric acid (20)

Table 4-1 Names and Structures of ligands 10-20

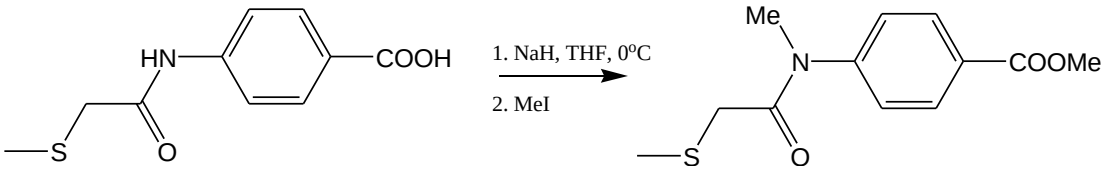

Scheme 4-2 Attempted synthesis of N-methylated ligand by deprotonation of amide using NaH and alkylation using MeI

The N-methyl derivative of **12** and is of interest because it cannot form intermolecular hydrogen bonds using the pendant amine group. A typical approach to synthesis of this type of amide is deprotonation of the amide using a strong base followed by alkylation with methyl iodide as shown in Scheme 4-2.[34] Two equivalents of sodium hydride and methyl iodide are required due to the deprotonation of the acid that will occur. This can then be hydrolysed by refluxing in aqueous acid. This route was unsuccessful and it was assumed that the presence of the dialkyl sulfide causes problems at both stages of the reaction. In the initial step, the sulfur atom promotes deprotonation at the methylene adjacent to the amide in competition to deprotonation of the amido nitrogen atom (Figure 4-12).

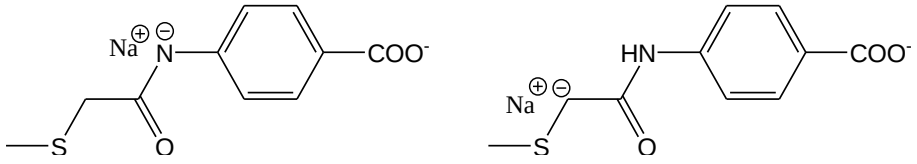

Figure 4-12 Alternative deprotonated forms of ligand 12

The addition of the methyl iodide is also potentially problematic since the sulfur can act as a nucleophile and react rapidly with alkyl halides. This reaction occurs by an S_N2 mechanism and forms trialkylsulfonium salts($R'R_2S^+$) as shown in Scheme 4-3.

Such salts can also act as alkylating agents when attacked by nucleophiles, displacing a sulphide as a leaving group. The generation of two possible nucleophiles in step 1 means the reaction can then form a complex mixture of products. This was found to be the case and N-methyl derivate was not obtained. It is possible that the synthesis of a N-methyl substituted derivative of **13** would not encounter the same difficulties however this reaction was not attempted

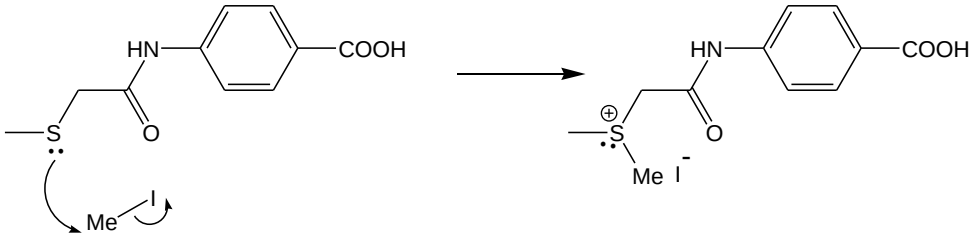

Scheme 4-3 The formation of a trialkylsulfonium salt from 12 on reaction with methyl iodide

4.8.2 Urea derivatives

The formation of ligand **14** was carried out by reaction of 4-aminobenzoic acid and 4-(methylthio)phenyl isocyanate. The latter was chosen because it is available commercially. Nucleophilic attack by the amine at the carbon atom in the isocyanate results in loss of planarity and proton transfer from the amine to the second nitrogen forms the urea linkage, Scheme 4-4.[34]

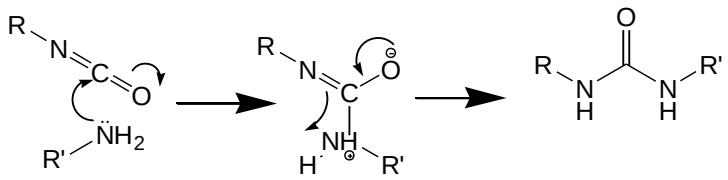

Scheme 4-4 Mechanism of reaction of an amine with an isocyanate to form a urea linkage.[34]

4.8.3 Thioamide

A ligand containing the thioamide group (L4.1), shown in Figure 4-13, was prepared from its amide analogue, **12** using Lawessons reagent, also shown in Figure 4-13.

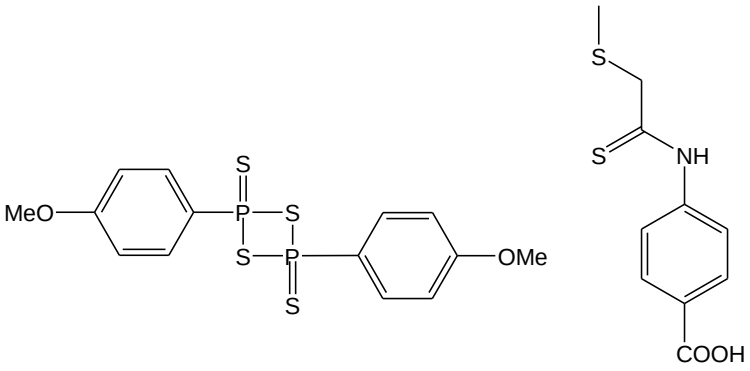

Lawessons Reagent Ligand L4.1

Figure 4-13 Structure of Lawessons Reagent and Ligand L4.1

4.9 Ligand Characterisation

All ligands successfully prepared were characterised by a combination of spectroscopic techniques and microanalysis.

4.9.1 NMR

Aromatic protons for ligands **10**-**14**, **16** and **19** are assigned α β, γ, δ, as shown in Scheme 4-5, **15** which contains the less symmetrical 3-aminobenzoic acid unit has the addition symbols κ, λ. Non-aromatic protons are assigned according to their location with respect to other functional groups.

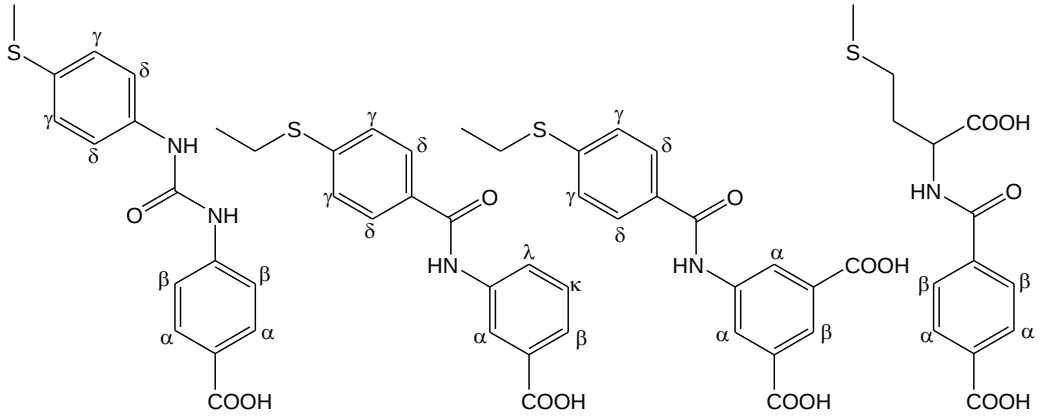

14 **15** **16** **19**

Scheme 4-5 Assignments for aromatic protons, ligands 10-19

The numbering scheme used for carbon atom assignment is shown in Scheme 4-6. Ligands **10**-**16** are numbered from the benzoic acid. Since ligands **17**-**20** have a significantly different structure and all contain the methionine unit they are labelled from the terminal methyl group attached to the sulfur atom.

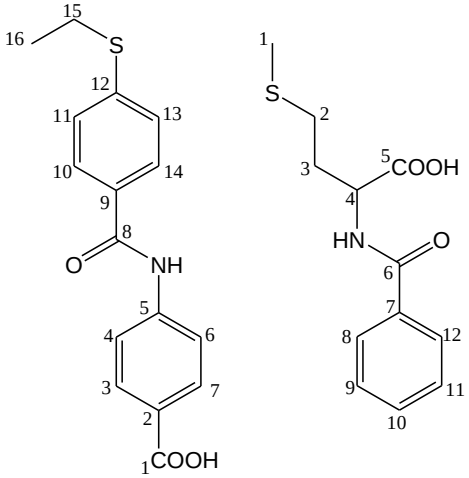

13 **18**

Scheme 4-6 ^{13}C NMR numbering scheme for ligands 13 and 18

4.9.2 UV-Vis

Ligand	λ_{max} /nm	E	Transition
10	281	15900	π-π*(Aromatic)
11	234	19500	π-π* (Aromatic)

12	268	17000	π-π*(Aromatic)
13	279	22000	π-π*(Aromatic)
14	284	54200	π-π*(Aromatic)
15	287	20000	π-π*(Aromatic)
16	222 298	2360 21000	n-π* C(O)NH π-π*(Aromatic)
18	233	13600	π-π*(Aromatic)
19	240	23900	π-π*(Aromatic)
20	241	75000	π-π*(Aromatic)
L4.1	226 309	5200 49000	n-π* C(S)NH π-π*(Aromatic)

Table 4-2 λ_{max} , ε and assignment of electronic transitions responsible for ligands 10-14, in 95 % MeOH/ H_2O

Ligands, **10**-**16**, all contain electronic absorptions due to aromatic π-π* transitions and the λ_{max} occur at a range of wavelengths from 234 to 309nm. The highest energy band is observed in ligand **11** which has no electron withdrawing group directly attached to the benzene ring other than the carboxylic acid which is present in all cases. Electronegative groups, such as amides, red shift the position of maxima to larger wavelengths. The effect is greatest for ligand **16**, which contains two electron withdrawing groups, an amide and a second carboxylic acid, and ligand L4.1 which has a thioamide group. The spectra of these two ligands also show the presence of the n-π* transition for the C(O)NH and C(S)NH groups respectively. These high energy absorptions are not observed for the other ligands since they occur at wavelengths below 200 nm.

4.9.3 IR Spectra

IR spectroscopy was used to identify functional groups within the ligands. All contain peaks arising from the carboxylic acid groups. These include sharp peaks for the C=O stretches, and OH bend, broad signals are seen for the OH stretch. Other

signals observed include those for amides, thioamides and ureas, and are listed in Table 4-3, these signals are characteristic of the functional groups and proves the presence .

Ligand	Wavenumber /cm^{-1}	Vibration
12	3291 1670	NH stretch C=O stretch
13	3390 1683	NH stretch C=O stetch
14	3310 1540	NH stretch C=O stretch
15	3300 1675	NH stretch C=O stretch
16	3292 1650	NH stretch C=O stretch
18	3314 1636	NH stretch C=O stretch
19	3307 1632	NH stretch C=O stretch
20	3309 1632	NH stretch C=O stretch
L4.1	3314 1170	NH stretch C-S strech

Table 4-3 Wavenumbers of bands in the IR spectra associated with the pendant functional groups in ligands 10-20

4.10 Binding studies of benzoic acid derivatives

4.10.1 Ligands **10** and **11**: Positive controls

The main purpose of this chapter is to investigate how ligand:ligand secondary bonding influences the strength of surface binding and the propensity for multilayering. As all the ligands in this chapter have a dialkyl or alkylaryl sulfide component to facilitate analysis by ICP-OES ligands **10** and **11** represent "controls" having no amido functionality and they differ from each other only slightly in the hydrophobicity of their sulfide tail groups, SCH_2CH_3 in **10**, cf. $CH_2SCH_2CH_2CH_3$ in **11**. Isotherms for uptake on goethite (Figure 4-14) are similar. The equilibrium

binding constants for **11**, obtained by fitting to a Langmuir isotherm (Table 4-4) as described in Chapter 2, is approximately double that of **10**. This may reflect the increase in the number of van der Waal forces associated with the additional CH_2 groups. In addition it is possible that more favourable sulfur-aromatic interactions, as discussed in Section 4.6.1, are occurring in **11** compared to **10** arising from a different location of the sulfur atom relative to the phenyl ring.

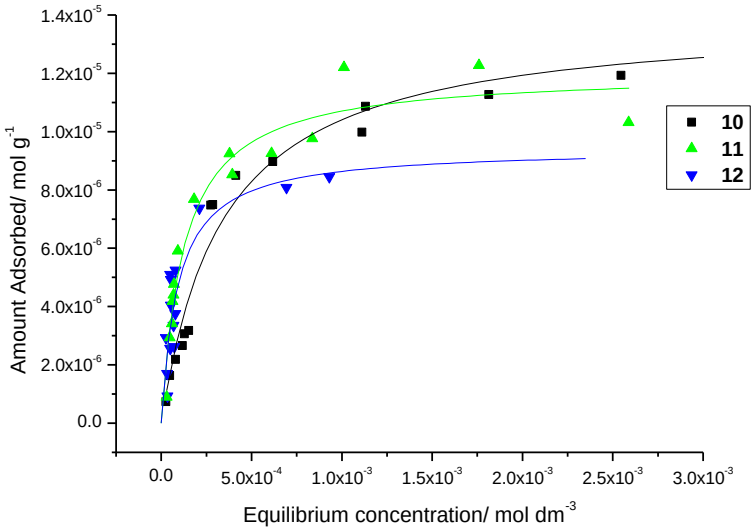

Figure 4-14 Uptake of Ligands 10, 11 and 12 on goethite from 95:5 MeOH/ H_2O

	10	**11**	**12**
Equilibrium binding constants (10^3)	2.9(4)	8(1)	11(3)
Surface Coverage(10^{-5})/ mol g^{-1}	1.40(6)	1.2(5)	1.0(1)
Required surface area per molecule/ $Å^2$	275(12)	318(132)	404(37)

Table 4-4 Adsorption data for ligands 10, 11 and 12, equilibrium binding constants, surface coverage and required area per molecule are derived from the Langmuir model.(errors in parenthesis)

4.10.2 Cooperative binding in a simple amide derivative, **12**

Ligands **12**, L4.1 and the N-methylated derivative were designed to study the importance of the presence and strength of hydrogen bonding between ligands on surface binding. Hydrogen bonding in an amide pair is usually stronger than that

found in a thioamide pair.[6] It is therefore reasonable to assume that **12** would show greater surface binding strength than L4.1.

Ligand L4.1 was successfully synthesised. However, it does not act as a surface ligand since sequestration of iron from the surface occurred. This was shown by the presence of iron in the solution phase as detected by ICP-OES. The synthesis of the N-methylated derivative was unsuccessful as stated in Section 0. Therefore this section deals only with the binding of ligand **12** and no direct comparison can be made with the other ligands.

The interpretation of the surface binding of **12** by the Langmuir equation gave a very poor goodness of fit parameter (R^2). This is probably due to the assumptions made by the equation, as described in Chapter 2, Section 2.4.2, that there is no cooperative binding between ligands. Thus as a binding site is used, it becomes progressively more difficult for another molecule to be adsorbed. Where the ligands contain functionality designed to make use of intermolecular bonding, binding of one ligand should promote the binding of further ligands.

The single Langmuir equation, see below, has only two parameters, binding strength and surface coverage. For simple systems such as **10** and **11**, this equation gives good R^2 values (R^2>90%). However, use of this equation for ligand **12** results in a lower value (R^2≈80%) and it follows that the equation should take into account some cooperativity of ligand binding and a third parameter is required. Introduction of this third term significantly improves the R^2 value. The binding strength and surface coverage remains the same within experimental error compared to the values found using the single Langmuir model.

From Chapter 2, the Langmuir equation is

$$K_{ads}[A] = \frac{\theta}{1-\theta} \quad \text{where} \quad \theta = \frac{[S_A]}{[S_M]}$$

K_{ads} = equilibrium adsorption constant

[A] = equilibrium concentration of adsorbate in the solution phase
S_A = equilibrium concentration of adsorbate on surface
S_M = maximum concentration of surface sites

For the simplest model of interactions, the mean-field model, the Langmuir equation changes to,

$$\frac{\theta}{1-\theta} = [K_{ads} \exp^{B\theta}][A]$$

B = Mean-field interaction constant

B is a measure of the interactions between ligands. Where B>0 the effective equilibrium constant, $K_{ads} \exp^{B\theta}[A]$, increases with increasing θ. This equation now requires a plot of [A] as a function of θ, *c.f.* θ as a function of [A] for the Langmuir form, to give

$$[A] = \frac{S_A}{S_M - S_A} \Big/ K_{ads} \exp^{\frac{BS_A}{S_M}}$$

Figure 4-15 shows the uptake of ligand **12** where the Equilibrium concentration is plotted as a function of amount adsorbed and Table 4-5 summarises the data obtained along with that using the Langmuir model for comparison.

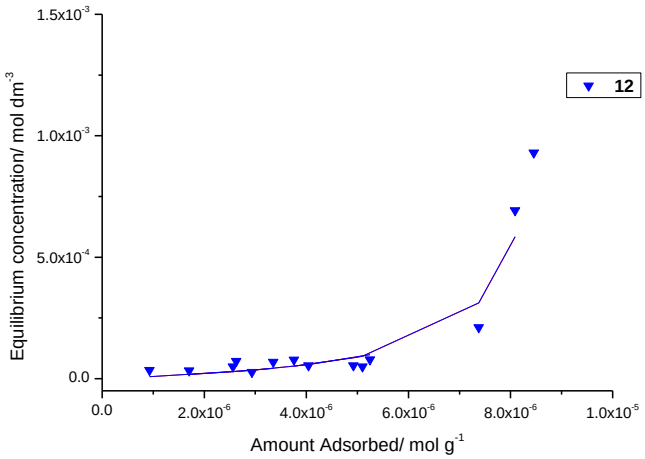

Figure 4-15 Uptake of 12 on goethite from 95:5 MeOH/ H_2O

	Langmuir	Mean field

	model	interaction model
Equilibrium binding constants (10^3)	11(3)	13(2)
Surface Coverage(10^{-5})/ mol g^{-1}	1.0(1)	0.9(1)
Required surface area per molecule/ $Å^2$	404(37)	420(47)
Mean field interaction constant		8.8E-15

Table 4-5 Adsorption isotherm data for ligand 12 using the Langmuir and Mean-field interaction models

This three parameter equation has been applied to the other ligands for comparison. In some cases it was not possible to fit the data, however, in all other cases the R^2 factor is reduced as shown in Table 4-6. Although many of the other ligands contain functionality for interligand bonding similar to **12**, the increase in number of parameters makes solving the equation more difficult.

Ligand	Langmuir Model	Mean Field Model
10	94	94.5
11	94	66
12	78	96.5
13	94	88
14	94.6	87.6
15	91	-
16	96	-
17	91.8	76
18	96.5	81
19	64	-
20	96	83

Table 4-6 R^2 values obtained from curve fitting using Langmuir and Mean-Field interaction models. Spaces indicate no curve fitting value was obtained.

In systems where two binding modes are taking place and a double Langmuir is required, an equation that takes into consideration a binding constant, surface coverage and an interacting term for each would be very difficult to fit. It was deemed unnecessary for this thesis because the application of the Langmuir equation to isotherms for all the other benzoic acids, **10**-**16**, results in R^2 values >90% whilst R^2 values from the mean field interaction model are all lower. Consequently binding constants and surface coverage data for all benzoic ligands with the exception of **12** have been calculated with the Langmuir model.

The incorporation of an amide group in **12** provides a hydrogen bond donor and acceptor. The presence of an amide enhances the binding strength compared to the analogous ligand without hydrogen bonding groups (**10**) as shown in Table 4-4. The surface coverage is smaller for **12** than **10** and therefore **12** requires a larger area per molecule. This could be due to hydrogen bonding defining the distance between ligands on the surface. Any such a difference also implies a different spacing of binding sites used by the "surface tethering" carboxylate group or the use of a different type of surface binding site.

The crystal structure of propylamidobenzoic acid, Figure 4-16,[35] could be considered to be analogous to ligands attached to the surface. The carboxylic acid dimerises in a manner which creates planar arrays of the COOH groups and perpendicular "tails". The distance between neighbouring amide units is 1.946Å, which is typical for an amide-amide hydrogen bond. The amide unit is rigid and planar and is inclined at 36.74^0 to the aromatic plane. The intermolecular spacing of the carboxylic acid carbon atoms defined by the amide hydrogen bonding is 5.12 Å. If a comparable separation is present in **12** then it would account for the lower surface density of ligands compared to ligand **10** and **11**.

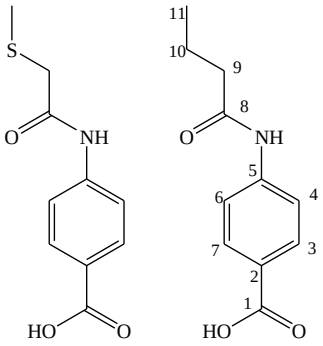

12 propylamidobenzoic acid

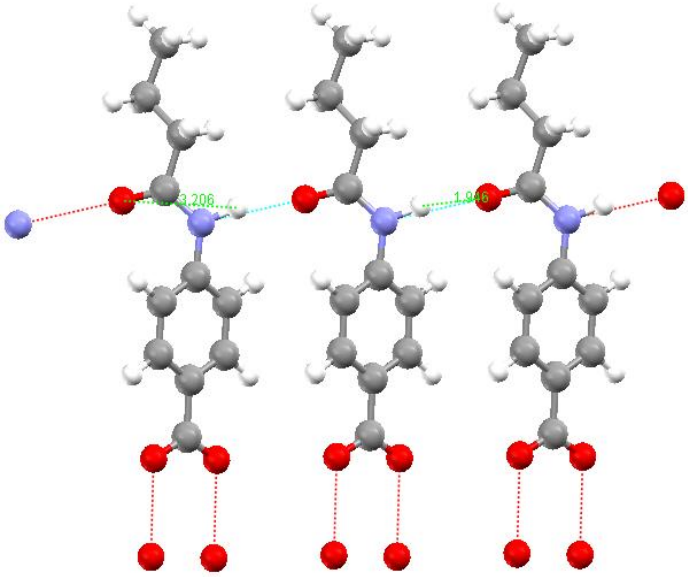

Figure 4-16 The crystal structure of 4-(n-propylacetamido)benzoic acid showing intermolecular hydrogen bonding between amides, [35]

In contrast to the separation distance between amides, carbon-sulfur bonds are usually about 1.8Å in length and the dialkylsulfide chain has free rotation about each atom since all are sp^3 hybridised. Therefore **10** and **11** have a greater flexibility than **12** and this would allow the ligands to pack more efficiently on the surface.[36-38]

4.10.3 Ligands **13**-**16**: Diarylamido derived benzoic acid

13 was designed to incorporate a second aromatic ring which might enhance the stability of a surface assembly by providing opportunities for intermolecular ligand-ligand aromatic stacking in addition to hydrogen bonding.

The data summarised in Table 4-7 show that the surface coverage is approximately double that of **12**, therefore a larger number of molecules are being adsorbed from the solution phase. It is possible that a second layer is forming with the two phenyl rings and amide groups interacting. Unfortunately, plotting the graph with the equilibrium concentration on a logarithmic scale as described in Chapter 3 gives no clear indication of two different layers. In addition, curve fitting to a double Langmuir also proved inconclusive.

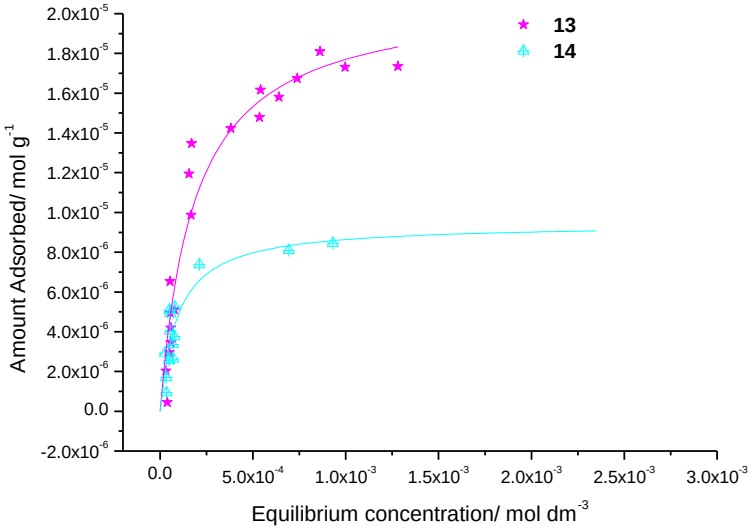

Figure 4-17 Adsorption isotherms for 13 and 14

	13	**14**
Equilibrium binding constants (10^3)	5.5(9)	43(17) 2(1.5)
Surface Coverage(10^{-5}) /mol g^{-1})	2.1(1)	1.2(2)
Required surface area per molecule/ $Å^2$	183(9)	285(48)

Table 4-7 Adsorption data for ligands 13 and 14

The binding strength of ligand **13** is, however, smaller than that of **12**. The high binding constant observed in **12** is due to the intermolecular forces between amide groups which are also present in **13**. Therefore the hydrogen bonding between amides in this ligand may be weaker. This weaker bonding could be due to the size of the phenyl ring. Since the benzene ring in **13** is larger than the methylene unit found in **12**, the aromatic group could increase the distance between the carbonyl and amino groups on neighbouring amides. A longer distance between the hydrogen bonding donor and acceptors would result in a weaker bond.

The ligand **14** contains a urea link (rather than an amide link as in **13**) between the two benzene rings, increasing the number of hydrogen bond donors by one. This was expected to and was observed to increase the surface binding strength; the binding constant is 43.1 x 10^3 for **14** compared to 5.5 x 10^3 for **13**. This comparison, along with that for **12** and **10**, support the idea that adding complementary hydrogen bond donors and acceptors enhances intermolecular interactions increasing the thermodynamic stability of the assembly at the surface.

The surface coverage for **14** is similar to that for **12** but approximately 50% of that observed for **13**. This is consistent with **13** forming a double layer compared to the other ligands discussed so far in this chapter which form just single layers.

Ligand **15** is the *meta* isomer of **13** and was synthesised to determine how the location of the amide link affects the surface binding. The *meta* orientation reduces the ability of the ligands to interact effectively, decreasing the binding strength considerably. The surface coverage is in the range expected for monolayer formation.

A carboxylic acid group added to ligand **15**, to give **16**, further increases the functionality. The isotherm for this ligand, fitted using a double Langmuir model, appears in Figure 4-19. The two binding constants obtained are summarised in Table 4-8. The initial slope of the graph is steep indicating strong binding. It is not possible to tell if the high strength is due to intermolecular interactions between ligands or an increase in ligand-surface interactions. The surface coverage observed is indicative of the formation of multiple layers which arises from the potential acid-acid, acid-amide and π-π interactions

Nagayasu *et. al.* studied the binding of various carboxylic acids and amines, some of which are shown in Figure 4-18 on stainless steel.[39] They found that compounds containing just one carboxylic acid group obeyed Langmuir type behaviour and binding was reversible. However, compounds containing two acid groups were found

to bind using both a reversible and irreversible mechanism as proved by desorption experiments. Since **16** contains two acid groups *meta* to each other, similar to isophthalic and trimesic acid, it is possible it will bind in a similar mode.

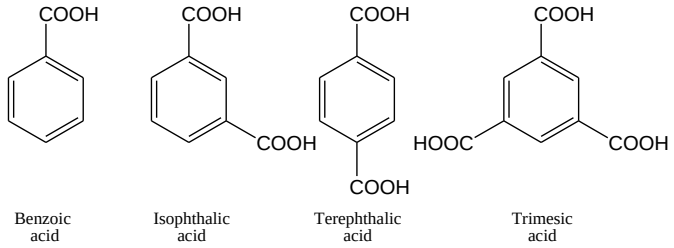

Figure 4-18 Names and structures of some carboxylic acids studied by Nagayasu *et. al.*

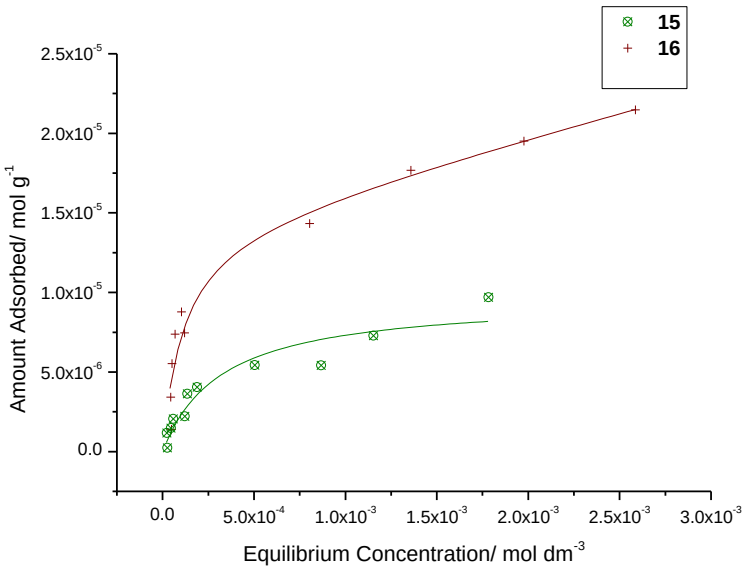

Figure 4-19 Adsorption isotherms for ligands 15 and 16

	15	**16**
Equilibrium binding constants (10^3)	3(1)	27(17) 0.4(2)
Surface Coverage(10^{-5})/ mol g^{-1}	1.0(1)	0.9(5) 3(2)
Required surface area per molecule/ $Å^2$	382(38)	473(263) 133(89)

Table 4-8 Adsorption isotherm data for ligands 15 and 16

4.11 Binding studies of amino acid derivatives

Ligands **10**-**16** all contain benzoic acid functionality, **17**-**20** are a series of carboxylic acid derivatives in which the acid group is attached to an alkyl chain rather than a phenyl ring. The ligands are structurally related as shown in Scheme 4-7. Their isotherms are shown in Figure 4-20.

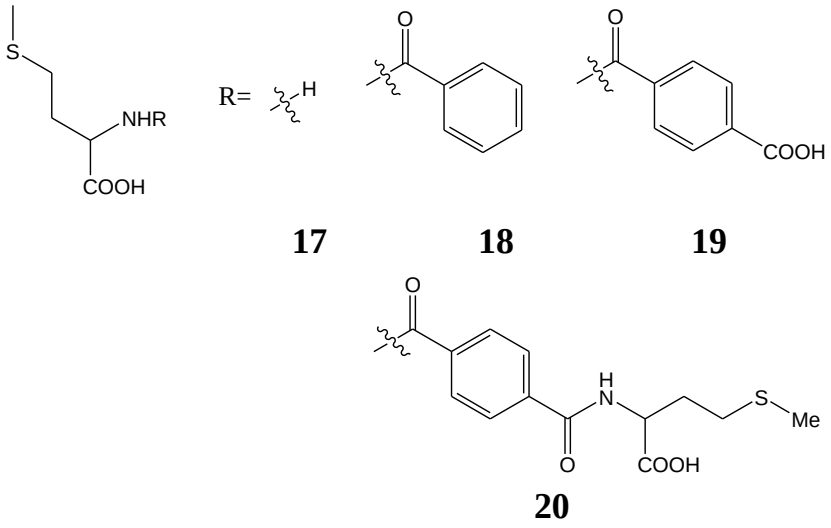

Scheme 4-7 Structural relationship between ligands 17-20

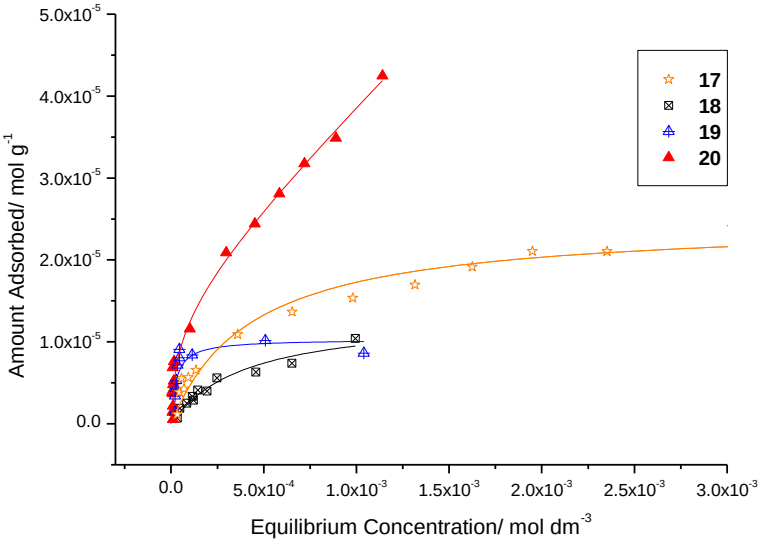

Figure 4-20 Uptake of ligands 17-20 on goethite from 95:5 MeOH:H_2O

Ligand	**10**	**17**	**18**	**19**	**20**
Equilibrium binding constant (10^3)/ k	2.9(4)	2.3(5)	2.5(5)	38(16)	4.7(5) 63(17)

Surface coverage (10^{-5})/ mol g^{-1}	1.40(6)	2.5(1)	1.3(1)	1.0(1)	0.9(1)
Required area per molecule/ $Å^2$	275(12)	155(6)	287(22)	371(37)	409(45)

Table 4-9 Data for Isotherms of 17, 18, 19, 20

The binding constant for the amino acid, methionine, **17**, is 2300 (Table 4-9). This is the same as that found for **10**, ethylthiobenzoic acid. It was expected to bind strongly due to the presence of a carboxylic acid group, and amino acids are known to chelate to Fe(III) in solution.[40] In addition, **17** contains hydrogen bond donors and an acceptor in the form of the primary amine group which could hydrogen-bond to surface oxo and hydroxyl groups, see Figure 4-21.

The surface coverage observed, 2.5 x 10^{-5} mol g^{-1}, which is higher than that found for the benzoic acids, might be accounted for by the small size of the ligand which has little steric bulk and can therefore pack easily.

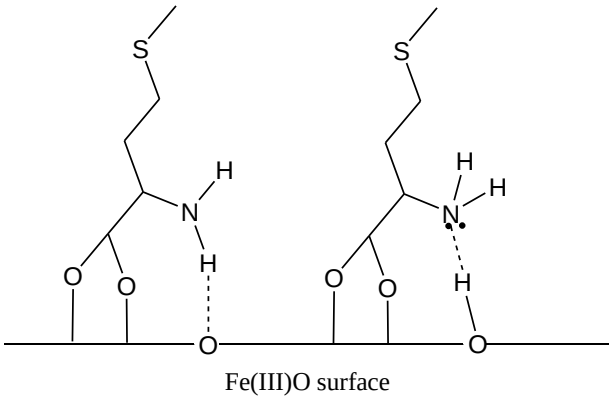

Figure 4-21 Schematic representation of the binding of 17 to the surface using a combination of Fe-O coordinate bonds from the carboxylate and hydrogen bonds from the amide to/from surface oxide/ hydroxide groups

Binding constants for **17** and **18** are the same within experimental error (Table 4-9). This is unsurprising since both ligands contain the same 4-thiohexanoic acid unit for surface attachment. i.e carboxylic acid attached to alkyl chain. Changing the 2-amino group in **17** to the 2-benzoylamido unit in **18** does not seem to have any effect on

binding strength. However, the surface coverage is reduced for **18** which is consistent with the size of the bulky benzoyl group on the amino nitrogen atom.

Ligand **19** has a binding strength which is an order of magnitude larger than those for **17** and **18**. It has two carboxylic acid groups present which gives three possible modes of binding, surface attachment using; aromatic or the aliphatic carboxylate groups, or both, see Figure 4-22. Coordination with two acids could give a high binding constant because both bind to the surface. Attachment using only one acid group could also give high binding constants since the ligand has uncoordinated acid functionality free for interligand bonding forming either carboxylic acid dimers or H-bonding to the amide group. The binding constant alone is insufficient to unambiguously assign which of the binding modes is being used. However, by comparison of surface coverage and required surface area per molecule the mode of surface attachments may be differentiated.

The surface coverage for **19** is similar to that for **18** but much lower than that found for **17**. The low surface coverage suggests that it is likely that the molecules attach with the carboxylate group from the amino acid because this arrangement would occupy a larger surface area compared to that using the benzoic acid group. However, since the binding constant for **19** is significantly higher than that of **18**, it is likely that the benzoic acid group must be involved in binding either to the surface or to other ligands. It is also possible that both modes of binding occur which alternate to allow interactions to take place.

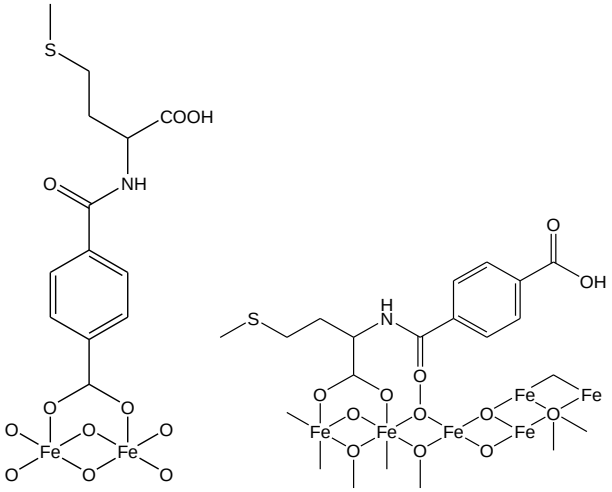

Figure 4-22 Suggested docking modes for ligands 19.

A double Langmuir model was required for the adsorption isotherm of **20** and the two binding constants obtained suggest that two different binding modes are taking place. The first binding constant is approximately double those found for **17** and **18**, and is associated with a low surface coverage. The second binding constant is an order of magnitude larger than **17** and **18**, and approximately twice that for **19**.

The presence of two sets of carboxylic acids and amides in **20** means that there are a large number of hydrogen bond donors and acceptors per molecule that can align with each other in the surface assembly. The very strong second binding constant is most likely due to a high degree of intermolecular ligand-ligand bonding and the lack of plateau region suggests the ligand is multilayering. Unfortunately, the nature of the methods used in this work for studying the adsorption equilibria at high residual ligand concentrations makes it difficult to define isotherms in multilayering cases.

4.12 Conclusions

The two aims of the work undertaken in this chapter,

1. to confirm the feasibility of introducing an element easily detectable by ICP-OES, such as sulfur, as an analytical label in adsorption isotherm determinations, and
2. to establish that introducing secondary bonding groups into the "tails" of simple carboxylic acid ligands enhances and "engineers" surface binding

have been confirmed.

The use of sulfur as an analytical label proved to be both convenient and effective in the determination of adsorption isotherms. Easy synthetic routes are available by use of starting materials containing sulfur atoms or by reaction of a thiol with an alkyl halide. Using this method allows testing of a wider range of ligands since UV-Vis chromophores are no longer required. It is likely that the introduction of other ICP-OES active elements purely for analytical purposed can be transferred to other surface binding studies. However, it is worth noting that the choice of element for analysis depends on the ligand-substrate binding system being studied. Soft sulfur atoms are rarely involved in coordination to a hard iron(III) oxide surface.

Ligands that contain functionality for secondary bonding, in general, show larger binding constants than those which do not. Introduction of such groups into ligand tails also appear, not unexpectedly, to influence the levels of uptake at surfaces and can lead to multilayering.

Trends established by comparing a range of substituent types have been identified.

- the hydrophobicity of a ligand, as provided by alkyl chains, is important for the stability of the surface bound complex. Ligands containing longer alkyl chains form more stable complexes than those containing shorter chains.

- the presence of hydrogen bond donors and acceptors can increase the binding strength. Complementary bonding pairs in the form of amides, enhance the stability of the surface bound complex. The addition of a further hydrogen

bond donor, in the form of a urea linkage, makes this effect more pronounced.

- ligands containing a second carboxylic acid group form more thermodynamically stable surface complexes. It is unknown whether this is due to ligand-ligand bonding or a larger number of ligand-surface bonds.

Overall, ligands which contain the highest number of potential hydrogen bond donor/acceptor interactions tend to form complexes with the largest stability constants. No attempt has been made to determine the mode of surface attachment. However, it is likely that providing a large number of potentially ligating groups allows the ligand to maximise interactions both to other ligands and the surface.

The next chapter investigates the design of different headgroups and considers how malonates bind to an iron(III)oxide surface. Malonic acid contains two carboxylic acid groups which also has the potential for intermolecular interactions.

4.13 Experimental

All reagents were used as obtained from Aldrich, Acros without further purification. ^{1}H and ^{13}C NMR were recordered on a DPX Bruker 360 MHz spectrometer. Fast atom bombardment (FAB) mass spectra were recorded on a Kratos MS50TC spectrometer. Infra-red (IR) spectra were obtained on a JABCO FTIR-460 spectrometer as potassium bromide discs. Electronic absorption measurements were made on a Unicam UV-2 Spectrophotometer.

4-Ethylsulfanyl-benzoic acid (10)

Was used as received from Aldrich.

4-Propylsulfanylmethyl-benzoic acid (11)

α-bromo,4-paratoluic acid was dissolved in ethanol (500 ml) and added to a warm solution of propanthiol (3.18g, 42 mmol) and sodium hydroxide (3.35g, 84 mmol) in ethanol (50 ml). This solution was then refluxed overnight. The solvent was then removed under reduced pressure to leave a white solid. To this was added diethyl ether (80 ml) creating two layers, the lower aqueous layer was removed and the organic layer was dried using magnesium sulphate. Removal of the diethyl ether left a white powder (6.5g, 73%). (Found C, 63.09; H, 6.82. $C_{11}H_{14}O_2S$ Requires C, 62.82; H 6.71.) λ_{max} (95:5 MeOH/ H_2O)/ nm 234.7 (ε/ dm^3 mol^{-1} cm^{-1} 19, 500) IR (cm^{-1}, KBr Disc): υ 2957 (OH), 1683 (C=O), 1428 (C-O-H). ^{1}H NMR (MeOD): δ 7.88-7.87 (d, 2H, J 9Hz, Ar-H (near COOH???)), 7.34-7.32 (d, 2H, J 9Hz, Ar-H), 3.63 (s, 2H, S*CH2*Ar), 2.29 (t, 2H, J 6Hz, CH3CH2*CH2*S), 1.52-1.37. ^{13}C NMR (MeOD): δ 170.1 (C1), 146.4 (C2), 131.3 (C3, C7), 130.8 (C5), 130.4 (C4, C6), 37.0 (C8), 34.8 (C9), 24.0 (C10), 14.1 (C11). *m/z* 211 (MH^+),

4-Ethylsulfanyl-benzoyl chloride

Ethylthiobezoic acid (0.53g, 2.9 mmol) was refluxed in thionyl chloride (8 ml) for 3 hours with a catalytic amount of DMF. The solvent was removed under reduced pressure and the product was used immediately without further purification.
(MH^+)

4-(2-Methylsulfanyl-acetylamino)-benzoic acid (12)

4-(2-chloroacetamido)benzoic acid (2g, 9.36 mmol) was dissolved in ethanol (50 ml) and added to a solution of sodium hydroxide (0.37g, 9.36 mmol) dissolved in ethanol (50 ml) with sodium thiomethoxide solution (21% wt by vol) (3.12g, 9.36 mmol) and refluxed for 48 hours. The solvent was then removed under reduced pressure and the resulting white solid was dissolved in water and acidified with sulphuric acid. The precipitated acid was the filtered, washed with water and recrystallised from a hot acetonitrile/ water solution. A white crystalline material was obtained (1.5g, 71%). (Found C, 43.12; H, 3.62; N, 4.88. $C_{10}H_{11}NO_3S$.NaCl requires C, 42.33; H, 3.90; N,

4.94. λ_{max} (95:5 MeOH/ H_2O)/ nm 268 (ε/ dm^3 mol^{-1} cm^{-1} 17, 000) IR (cm^{-1}, KBr Disc): υ 3291 (NH), 2550 (OH), 1684 (C=O), 1670 (C=O). ^{1}H NMR (D_2O): δ 7.81-7.76 (d, 2H, J 9Hz, α Ar-H), 7.43-7.34 (d, 2H, J 9Hz, β Ar-H), 3.27 (s, 2H, *CH2*), 2.05 (s, 3H, *CH3*). ^{13}C NMR (D_2O): δ 175.9 (C1), 171.9 (C8), 150.7 (C2), 131.1 (C3), 130.5 (C5), 130.1 (C7), 123.2 (C4), 115.3 (C6), 15.2 (C10). *m/z* 224 (M^+)

4-(4-Ethylsulfanyl-benzoylamino)-benzoic acid (13)

4-Ethylsulfanyl-benzoyl chloride (0.5g, 2.49 mmol) was dissolved in chloroform (50 ml) and cooled to 0^{o}C. To this solution was added 4-amino benzoic acid (0.376g, 2.49 mmol) and 2M NaOH (aq) and stirred at 0^{o}C for one hour. The layers were then separated and the aqueous layer was extracted with further chloroform (2 x 30 ml). This was then dried over anhydrous magnesium sulphate and the solvent was removed under reduced pressure to leave a brown solid. This was recrystallised from MeCN/ H_2O. (0.4g, 53 %) (Found C, 55.42; H, 4.55; N, 4.3. $C_{16}H_{15}NO_3S$.(0.73NaCl) requires C, 55.85; H, 4.39; N, 4.07) λ_{max} (95:5 MeOH/ H_2O)/ nm 278.8 (ε/ dm^3 mol^{-1} cm^{-1} 22, 000) ^{1}H NMR (DMSO): δ 8.02 - 7.96 (m, 6H, Ar-H), 7.46 - 7.42 (d, 2H, J 8Hz, Ar-H near S), 3.13 – 3.05 (q, 2H, J 7Hz, CH3*CH2*S), 1.33 - 1.30 (t, 3H, J 7Hz, *CH3*CH2S). ^{13}C NMR (DMSO): δ 167.3 (C1), 165.7 (C8), 143.7 (C2), 142.3 (C9), 131.2 (C5), 130.5 (C3, C7), 128.8 (C10, C14), 126.5 (C4, C6), 125.8 (C12), 119.8 (C11, C13), 25.5 (C16), 14.2 (C15). *m/z* 302

4-[3-(4-Methylsulfanyl-phenyl)-ureido]-benzoic acid (14)

4-(methylthio)phenyl isocyanate (0.5g, 3mmol) and 4-aminobenzoic acid (0.46g, 3mmol) were refluxed in acetonitrile for 3 hours. The product precipitates pure during reflux as a white solid. (0.68g, %) (Found C, 59.64; H, 4.51; N, 9.17. $C_{15}H_{14}N_2O_3S$ requires C, 59.58; H, 4.67; N, 9.27.) IR (cm^{-1}, KBr Disc): υ 3310 (NH), 2985 (OH), 1646 (C=O), 1540 (C=O). ^{1}H NMR (DMSO): δ 8.91 (s, 1H, NH), 8.64 (s, 1H, NH), 7.76 (d, 2H, J 8Hz, α Ar-H), 7.44 (d, 2H, J 8Hz, βAr-H), 7.32 (d, 2H, J 8Hz, δAr-H), 7.10 (d, 2H, J 8Hz, γAr-H), 2.31 (s, 3H, *CH3*). ^{13}C NMR (DMSO): δ 165.9 (C1), 151.0 (C8), 142.8 (C2), 135.9 (C5), 129.4 (C2), 129.3 (C7),

126.6 (C4, C6), 122.5 (C9), 118.1 (C10, C14), 116.9 (C12), 116.1 (C11, C13), 14.8 (C15). *m/z* (M^+)

3-(4-Ethylsulfanyl-benzoylamino)-5-(1-hydroxy-vinyl)-benzoic acid(16)

Aminoisothalic acid dissolved in acetonitrile (30 mls) with 2 M NaOH (30 mls) was added to a solution of 4-Ethylsulfanyl-benzoyl chloride in acetonitrile (30 mls) cooled to 0^0C in an ice bath and stirred for 2 hours. The solvent was then removed under reduced pressure and water (50 mls) was added. The solution was then acidified using HCl (aq) and the white solid was then recrystallised from hot acetic acid and water. (Found C, 56.88; H, 4.51; N, 3.82. $C_{17}H_{15}NO_5S.0.2NaCl$ requires C, 59.11; H, 4.38; N, 3.82.) λ_{max} (95:5 MeOH/ H_2O)/ nm 222 (ε/ dm^3 mol^{-1} cm^{-1} 23, 600) 298.5 (21, 000)^{1}H NMR (D2O): δ 7.98 (s, 1H, αAr), 7.89 (s, 2H, βAr-H), 7.56-7.42 (d, J 8 Hz, 2H, δAr-H), 6.91-6.88 (d, 2H, J 9Hz, γAr-H near S), 2.57-2.48 (q, 2H, J 7Hz, CH3*CH2*S), 1.00 – 0.94 (t, 3H, J 7Hz, *CH3*CH2S). *m/z* 346 (M^+)

3-(2-Methylsulfanyl-thioacetylamino)-benzoic acid

4-(2-Methylsulfanyl-acetylamino)-benzoic acid (1.0g, 4.44 mmol) and Lawessons reagent (1.08, 2.66 mmol) were heated under reflux in toluene (75ml) for one hour. The solvent was then removed under reduced pressure to leave a red solid. This was purified by column chromatography using DCM, the desired product was obtained as a green solid (R_f = 0.61). (0.35, 33%) Found C, 46.71; H, 3.91; N, 5.09. $C_{10}H_{11}NO_2S_2$.(0.3NaCl) requires C, 46.39; H, 4.28; N, 5.41. λ_{max} (95:5 MeOH/ H_2O)/ nm 226 (ε/ dm^3 mol^{-1} cm^{-1} 52, 000), 309 (49, 000) IR (cm^{-1}, KBr Disc): υ 3314 (NH), 2984 (OH), 1644 (C=O), 1170 (C=S). ^{1}H NMR (MeOD): δ 8.09-8.03 (d,d 2H, J 8,2 Hz, α Ar-H), 7.94-7.88 (d,d, 2H, J 8,2 Hz, β Ar-H), 3.69 (s, 2H, *CH2*), 2.13 (s, 3H, *CH3*). ^{13}C NMR (MeOD): δ 201.3 (C1), 145.7 (C8), 136.5 (C2, C5), 130.6 (C3), 130.2 (C7), 123.9 (C4), 123.2 (C6), 50.1 (C9), 16.2 (C10).

DL-methionine (17)

Was used as received from Aldrich.

2-Benzoylamino-4-methylsulfanyl-butyric acid (18)

A solution of DL-methionine (1.06, 7.11 mmol) in acetonitrile with 2M NaOH (20 mls) was added to a solution of benzoyl chloride (1g, 7.11mmol) in acetonitrile cooled to 0^0C in an ice bath and stirred for two hours. The solvent was removed under reduced pressure and water (30 mls) was added. The solution was then acidified using HCl (aq) and the white solid was then recrystallised from THF and hexane. (Found C, 55.46; H, 5.65; N, 5.08. $C_{15}H_{14}N_2O_3S.0.1NaCl$ requires C, 55.61; H, 5.83; N, 5.41.) λ_{max} (95:5 MeOH/ H_2O)/ nm 233 (ε/ dm^3 mol^{-1} cm^{-1} 6, 800) IR (cm^{-1}, KBr Disc): υ 3314 (NH), 2917 (OH), 1734 (C=O), 1636 (C=O). ^{1}H NMR (MeOD): δ 7.81 (d,d, 2H, J 9, 2 Hz, A-ArH), 7.49-7.38 (m, 3H, remaining Ar-H), 4.73 (q, 1H, J 5Hz, C*H*), 2.55 (m, 2H, *CH_2* near acid), 2.05 (m, 2H, *CH_2* near S), 1.97 (s, 3H, *CH_3*). ^{13}C NMR (MeOD): δ 175.8 (C5), 170.9 (C6), 135.7 (C7), 134.5 (C12), 133.3 (C8), 131.2 (C11), 130.0 (C9), 129.0 (C10), 53.7 (C4), 32.4 (C2), 32.0 (C3), 15.7 (C1). *m/z* 254 (MH^+)

Terephthaloyl dichloride

Terephalic acid was refluxed in thionyl chloride(8 mls) for two hours with a drop of DMF as catalyst. The solvent was removed under reduced pressure to yield a yellow crystalline material that was used without further purification.

N-(1-Carboxy-3-methylsulfanyl-propyl)-terephthalamic acid (19)

DL-methionine dissolved in acetonitrile (30 mls) with 2 M NaOH (30 mls) was added to a solution of Terephthaloyl dichloride in acetonitrile (30 mls) cooled to 0^0C in an ice bath and stirred for 2 hours. The solvent was then removed under reduced pressure and water (50 mls) was added.The solution was then acidified using HCl (aq) and the white solid was then recrystallised from hot acetonitrile and water. IR (cm^{-1}, KBr Disc): υ 3307 (NH), 2916 (OH), 1693 (C=O), 1632 (C=O). ^{1}H NMR (MeOD): δ 8.16 (d, 4H, J 15Hz, Ar-H), 4.67 (q, 1H, J 5Hz, *CH*), 2.50 (m, 2H, *CH_2*

near acid), 2.11 (m, 2H, *CH_2* near S), 1.91 (s, 3H, *CH_3*) ^{13}C NMR (D2O): δ 1.79.0 (C13), 175.6 (C5), 170.0 (C6), 161.6(C10) 139.0 (C7), 129.3 (C9) 129.0 (C11), 128.0 (C12), 127.6 (C8), 55.5 (C4), 31.4 (C2), 30.5 (C3), 14.7 (C1).

2-[4-(1-Carboxy-3-methylsulfanyl-propylcarbamoyl)-benzoylamino]-4-methylsulfanyl-butyric acid (20)

DL-methionine dissolved in acetonitrile (30 mls) with 2 M NaOH (30 mls) was added to a solution of Terephthaloyl dichloride in acetonitrile (30 mls) cooled to 0^0C in an ice bath and stirred for 2 hours. The solvent was then removed under reduced pressure and water (50 mls) was added.The solution was then acidified using HCl (aq) and the white solid was then recrystallised from hot acetonitrile and water. (Found C, 46.39; H, 5.76; N, 5.79. $C_{24}H_{18}N_2O_6S_2$.0.7NaCl requires C, 46.05; H, 5.15; N, 5.97.) λ_{max} (95:5 MeOH/ H_2O)/ nm 241 (ε/ dm^3 mol^{-1} cm^{-1} 7, 500) IR (cm^{-1}, KBr Disc): υ 3309 (NH), 2916 (OH), 1731 (C=O), 1632 (C=O). ^{1}H NMR (MeOD): δ 7.82 (s, 4H, Ar-H), 4.67 (q, 2H, J 5Hz, *CH*), 2.50 (m, 4H, *CH_2* near acid), 2.11 (m, 4H, *CH_2* near S), 1.91 (s, 6H, *CH_3*). ^{13}C NMR (MeOD): δ 175.5 (C5), 170.1 (C6), 138.6 (C7), 129.1 (C8), 53.7 (C4), 32.3 (C3), 32.0 (C2), 15.6 (C1).

4.14 References

1 M. Frey, S. G. Harris, J. M. Holmes, D. A. Nation, S. Parsons, P. A. Tasker, and R. E. P. Winpenny, *Chemistry--A European Journal*, 2000, **6**, 1407.
2 K. Autumn, M. Sitti, Y. A. Liang, A. M. Peattie, W. R. Hansen, S. Sponberg, T. W. Kenny, R. Fearing, J. N. Israelachvili, and R. J. Full, *Proceedings of the National Academy of Sciences of the United States of America*, 2002, **99**, 12252.
3 A. K. Geim, S. V. Dubonos, I. V. Grigorieva, K. S. Novoselov, A. A. Zhukov, and S. Y. Shapoval, *Nature materials*, 2003, **2**, 461.
4 W. M. Latimer and W. H. Rodebush, *Journal of the American Chemical Society*, 1920, **42**, 1419.
5 P. J. Atkins, Lorette, 'Chemical Principles, The Quest for Insight', Library of Congress Cataloging-in-Publications Data, 1999.
6 L. Hagegman, C. Lindblad, H. Oskarsson, A.-S. Ullstrome, and I. Persson, *Journal of the American Chemical Society*, 2003, **125**, 3631.
7 P. E. Allegretti, E. A. Castro, and J. J. P. Furlong, *Theochem*, 2000, **499**, 121.
8 G. J. Pernia, J. D. Kilburn, J. W. Essex, R. J. Mortishire-Smith, and M. Rowley, *Journal of the American Chemical Society*, 1996, **118**, 10220.
9 http://www.accelrys.com/reference/gallery/ls_dna.html.
10 R. Valiokas, M. Oestblom, S. Svedhem, S. C. T. Svensson, and B. Liedberg, *Journal of Physical Chemistry B*, 2002, **106**, 10401.
11 B. K. Min, H.-J. Lee, Y. S. Choi, J. Park, C.-J. Yoon, and J.-A. Yu, *Journal of Molecular Structure*, 1998, **471**, 283.
12 A. Shukla, E. D. Isaacs, D. R. Hamann, and P. M. Platzman, *Physical Review B: Condensed Matter and Materials Physics*, 2001, **64**, 052101/1.
13 Q. Lin, Y.-M. Zhang, T.-B. Wei, and H. Wang, *Acta Crystallogr.,Sect.E:Struct.Rep.Online*, 2004, **60**, o696.
14 F. H. Allen, *Acta. Crystallogr.*, 2002, **B58**, 380.
15 M. Fujita, 'Molecular Self Assembly: organic versus inorganic approachs', ed. M. Fujita, Springer, 2000.
16 A. Parkin, G. Barr, W. Dong, C. J. Gilmore, and C. C. Wilson, *CrystEngComm*, 2006, **8**, 257.
17 B. H. Hong, J. Y. Lee, S. J. Cho, S. Yun, and K. S. Kim, *Journal of Organic Chemistry*, 1999, **64**, 5661.
18 T. Steiner and G. Koellner, *Journal of Molecular Biology*, 2001, **305**, 535.
19 H. Adams, K. D. M. Harris, G. A. Hembury, C. A. Hunter, D. Livingstone, and J. F. McCabe, *Chemical Communications (Cambridge)*, 1996, 2531.
20 H. Adams, F. J. Carver, C. A. Hunter, J. C. Morales, and E. M. Seward, *Angewandte Chemie, International Edition in English*, 1996, **35**, 1542.
21 E. Huckel, *Zeitschrift fuer Physik*, 1931, **70**, 204.
22 E. Huckel, *Zeitschrift fuer Physik*, 1931, **72**, 310.
23 K. O. Boernsen, H. L. Selzle, and E. W. Schlag, *Journal of Chemical Physics*, 1986, **85**, 1726.
24 L. F. Newcomb and S. H. Gellman, *Journal of the American Chemical Society*, 1994, **116**, 4993.

[25] H. J. Schneider, K. Philippi, and J. Poehlmann, *Angewandte Chemie*, 1984, **96**, 907.
[26] B. Askew, P. Ballester, C. Buhr, K. S. Jeong, S. Jones, K. Parris, K. Williams, and J. Rebek, Jr., *Journal of the American Chemical Society*, 1989, **111**, 1082.
[27] C. A. Hunter and J. K. M. Sanders, *Journal of the American Chemical Society*, 1990, **112**, 5525.
[28] F. J. Carver, C. A. Hunter, and E. M. Seward, *Chemical Communications (Cambridge)*, 1998, 775.
[29] F. J. Carver, C. A. Hunter, D. J. Livingstone, J. F. McCabe, and E. M. Seward, *Chemistry--A European Journal*, 2002, **8**, 2847.
[30] F. Kraus, T. Hanauer, and N. Korber, *Inorganic Chemistry*, 2006, **45**, 1117.
[31] B. W. Gung, X. Xue, and H. J. Reich, *Journal of Organic Chemistry*, 2005, **70**, 7232.
[32] M. Egli and S. Sarkhel, *Accounts of Chemical Research*, ACS ASAP.
[33] R. J. Zauhar, C. L. Colbert, R. S. Morgan, and W. J. Welsh, *Biopolymers*, 2000, **53**, 233.
[34] J. G. Clayden, 'Organic Chemistry', Oxford University Press, 2001.
[35] N. Feeder and W. Jones, *Molecular Crystals and Liquid Crystals Science and Technology, Section A: Molecular Crystals and Liquid Crystals*, 1994, **240**, 231.
[36] I. Yarovsky, M.-I. Aguilar, and M. T. W. Hearn, *Analytical Chemistry*, 1995, **67**, 2145.
[37] S. Soubatch, R. Temirov, and F. S. Tautz, *Langmuir*, 2006, **22**, 9572.
[38] A. Gavezzotti, *Acta Crystallographica, Section B: Structural Science*, 1990, **B46**, 275.
[39] T. Nagayasu, C. Yoshioka, K. Imamura, and K. Nakanishi, *Journal of Colloid and Interface Science*, 2004, **279**, 296.
[40] R. N. Puri, R. O. Asplund, and W. F. Tucker, *Inorganica Chimica Acta*, 1982, **66**, 7.

Contents

5 Determination of the binding mode(s) of Malonic acid to iron(III) oxide surfaces

Work presented in Chapter 3 suggests that shortening the chain between a carboxylic acid and keto group (n=2 compared to n=3 in Figure 5-1) increases the strength of surface binding. Consequently it was decided to investigate how reducing the length further to a single carbon atom would affect the binding strength. 2-Substitued malonic acids were considered first. Monoesterification to give systems analogous to L2-L5 were also considered but the low hydrolytic stability of β-keto esters was thought likely to present major complications in studies of isotherms.[1]

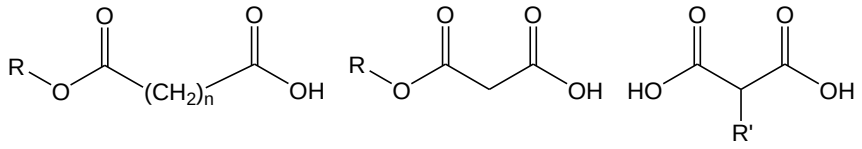

L1-L6 Malonate 2-substituted malonic acids

Figure 5-1 Representation of n-keto group in ligands L1-L6 and malonic acid

The potential for the R group to provide further functionality suggests that malonic acid is a good candidate as a corrosion inhibition ligand worthy of further study. It was hoped that synthesising derivatives could generate very useful surface ligands.

5.1 Introduction: Surface binding of malonates and related dianions

Extensive studies have been carried out on many natural organic acids which interact with mineral surfaces in environmental systems.[2] It has been suggested, that studying well defined systems, such as small organic acids, will give a better understanding of the interactions of larger ill-defined organic molecules such as hummic acids since the functional groups of larger molecules are often composed of these smaller units. Several of these small organic compounds contain dicarboxylic acid groups such as oxalate, malonate and succinate.

Several of these studies have focused on surface charges and the dependence of binding on pH as discussed in Section 5.1.1. The use of first and second coordination sphere binding is also considered. Section 0 discusses other methods, such as database mining, which have been used to investigate the possible modes of inner coordination sphere complex formation by carboxylates and malonates.

5.1.1 Surface charges and pH dependence of binding

The adsorption of carboxylic acids to metal oxide surfaces can be via inner or outer sphere mechanisms, the former involving direct bonds to the metal atoms in the surface and the latter involving interactions which occur via surface groups. [2] Filius *et. al* studied the binding of some weak acids on an iron(III)(hydr)oxide mineral surface, goethite, and investigated the effect of concentration, pH and salt dependency on binding using a charge distribution multisite attachment model (CD-MUSIC) with comparisons to literature IR data.[2, 3]

The CD-MUSIC model considers the surface structure and the charge distribution at the interfaces. The goethite prepared by Hiemstra consists of needle shaped crystals which are dominated by a 110 face with 021 faces on the ends of the needles as shown by Figure 5-2.[3, 4] This gives rise to surface groups which are either singly, doubly and triply coordinated. The oxygens at the surface are then bound to either one, two or three Fe(III) ions in the goethite.

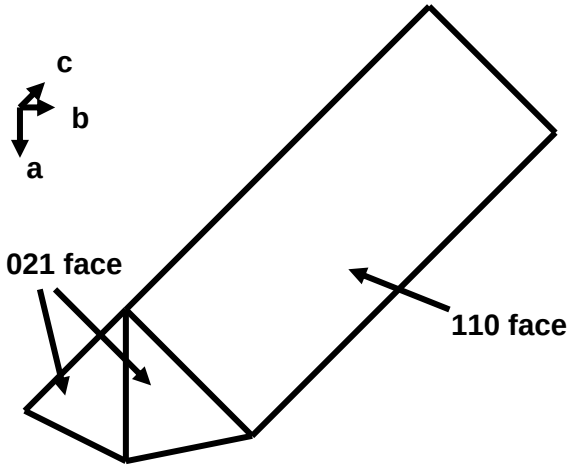

Figure 5-2 Schematic representation of the goethite crystal morphology[4]

Introduction

The charge of the Fe(III) ions is compensated by neighbouring oxygen atoms by the principle of electroneutrality. Each Fe-O bond has a +½ valence unit (vu) per bond using the theory described by Pauling.[5] Each oxygen ion has a charge of -2 vu and depending on the number of bonds with Fe(III) ions, the surface oxygens are charged differently. These groups are protonated under acidic conditions and each proton donates a +1 vu charge. Further protonation can occur depending on pH to make terminal water ligands and again each group will have a different charge. For example, an oxygen which is coordinated to one iron(III) atom and is doubly protonated has:

-2 vu, from the oxygen

+½ vu from the Fe-O bond

(2 x +1) vu from the H^+

= +½ vu ➔ $FeOH_2^{+½}$

The other possible species are: $FeOH^{-½}$, Fe_2OH^0, $Fe_3O^{-½}$. The authors claim the uncharged surface group consisting of an oxygen which is coordinated by two irons, remains singly protonated over a wide pH range, 2 to 12.[6]

When ligands bind to the surface, the reaction equations can be considered as:

$$-FeOH^{-½} + nH^+ + L^{-m} \rightleftharpoons -FeOH_{(1+n)}L(^{-½+n-m}) \quad \text{Outer-sphere}$$

$$n(-FeOH^{-½}) + nH^+ + L^{-m} \rightleftharpoons -Fe_nL(^{-m-½n}) + nH_2O \quad \text{Inner-sphere}$$

The overall charge of the completely deprotonated ligand can then be distributed over the three electrostatic planes as shown in Figure 5-3.These three planes are made up of a surface 0-plane which contains adsorbed protons and surface bound ligands. The remaining ligating atoms of a bound ligand or those which form by outer-sphere mechanisms lie in the intermediate solution directed 1-plane. The diffuse double layer contains the remaining ion-pairs.

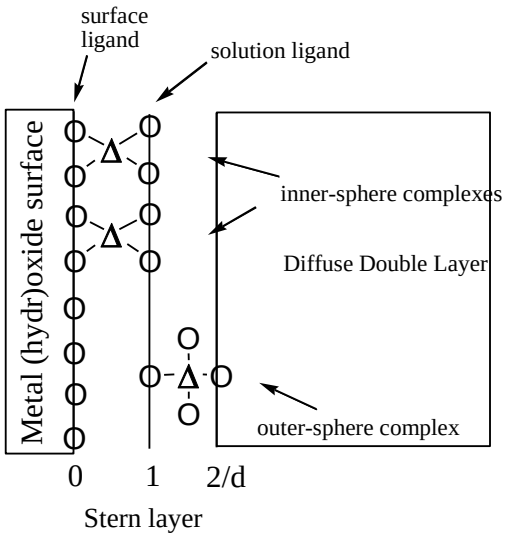

Figure 5-3 Schematic representation of inner and outer-sphere complexes showing the location of the three electrostatic planes.[3]

In the case of a carboxylate ligand, if the charge is equally distributed over both oxygens then each carries a net -½ vu. It is then neutralised by the Pauling charges of two Fe-O bonds, which is favourable for adsorption. The total change in charge of a surface plane can be calculated on the basis of the number of oxygens and the number of protons that react with surface hydroxyls to form water.

The acids studied by Filius were all dicarboxylic acids, and an increase in adsorption was observed with decreasing pH. At high pH values the goethite surface and ligand are both negatively charged and the binding is low. As the pH is lowered they become oppositely charged and the adsorption increases linearly with decreasing pH, pointing to binding of an electrostatic nature. The dependence then changes as the ligand becomes protonated and the charge of the anion diminishes. The adsorption of malonic acid is also lowered by increasing salt strength. The authors suggest that the malonate binds using two different modes, as discussed below, at different pH values. Also at the time of print, 1997, the authors note that there were no data in the literature for comparison. The modes of binding were inferred from the species which was considered the most chemically realistic and which gave an adequate description of the results.

Introduction

All modes involve inner sphere coordination of a single carboxylate group with the surface. At low pH, the surface oxygens are involved in bonds to protons, A in Figure 5-4. As the pH is increased, the free terminal carboxylate hydrogen bonds to a surface water group. When the concentration of Na(I) is high a third species can form involving a complex between the non-surface coordinated carboxylate with a sodium ion.

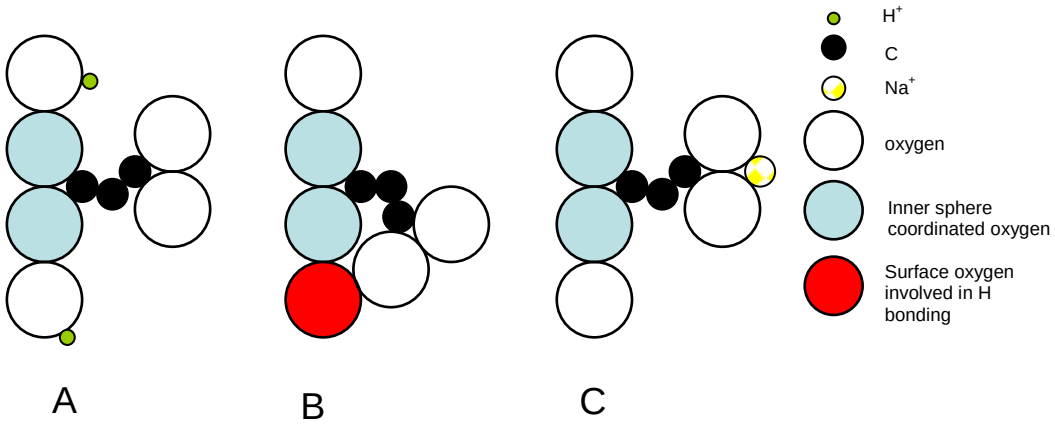

Figure 5-4 Models of malonate binding at A- low pH, B-higher pH values, C- high salt concentration, as suggested by Filius[2]

Persson and Axe have studied the adsorption characteristics and pH-dependence of oxalate and malonate on goethite from an aqueous solution. [7] Adsorption isotherms, in addition to *in-situ* attenuated total reflectance fourier transform infrared spectroscopy (ATF-FTIR) were used. Adsorption was measured using the uptake of ligand solutions containing the ^{14}C isotope. A model complex for the malonate binding, $[Fe(H_2C_3O_4)_3]^-$, as shown in Figure 5-5, was studied using EXAFS, and the theoretical vibration frequencies were calculated with DFT. The model involves a bidentate chelating 6 membered ring and the authors assume this is the main mode of surface coordination. The structures of the malonate surface complexes were then assessed by comparison of its characteristic IR features to those of the model. Since IR signals depend greatly on local chemical interactions if the local chemical environments in solution and at the surface are similar then virtually identical IR spectra are expected.

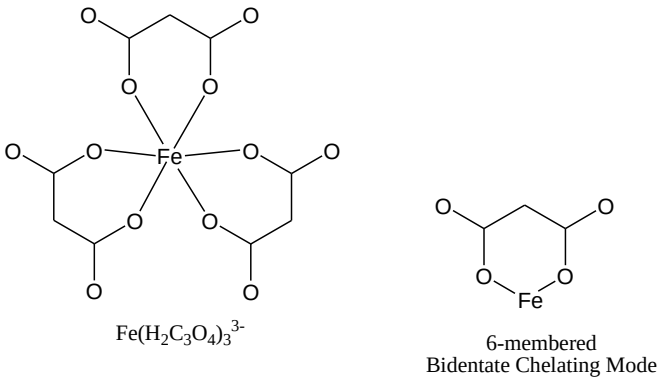

Figure 5-5 Structure of model compound and bidentate chelating mode used by Persson and Axe for IR comparisons[7]

For the surface-bound malonate complex the authors found that upon changing pH from 7.6 to 2.8 a broad peak at 1560 cm^{-1} moved to 1582 cm^{-1}. In addition, the intensity of the peak at 1340 cm^{-1} increased relative to that of a peak at 1430 cm^{-1} with increasing pH. This was attributed to the existence of at least two surface complexes. The first is described as a hydrogen bonded surface complex with no direct bond between the malonate and iron(III). The second is an inner-sphere complex where the malonate forms a six membered chelate ring and contains no protonated outer-sphere surface complexes, i.e. no secondary surface bonds form. In addition the authors noted that no dissolution of iron occurred over the whole range of experimental conditions used.

More recent studies by Hug and Bahnemann also used *in-situ* ATR-FTIR to study the adsorption of oxalate, malonate and succinate on TiO surfaces, anatase and rutile, and the γ-FeOOH surface, lepidocrocite [8] For the malonate-lepidocrocite binding, they discovered that the ligand uptake increased with decreasing pH and claim this is consistent with adsorption being an exchange of surface hydroxyl groups with carboxylate anions.[9] Possible modes of binding are discussed by comparison of the FTIR spectra obtained with free ligands in solution with a surface bound complex. The most noticeable difference between the adsorbed and free malonate is the absence of the carbonyl frequencies in the surface complex, suggesting the lack of carbon to oxygen double bonds. The authors interpret this difference between spectra as clear evidence for inner-sphere coordination with direct bonds to metal atoms.

Also, in this case the location of peaks in the spectra show virtually no dependence on pH and hence the authors argue that the surface complex consists of just one structure.

The authors propose a different structure from that of Persson and suggest it is likely to be one of those shown in Figure 5-6. In addition, they note that hydrogen bonding to surface hydroxyls lowers the double bond character of the non-coordinated carbon to oxygen bond such that typical carbonyl frequencies are not observed.

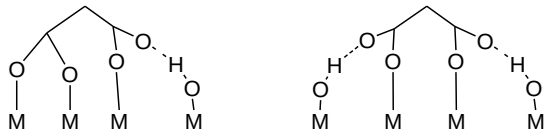

Figure 5-6 Schematic representation of possible modes of binding suggested by Hug and Bahnemann for malonate on lepidocrocite surfaces

It is therefore difficult to determine the definitive mode(s) of binding using IR without better models of the ligand bound surface complex for IR comparison.

5.2 Polynuclear complexes as models for surface binding

Polynuclear clusters with a large number of metal atoms are likely to give better models for surface ligand binding than mononuclear complexes since a metal oxide surface is necessarily a polynuclear structure. Studies carried out by Frey *et. al* showed that synthesis of clusters of this type could be used to rationalise the performance of a corrosion inhibitor ligand, **1**.[10, 11]

Adsorption isotherm experiments on a series of ligands structurally similar to **1**, demonstrated that ligands containing a keto group on the alkyl chain of the phenylbutanoic acid functionality gave significantly stronger binding than those without. This compared well with corrosion inhibition tests, which suggested that the

presence of a carbonyl and the terminal methyl group was also of importance in determining its effectiveness.

Synthesis of the $Fe_{11}O_6(OH)_6$(**1**-H)$_{15}$ cluster shown in Figure 5-7 was achieved by appropriate choice of solvents/ conditions. The complex contains 15 ligands binding using carboxylate groups attached to 11 iron(III) ions. Intramolecular hydrogen bonding occurs on four of the ligands between the keto group and hydroxyl groups attached to the iron oxide core. Three of these have almost identical conformations and are superimposed on each other in Figure 5-8.

Pattern matching was carried out with the arrangement of the iron-oxide unit on a lepidocrocite iron(III) oxide surface with minimal structural rearrangement.[12] Energy minimisation calculations showed that only minor changes in energy were required to allow the ligands in the model complex (as in Figure 5-8) to adopt the structure needed for surface binding, which suggests that this is a plausible mode of surface binding. This multisite attachment is similar to B in Figure 5-4.

Modelling of the surface generated by the side-by-side alignment of multiple ligands at this surface produced a close packed hydrophobic layer over the iron(III) oxide. The presence of the tolyl methyl group optimises the packing to obtain a coherent hydrophobic layer.

The efficacy of **1** as a corrosion inhibitor was thus attributed to both the hydrogen bonding between the keto-group and surface hydroxyls and to the hydrophobic layer that is produced by efficient packing of the tolyl "tails".

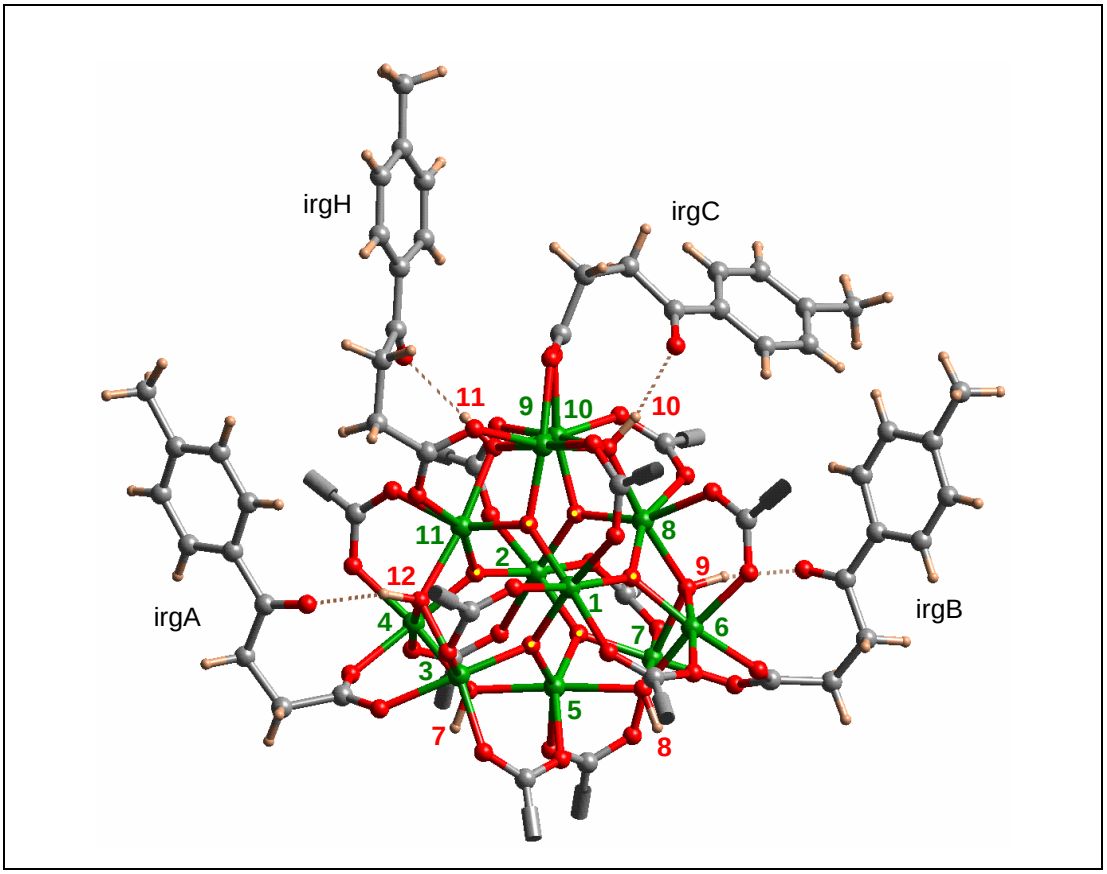

Figure 5-7 Molecular core of crystal structure of $Fe_{11}O_6(OH)_6(1\text{-}H)_{15}$ viewed along the pseudo 3-fold axis. The eleven iron atoms are shown as green balls and labelled with green numbers. The six oxide ions are highlighted with a yellow dot. The six hydroxide ions are labelled with red numbers. The four 1 ligands (A, B, C, H) which form hydrogen bonds (beige dashes) are shown in full. For the others, only the acetate head group is shown for clarity.[12]

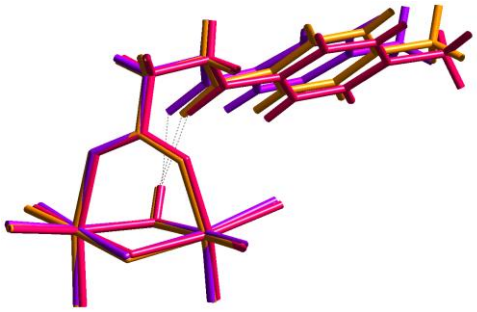

Figure 5-8 Overlay of the three hydrogen bonded ligands in Figure 5-7. Each of the four fragments has the formula $\{Fe_2O_7(OH)1\}$. Hydrogen bonding shown by dashed lines.[12]

5.3 Overview of chapter

This chapter looks at the binding characteristics of phenyl malonic acid on goethite from 95:5 MeOH/ H_2O. Using methods similar to those carried out by Harris *et. al*, attempts were made to discover its mode of binding.[10-12] Molecular modelling, and synthetic work to obtain polynuclear malonic acid complexes as models for surface structures are described.

5.4 Adsorption Isotherms

The adsorption isotherm for **21** is shown in Figure 5-10, along with **1**, the commercial corrosion inhibitor from Chapter 2 and **22** as a "control" to establish what benefit; if any, arises from the second carboxylic acid group. Each of these structures are shown in Figure 5-9.

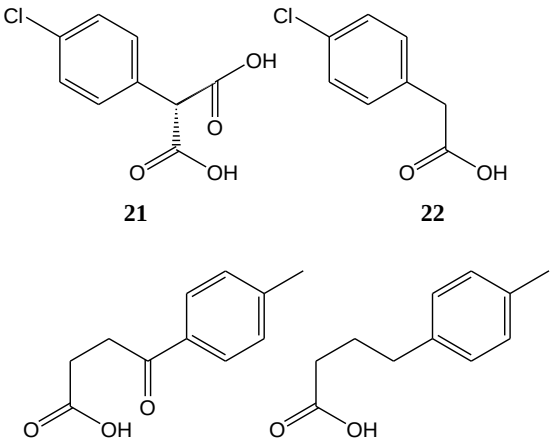

21 **22**

1 4-*p*-tolyl-butyric acid

Figure 5-9 Structures of Ligands 1, 21, 22 and 4-p-tolyl-butyric acid

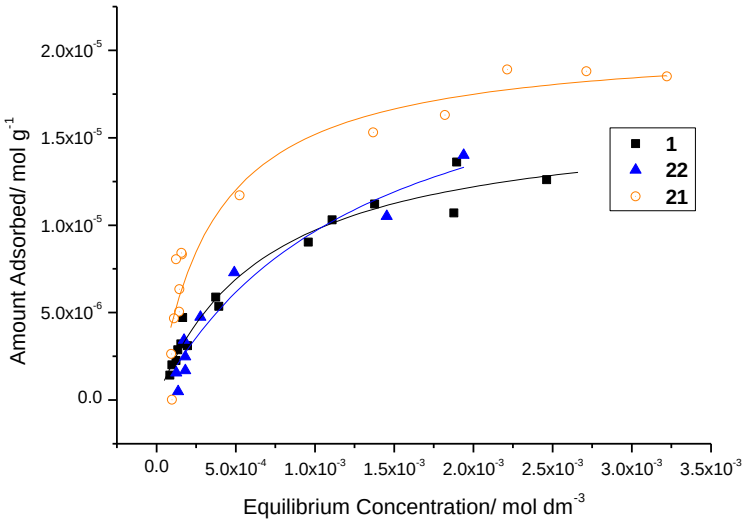

Figure 5-10 Uptake of 1, 21, 22 onto goethite from 95:5 MeOH/ H_2O

	1	**21**	**22**
Equilibrium binding constant(10^{-3}) / k	1.5(2)	2.8(6)	0.8(3)
Surface coverage(10^{5})/ mol g^{-1}	1.6(1)	2.1(1)	2.2(4)
Required surface area per molecule/ $Å^2$	238(15)	185(9)	170(31)

Table 5-1 Adsorption isotherm data for 1, 21 and 22

As can be seen in Table 5-1 the binding strength of **21** is higher than that found for **22**. Therefore, the presence of the second carboxylic acid group forms favourable secondary interactions which is consistent with the hypothesis of intermolecular bonding with surface oxygens, B in Figure 5-4.

The presence of an additional carbonyl group in a ligand, by comparison of **1** with 4-p-tolyl-butyric acid , has already been shown to enhance binding strength and was therefore expected to have a similar effect.[11] However, the relative increase of **21** over **22** compared with **1** with 4-*p*-tolyl-butyric acid is significantly higher in the malonate case. This could be due to either the pendant COOH group hydrogen bonding to the surface more effectively than the keto group or the hydrogen bonding acceptor group in **21** being closer to the surface, indicating better preorganisation, than in **1** and is investigated further in the next section.

The significantly stronger binding and higher surface coverage of **21** over **1** could indicate that it is a good candidate for corrosion protection or surface engineering of iron.

5.5 Molecular modelling and database mining

Molecular modelling was attempted to determine an explanation for this increase in binding strength and to suggest a potential mode of surface attachment. This modelling was carried out by Fraser White on a Silicon Graphics Octane Workstation running Cerius 2.[13, 14] The universal force field was used and partial atomic charges calculated using the charge equilibration.[15]

Database mining to identify potential binding modes of malonic acids were undertaken in a similar manner to the work on salicylaldoxime ligands (see Section 3.3) The modes are described using the Harris notation which is a concise method of describing the connectivity of a ligand, and was also used in Section 3.3.[12]

Various models can be suggested for malonate coordination, based on the main binding modes displayed by a monocarboxylate coordination. Statistical analysis of the CSD of the binding of carboxylates to metals has been carried out by Harris and more recently by White.[12, 16] The Harris nomenclature, of various modes of binding is shown in Figure 5-11, the number of complexes containing iron in the CSD is also shown.

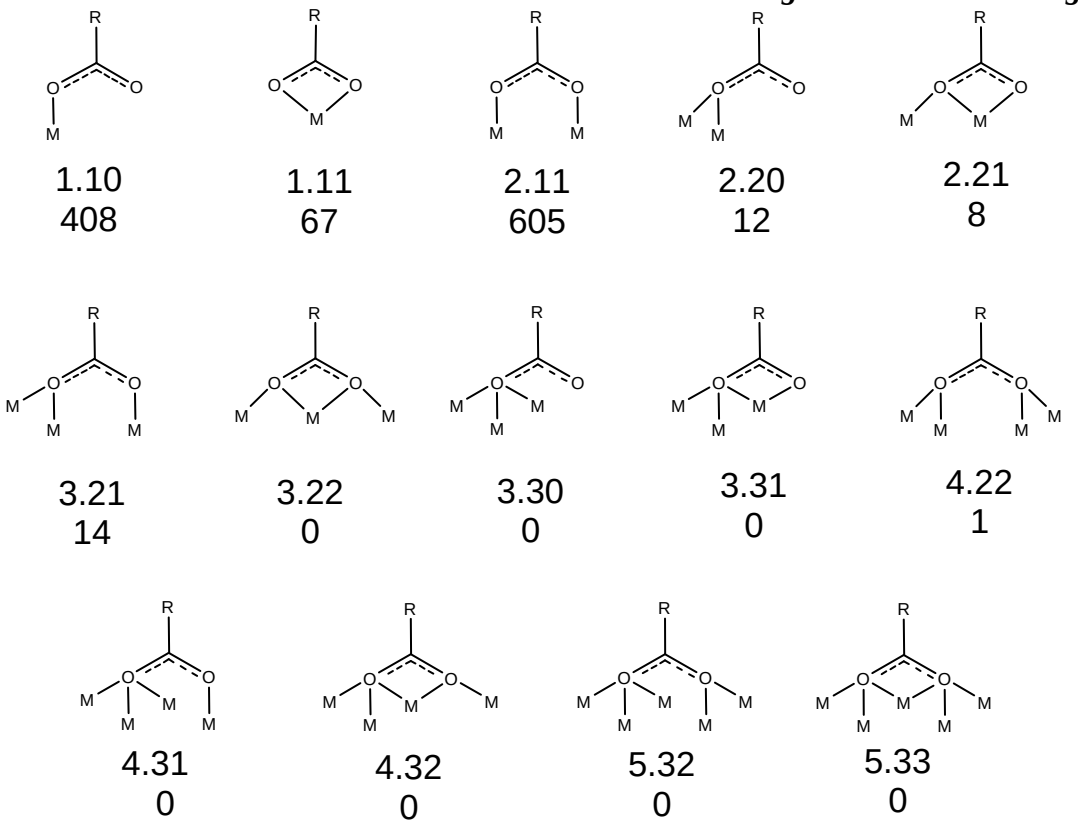

Figure 5-11 Binding modes observed for carboxylates in the CSD, stating Harris notation and, below, number of occurrences in CSD where M = Fe.[16]

There is significant preference for the 1.10 and 2.11 modes over any of the others. The large number of 1.10 mode complexes found was slightly unexpected, however, these complexes often contained large organic molecules with extensive functionality which dominated the coordination chemistry available to the COO^- group.[12]

The coordination preference displayed by single carboxylates was used as a basis to provide malonate binding modes. The Harris notation was extended to the malonate complexes, such that N.ABCD_m, where N is the total number of metal atoms bonded to the entire fragment and the positions of A-D are shown in Figure 5-12. In the cases where multiple orientations/ options are available, an arbitrary number is assigned, m. Four modes of binding for malonate to an iron oxide surface are shown which involve at least two Fe atoms in the surface.[16] Monodentate coordination

modes were not considered because these would not account for why malonate binds much more strongly than single carboxylic acids.

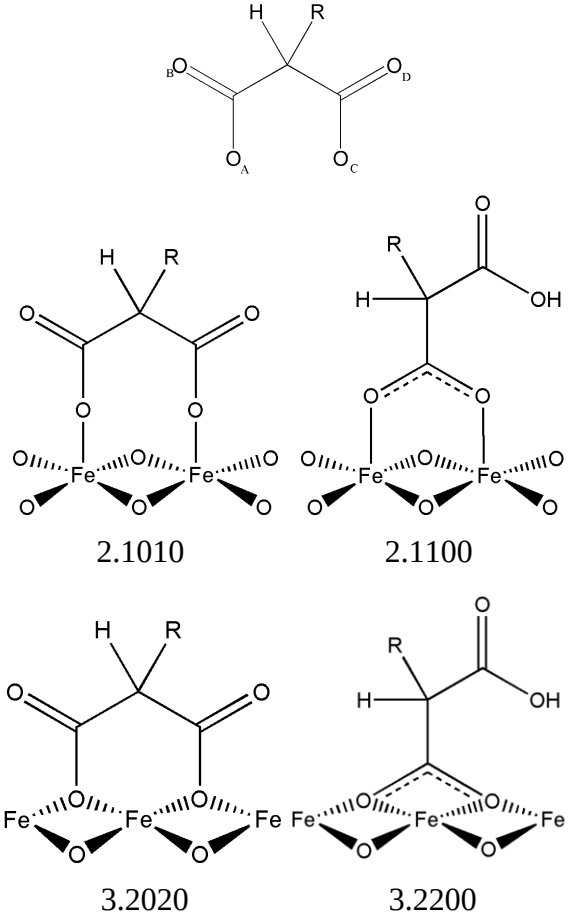

Figure 5-12 Positions of binding atoms A-D in malonate fragment and four different modes of binding with Harris notation

The modelling by molecular mechanics considered how the energy of the system is altered by attachment of a ligand to an iron(III) oxide surface. This depends mainly on charges in energies associated with changing bond lengths, bond angles and torsion angles to form the complex. In addition, the impact of van der Waal forces and electrostatic terms were also examined.

The surface chosen for modelling was the 010 plane of goethite as used by Harris.[12] This is found in lepidocrocite, the most predominant corrosion product on steel, and goethite, the substrate used in the ligand binding studies. In addition, interactions with carboxylate ligands were chemically viable without major surface reconstruction.

Initially modelling was carried out with unsubstituted malonic acid, R=H in Figure 5-12, for simplicity. The bidentate bridging 2.1010 mode allowed energy minimisation calculations to be carried out but the lack of intermolecular hydrogen bonding available does little to explain the high surface binding strength observed by malonates.

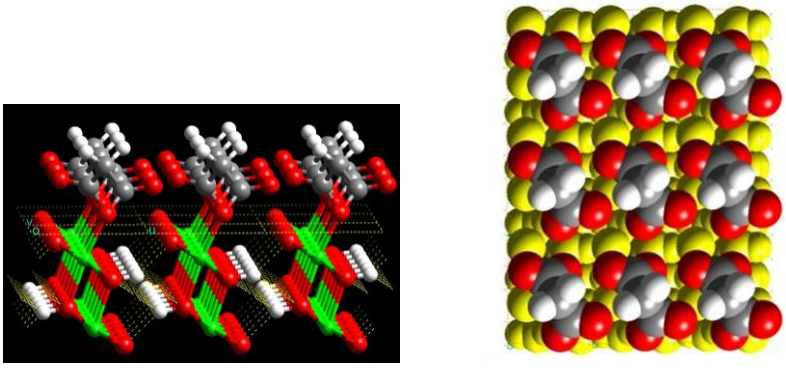

Figure 5-13 Molecular modelling simulations of docking mode for the 1.1010 type and spacefilling model showing packing of ligands on surface. Yellow colour shows uncovered iron oxide surface

The 2.1100 type has two different orientation possibilities for docking, labelled 1 and 2 as shown in Figure 5-14 and leads to the second carboxylate group being either approximately parallel or perpendicular to the surface. Molecular modelling suggests that both modes are possible.

Figure 5-14 Possible orientations for secondary functionality

The bidentate chelating 3.2020 mode is similar to the 2.1010 mode but two oxygen atoms from the malonate replace those of the surface oxide layer and the malonate is therefore 'embedded' into the surface. Modelling for this mode calculates the lowest energy of those discussed.

No calculations were carried out for the 3.2200 mode. The C-O distances of the surface bound carboxylate are too large to be chemically viable and the dispositions of the electrons on the oxygen atoms are unreasonable unless they lie in the plane of the iron oxide surface.

Adding the phenyl ring to the modelling adds further complexity to the system. Again, considering the 2.1010 case first, two possible orientations of the phenyl ring are available as shown in Figure 5-15. Simulation using the first mode failed, due to the unreasonable geometry obtained by forcing the aromatic ring parallel with the surface. The second gives an acceptable geometry with gaps between aromatic rings that may allow for some π-π interactions.

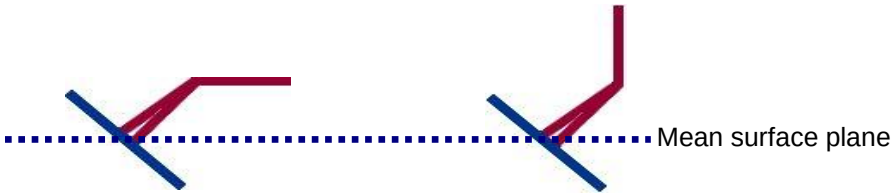

Figure 5-15 Possible orientations for phenyl ring in phenyl malonate case

In the case of the 2.1100 mode, the α carbon is chiral. Two different modes can occur and both result in allowed geometries. The first has a much higher energy than the second but free carboxylate groups are available for inter-ligand binding that could be involved in multilayering. The second mode gives a much lower energy than the first since the second carboxylate group is used in hydrogen bonding to near-by malonate molecules which are bound to the surface.

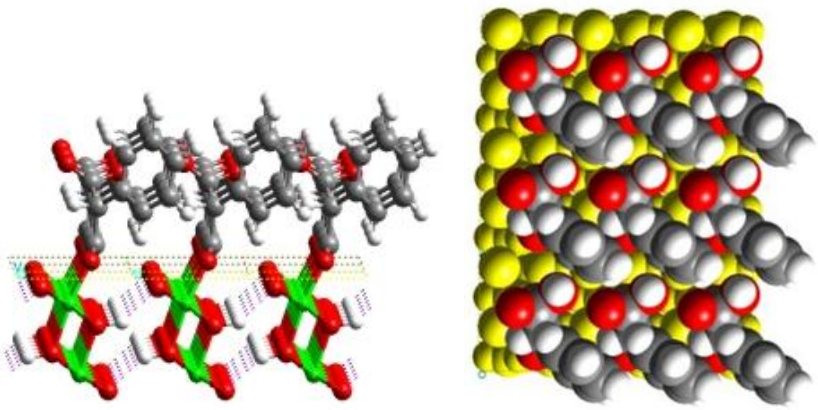

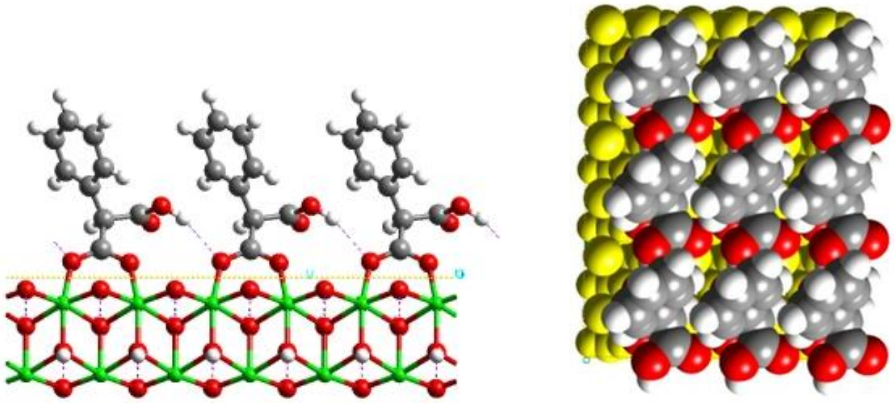

Figure 5-16 Molecular modelling simulations of 2.1100_1 (top) and 2.1100_2 (bottom) binding modes and spacefilling model showing packing of ligands on surface. Yellow colour shows uncovered iron oxide surface

The 3.2020 modes result in two very low energy binding modes, intermolecular hydrogen bonding occurs between carboxylate groups on neighbouring docked malonate molecules and the aromatic rings are much closer together.

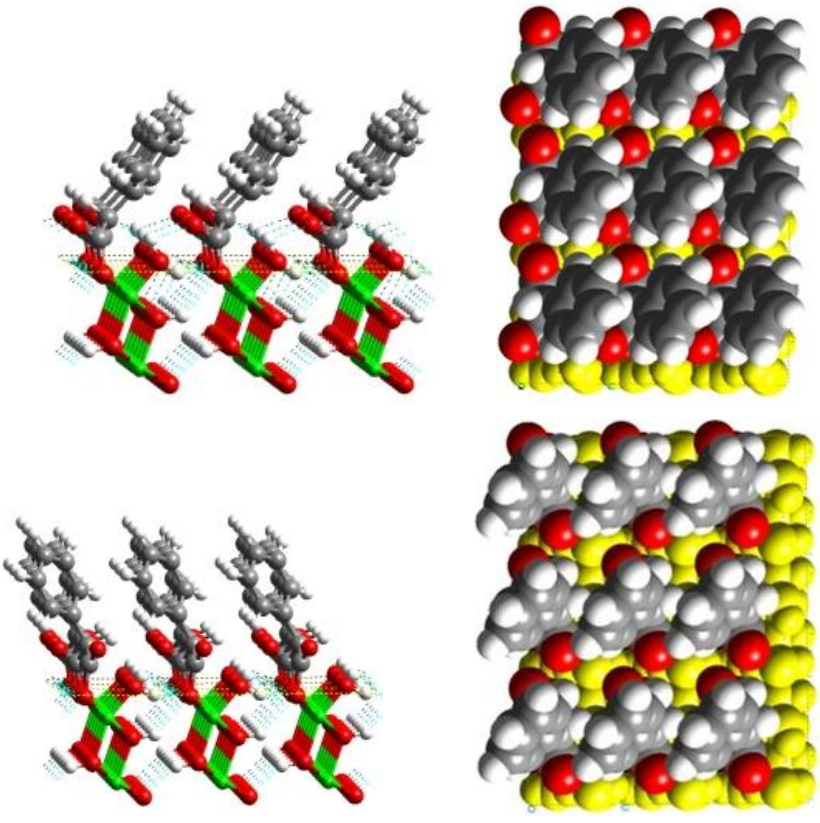

Figure 5-17 Molecular modelling simulations of 3.2020_1 (top) and 3.2020_2 (bottom) binding modes and spacefilling model showing packing of ligands on surface. Yellow colour shows uncovered iron oxide surface

5.6 Polynuclear clusters

It was hoped that polynuclear iron oxide clusters containing the malonate functionality could be prepared which would provide structural evidence to assist in defining possible binding modes. Several attempts were made to form polynuclear iron(III) oxide clusters, most of which were unsuccessful. They resulted in either polycrystalline material or crystals unsuitable for X-ray diffraction. However, it is widely known that the synthesis of polynuclear cluster is notoriously serendipitous.[17]

Crystals grown from a solution of iron(III) bromide in pyridine with phenyl malonic acid added gave the structure shown in Figure 5-18. It is important to note that the malonate ligand has undergone decarboxylation to phenyl acetate. This decarboxylation is discussed further in Section 5.7. The asymmetric unit consists of two $[Fe_3O(C_6H_5CH_2COO)_3(py)_3]$ complexes. Each contains an iron(III) oxide trimer with six phenyl acetate acid ligands. The structure is very similar to other (REF) $[Fe_3O(RCO_2)L_3]^+$ complexes in the CSD with three iron atoms and a μ_3 oxide ion in a plane and with pyridine molecules arranged *trans* to the iron-oxide bonds. The pyridine ligands are twisted out of the Fe_3O core by 140^0 along the OFeNC bonds.

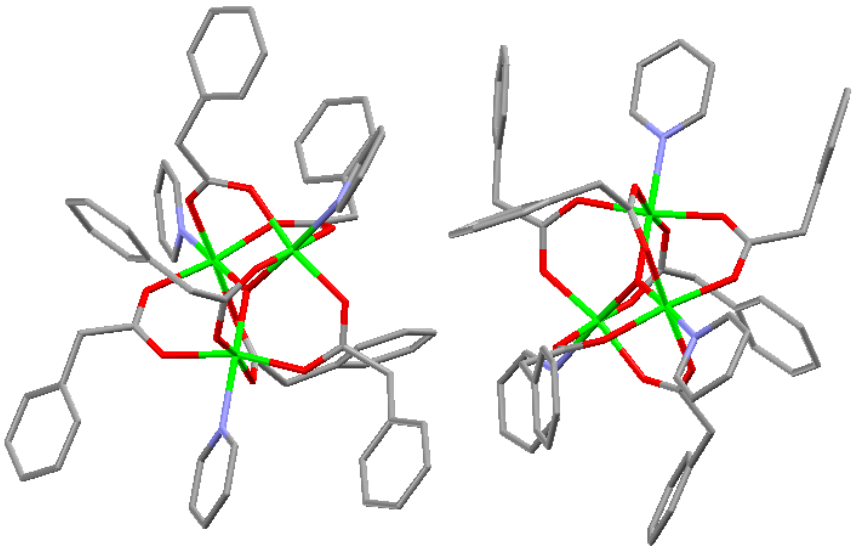

Figure 5-18 Crystal structure of $[Fe_3O(C_6H_5CH_2COO)_3(py)_3]$ showing two complex in the asymmetric unit. Iron atoms are coloured green. The hydrogen atoms have been omitted for clarity.

Each iron centre is *pseudo* octahedral, with bond angles between the oxygen atoms from the acid groups and μ_3 oxide, or nitrogen from the pyridine falling in the range 98^0 to 82^0 respectively. On each side of the Fe_3O plane, two phenyl acetate ligands have their aromatic rings parallel with the plane of the Fe_3O core. The third is twisted such that a hydrogen atom on the edge of the benzene ring lies above the bridging oxide ion (see Figure 5-19).

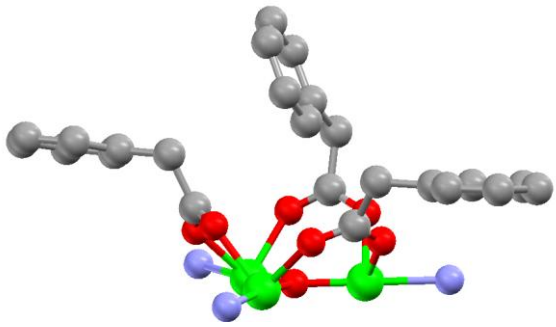

Figure 5-19 Part of the crystal structure of $[Fe_3O(C_6H_5CH_2COO)_3(py)_3]$ Showing arrangement of phenyl rings in relation to the iron oxide core. Iron atoms are coloured green. Carbon atoms of pyridine rings and hydrogen atoms have been omitted for clarity.

5.7 Malonic acid derivatives

Several attempts were made to synthesis derivatives of phenylmalonic acid. It was hoped that these could be used in conjunction with modelling studies to provide evidence for or against the suggested models and by comparing the observed binding strengths for each system. These derivatives were also planned to include the ICP-OES detectable atom, sulfur, for isotherm determination as discussed in Chapter 4.

4-chlorophenyl malonic acid was synthesised by reaction of 4-chlorophenyl acetic acid with butyl lithium and addition of solid CO_2 as shown in Figure 5-20. Deprotonation occurs at the α-carbon and is due to stabilisation by keto-enol resonance forms.

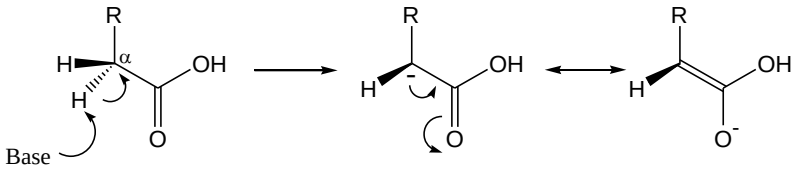

Figure 5-20 Mechanism of deprotonation at α-carbon atom and stabilisation due to keto-enol resonance forms

Nucleophilic attack at the δ+ carbon atom of the carbon dioxide molecule generates the malonic functionality, Figure 5-21.

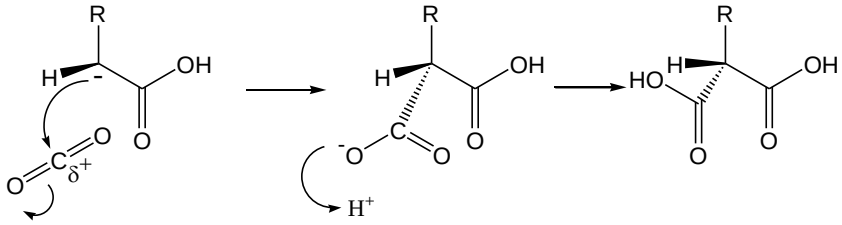

Figure 5-21 Mechanism of nucleophilic attack of carbon dioxide to form malonic acid functionality

It is thought that the reaction between 1-propanthiolate and the aryl chloride generated the product shown in Figure 5-22. However, attempted removal of the high boiling point solvent 1-methyl pyrrolidinone (NMP) resulted in decomposition of the product to an unidentifiable material.

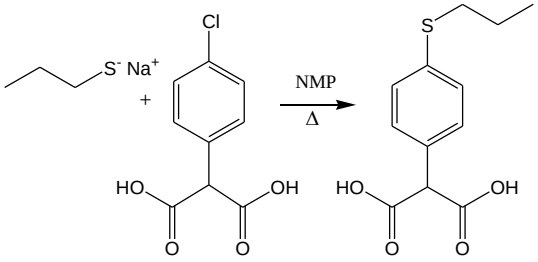

Figure 5-22 Reaction of sodium propanethiolate with 4-chlorophenyl acetic acid

Alternative synthetic routes were tried using phenylmalonic acid as a starting material. Both nitration and sulfonation reactions produced impure products that could not be separated and purified.

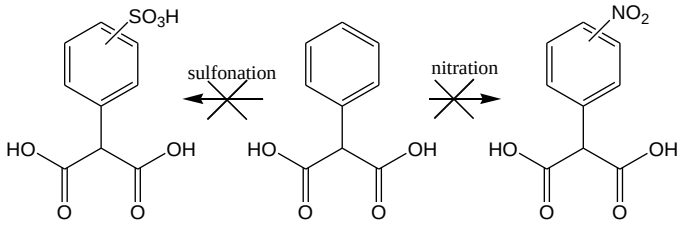

Figure 5-23 Attempted nitration and sulfonation of phenyl malonic acid

Reactions between alkyl halides and dimethyl propandioate, commonly known as dimethyl malonate, are well known and occur readily under basic conditions.[18] The α-carbon is next to two keto groups and therefore its protons are easily removed. Several attempts were made using malonate esters to attempt to form malonic acid compounds.

4-nitrophenyl malonate ester was successfully synthesised from dimethyl malonate and 1-fluoro-4-nitrobenzene as shown in Figure 5-24. The nitrogroup on the phenyl ring assists the reaction since resonance forms delocalises the negative charge.

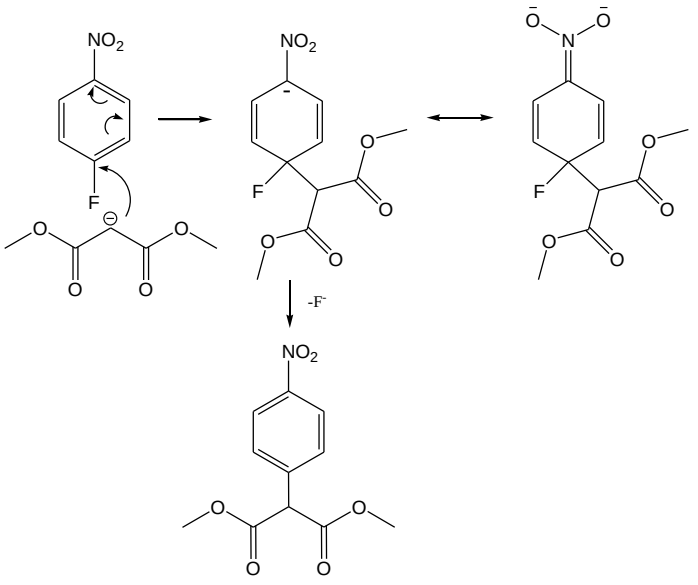

Figure 5-24 Formation of 4-nitrophenyl malonic ester from dimethyl malonate and 1-fluoro-4-nitrobenzene

However, decarboxylation occurred upon hydrolysis to make the malonate acid. The cyclic mechanism is shown in Figure 5-25 and occurs via an acid enol intermediate. Loss of gaseous carbon dioxide ensures that the reaction goes to completion.

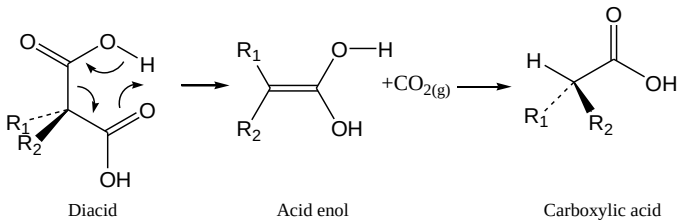

Figure 5-25 Mechanism of decarboxylation of malonic acid

Other attempts using alkyl halides with dimethyl malonate to form malonic acids also resulted in decarboxylation upon hydrolysis.

5.8 Conclusions

Chapter 3 showed that having a smaller alkyl chain link between a carbonyl group and a carboxylic acid group compared to a longer link was beneficial to the strength of surface binding. This chapter has shown that reducing the link further to just one carbon increases the binding strength further. This suggests that the malonic acid functionality is therefore a good candidate as a ligand for corrosion inhibition. In order to find ways to improve its efficiency attempts were made to determine the mode of binding using molecular modelling. The two most possible modes involve a binucleating mode which contains a free carboxylic acid group available for intermolecular hydrogen bonding and a dianionic malonate trinucleating mode. The serendipitous nature in synthesising polynuclear clusters failed to yield any useful crystal structure data on the malonate binding. The formation of a trinuclear iron oxide compound binding phenyl acetate ligands implies an inherent instability of the malonate species. This decarboxylation to phenyl acetic acid was also observed when attempting to synthesise malonic acid derivatives and limits the usefulness of

malonate as a surface engineering ligand except in systems where the loss of surface activity over time is beneficial.

5.9 Experimental

All reagents were used as obtained from Aldrich, Acros without further purification. ^{1}H and ^{13}C NMR were recordered on a DPX Bruker 360 MHz spectrometer. Fast atom bombardment (FAB) mass spectra were recorded on a Kratos MS50TC spectrometer. Infra-red (IR) spectra were obtained on a JABCO FTIR-460 spectrometer as potassium bromide discs. Electronic absorption measurements were made on a Unicam UV-2 Spectrophotometer.

2-(4-chloro-phenyl)-malonic acid (21)

4-chlorophenyl acetic acid (5g, 29 mmol) was dissolved in anhydrous THF (30 mls) and cooled to -78^{o}C in a dry-ice/acetone bath. A solution of butyl lithium (2.5 M, 27 mls) in hexane was then added dropwise with stirring. The mixture was stirred for a further two hours after addition was complete. Solid carbon dioxide (23 g) was then added in four portions over a period of 30 minutes. The mixture was stirred for a further two hours at -78^{o}C then at room temperature for 30 minutes. HCl (2M, 100 mls) and diethyl ether (50 mls) were then added and the layers separated. The aqueous layer was then extracted with further diethyl ether (2 x 30 mls) and the combined extracts were dried over magnesium sulfate and the solvent was removed under reduced pressure. Anhydrous ether was then added (20 mls) with excess hexane (100 mls) and was left to cool in a fridge overnight. The solvent was decanted off and the solid was recrystallised from a 2:1 mix of toluene and dichloromethane to give a white powder (1.4g, 22%) λ_{max} (95:5 MeOH/ H_2O)/ nm 224.5 (ε/ dm^3 mol^{-1} cm^{-1} 10, 000) ^{1}H NMR (MeOD) δ: 7.65-7.27 (d,d, 4H, J 5, 7 Hz, Ar-H). ^{13}C NMR: 169.6 C(8), C(9), 133.0 C(1), 132.1 C(7), 130.1 C(2), C(6), 127.5 C(3), C(5), 56.3 C(7). m.p. 119-121.

4-chlorophenyl acetic acid (22)

Was used as received from Aldrich.

2-(4-propylsulfanyl-phenyl)-malonic acid

Sodium hydride (0.43g, 18.6 mmol) was suspended in anhydrous 1-methyl 2-pyrrolidinone (NMP) (20 mls) and 1-propanethiol (1.42g, 18.6 mmol) was added slowly with stirring. 4-chlorophenyl malonic acid was dissolved in NMP (5 mls) and added to the reaction flask and was stirred at 100^{o}C during which time the mixture turns orange. Upon cooling, 0.1M HCl (aq) (15 mls) and diethyl ether was added. The layers were separated and the aqueous layer extracted with diethyl ether (2x10 mls). The organic layers were combined, washed with water (15 mls), and dried over anhydrous magnesium sulphate. Removal of the diethyl ether resulted in an orange liquid that was mainly NMP solvent. Attempted removal of this solvent under high vacuum and temperature resulted in an unidentifiable oil.

5.10 References

1 W. M. Kutz and H. Adkins, *Journal of the American Chemical Society*, 1930, **52**, 4391.

2 J. D. Filius, T. Hiemstra, and W. H. Van Riemsdijk, *Journal of Colloid and Interface Science*, 1997, **195**, 368.

3 T. Hiemstra and W. H. van Riemsdijk, *Journal of Colloid and Interface Science*, 1996, **179**, 488.

4 P. Venema, T. Hiemstra, and W. H. van Riemsdijk, *Journal of Colloid and Interface Science*, 1996, **183**, 515.

5 L. Pauling, *Journal of the American Chemical Society*, 1929, **51**, 1010.

6 T. Hiemstra, P. Venema, and W. H. van Riemsdijk, *Journal of Colloid and Interface Science*, 1996, **184**, 680.

7 P. Persson and K. Axe, *Geochimica et Cosmochimica Acta*, 2005, **69**, 541.

8 S. J. Hug and D. Bahnemann, *Journal of Electron Spectroscopy and Related Phenomena*, 2006, **150**, 208.

9 W. M. Stumm, J. J; , 'Aquatic Chemistry, Chemical Equilibria and Rates in Natural Waters', John Wiley and Sons Inc., 1996.

10 M. Frey, S. G. Harris, J. M. Holmes, D. A. Nation, S. Parsons, P. A. Tasker, S. J. Teat, and R. E. P. Winpenny, *Angewandte Chemie, International Edition*, 1998, **37**, 3246.

11 M. Frey, S. G. Harris, J. M. Holmes, D. A. Nation, S. Parsons, P. A. Tasker, and R. E. P. Winpenny, *Chemistry--A European Journal*, 2000, **6**, 1407.

12 S. G. Harris, 'Crystallographic and modelling studies of organic ligands on metal surfaces', Edinburgh University, Edinburgh, 1999.

13 F. J. White, 'PhD thesis', University of Edinburgh, Edinburgh, In Preparation.

14 M. S. Incorportated, in 'Cerius 2', San Diego, 2000.

15 A. K. Rappe, C. J. Casewit, K. S. Colwell, W. A. Goddard, III, and W. M. Skiff, *Journal of the American Chemical Society*, 1992, **114**, 10024.

16 F. J. White, in 'Unpublished work', 2005.

17 R. E. P. Winpenny, *Journal of the Chemical Society, Dalton Transactions*, 2002, 1.

18 J. G. Clayden, 'Organic Chemistry', Oxford University Press, 2001.

Contents

6 Conclusions and Future work

The design and development of organic ligands has been considered in this thesis and multisite attachment has been shown to be useful to provide strong surface binding. The use of adsorption isotherms provide a means of determining the thermodynamic stability of a ligand-surface complex and data fitting to the Langmuir equation often provides information about the binding strength and surface coverage of a ligand. Analysis of the data is more complex in situations where multilayering processes occur. In some circumstances double Langmuir equations can be used although they give no information about the different binding processes which occur.

Attempts have been made to use alternative tools to study binding and obtain kinetic information through use of a QCM. However, the equipment investigated was overly sensitive to the surrounding laboratory environment and was not used.

Investigation of a patent by ICI suggested that the synergistic performance observed by combining two corrosion inhibitors was not due to an increase in multisite attachment to the surface but more likely due to multilayering and the hydrophobic effect. These generate so-called “thick films” which are effective at engineering surfaces.

The deliberate inclusion of functional groups which allow intermolecular interactions between surface bound ligands has been shown to be beneficial to the thermodynamic stability of the surface assembly. Increasing the amount of favourable functionality often generates complexes which give rise to larger stability constants. Some groups that are useful for providing secondary ligand-ligand bonds are also good at surface ligation. This creates the possibility of enhancing binding due to the larger number and types of bonds possible between the ligand and the surface, thus making it harder to suggest a single definitive mode of attachment.

The binding of the malonate functionality was investigated in detail by molecular modelling calculations. The models suggested, proved inconclusive at defining a

mode of binding due to the various charge balance and energy difference issues although the most likely are a binucleating mode which contains a free carboxylic acid group available for intermolecular bonding or a dianionic malonate trinucleating mode. Attempts to synthesise polynuclear iron(III)oxide clusters were unsuccessful in providing evidence to confirm any of the models proposed. This was complicated by the ease of malonate decarboxylation as shown by the iron (III) trimer complex formed, that contained a decarboxylated ligand, and also the attempts to synthesise malonate derivates which underwent decarboxylation reactions. However, this tendency to decarboxylate has the potential to be exploited by industry in friction additives which are designed to deliberately decrease in surface activity over time.

Continuation of these studies should attempt to investigate further methods to study ligand binding from both an academic and industrial viewpoint. Spectroscopic techniques could provide some insight into the types and strengths of bonds that occur. The ability of the ligands that have been synthesised to act as corrosion inhibitors would allow further correlations between functionality and corrosion inhibition performance to be determined allowing the design of better surface actives.

Contents

A1. Quartz Crystal Microbalance

The quartz crystal microbalance is a highly sensitive piece of equipment capable of detecting very small mass changes with real-time data capture. As a change in mass is observed as a function of time, kinetic information can be obtained. The device operates due to the piezoelectric effect and functions as a gravimetric tool.

In 1880, Pierre and Jacques Curie observed that exerting pressure on a small piece of quartz caused an electric potential between the deformed surfaces.[1] They also discovered the inverse was true and that application of a voltage effected physical displacements. This pressure-electric effect was named the "piezoelectric" effect.

When an oscillating electric field is applied to a piezoelectric material, an acoustic wave can be induced which spreads through the material. A resonant frequency can then be obtained when the electric and mechanical oscillations are near the fundamental frequency of the crystal. This oscillation frequency depends on the thickness, density and shear modulus of the quartz.

There are many materials which exhibit the piezoelectric effect. Some such as ammonium dihydrogen phosphate have very large piezoelectric coefficients. The usefulness of the material depends on its mechanical and thermal stability. A large amount of information about the design and behaviour of quartz crystal resonators has been obtained and they are used exclusively for use in devices requiring piezoelectric materials. Since quartz is cheap and easy to obtain there has been little reason to look at other piezoelectric materials for resonators.

An ordinary piece of quartz crystal can have many modes of resonance. To be useful a mode must be selected and suppress all others. This is done by cutting the quartz at a specific crystallographic orientation.[2] The mode of vibration found to be most sensitive to change of mass is the high-frequency thickness-shear mode. The analysis of this thickness-shear mode is relatively simple because the plate motions are essentially one-dimensional as shown in Figure 1.

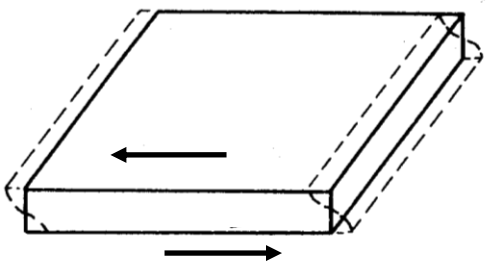

Figure 1 One dimensional thickness shear motions of plate[3]

In order to make the quartz crystal resonate in the thickness-shear mode it needs to be cut in the correct orientation.[3] Figure 2 shows the x, y and z axis on the crystal and rotations of the AT and BT cuts. The AT-cut is the most commonly used.

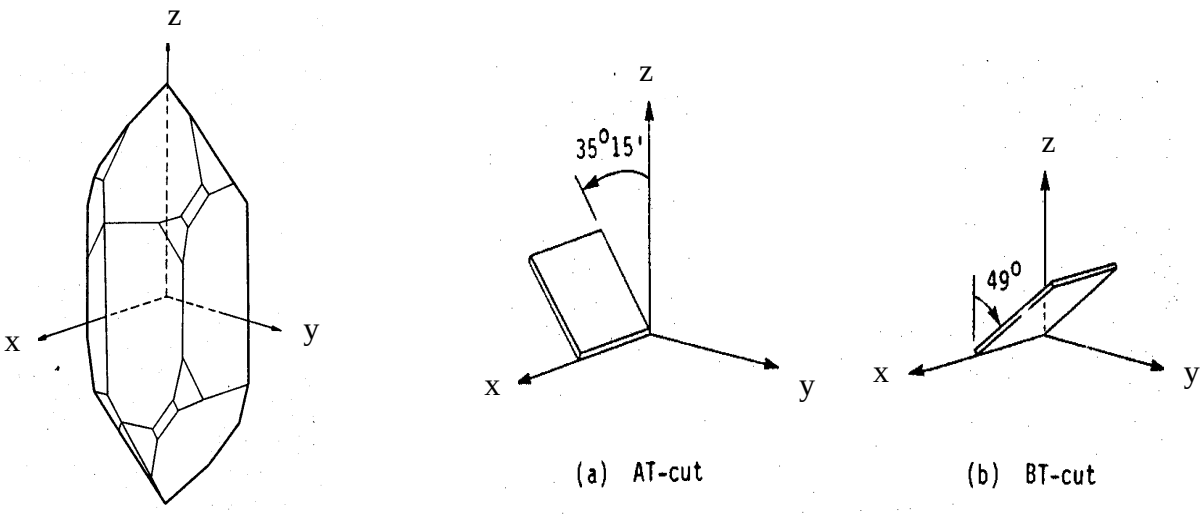

Figure 2 Axes of quartz crystals and orientations of the AT and BT cuts[4]

The resonant frequency can also be affected by temperature and stress.[1] Figure 2 shows the frequency-temperature dependence of different cuts of quartz crystals. In order to use a QC effectively, the resonance needs to have virtually zero dependence on temperature in the region where the work is to be carried out. The AT- cut, which has a cut angle of $35^0$15', has a near zero dependence on temperature in the range 10-50^0C.

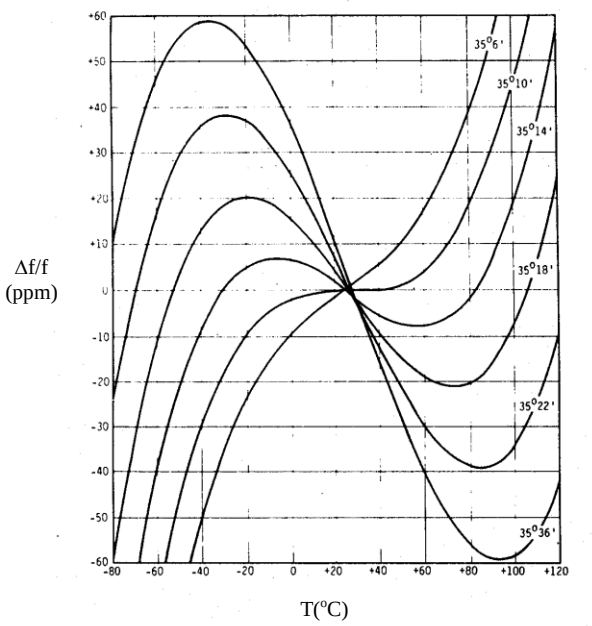

Figure 3 Frequency-temperature dependence for a range of cutting angles[4]

Lord Rayleigh's work showed that "a small change in the inertia of a mechanically vibrating system perturbs the resonant frequency", which means that the adsorption onto the surface will change the resonant frequency .[5] Sauerbrey developed the theory and suggested using a QC oscillator as a sensing device for measuring the thickness of thin films.[6] Equation 1, derived by Sauerbrey, shows the relationship between the oscillation frequency of the fundamental mode of the QCM (f_0), the overtone number (n), the density (ρ_q), the shear modulus of quartz (μ_q), the change in frequency (Δf) and the change in mass (Δm).

$$\Delta f = -\frac{2\Delta m n f_0^2}{A\sqrt{(\mu_q \rho_q)}} \qquad \text{Equation 1}$$

For a given crystal of quartz the values of f_0, n, ρ_q, μ_q are constant and the frequency changes only with respect to mass per unit area. This means that the QCM is most effective when used to study processes that are uniform across the whole surface of the crystal.

For optimal use of the QCM, there are four important conditions:[1]

1) uniform distribution of mass over the QC plate,
2) complete cover of the active area of vibration,

3) attachment of the deposited material to the QC plate, and
4) knowledge of the area of material.

When these conditions are met, by either a monolayer or a thin film that exhibits rigid-layer behaviour the relationship shown in equation 2, which is a simpler version of equation 1, can be used where m is the mass of the unloaded resonator.[7]

$$\frac{\Delta f}{f_0} = -\frac{\Delta m}{m} \qquad \text{Equation 2}$$

It is this simple relationship between the frequency change and the mass on the surface of the crystal which provides the basis for our proposal to use the QCM for competitive binding studies of surface ligands. The sensitivity of the QCM depends on the fundamental frequency which usually ranges between 2-20 MHz.[8] Such balances are commercially available but some custom built QCMs have been shown to be able to operate at 27MHz.[9] Thinner crystals have higher frequencies but are very fragile, crystals with fundamental frequencies at about 2MHz are very robust but much less sensitive. The trade off is therefore sensitivity against robustness and the standard compromise is usually 10 MHz.

Initially the QCM has been used by others purely to study gaseous systems. It was thought that liquids would dampen the oscillation frequency to the extent that measurement would be impossible. However, later it was shown, that it is possible to use QCMs in liquids and to study processes occurring at the liquid-solid interface.[10, 11] These studies led to a modified expression, equation 3, to describe the behaviour of the electrode in contact with a liquid phase.

$$\Delta f = -f_0^{3/2}\left[\frac{\eta_s \rho_s}{\pi \eta_q \rho_q}\right]^{1/2} \qquad \text{Equation 3}$$

where η_s is the solution viscosity and ρ_s is the solution density.

As can be seen, the frequency depends on both the viscosity and density of solution in contact with the QC, any viscosity changes that may occur during the reaction being studied, must be

taken into account. It has been shown that the change in frequency is independent of volume of solution present or height above crystal surface.[12]

The simpler Equation 1 can still be used, provided that the density and viscosity of the solution do not change during the experiment.

The QCM is set-up such that the results are captured in real-time by computer. This means that changes are measured in-situ as they happen rather than after reaction.The reaction vessel involved can vary depending on the system being measured, these include flow cells where reactants are continuously flowed around the cell and pass the surface of the quartz, open containers have also been used where reactants can simply be injected or added to the solution as data capture occurs.

Figure 4 shows how the quartz crystal is sandwiched between two electrodes, usually gold, with the electrical connections attached.

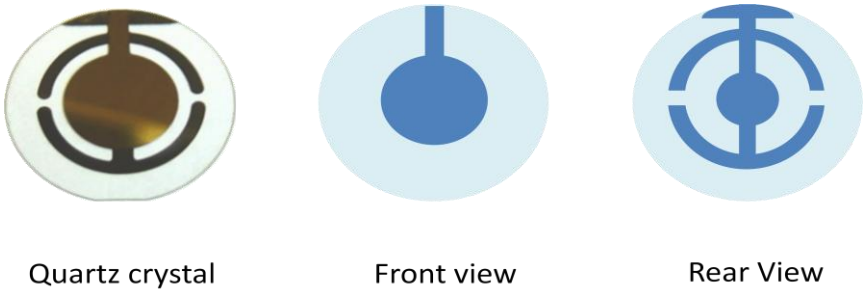

Figure 4 Photograph of Quartz crystal showing schematic of the front and rear view of crystal surface. The darker blue shading indicates gold plating on the light blue quartz surface.

The QCM apparatus contains the crystal sandwiched between two O-rings. One side of the surface is exposed to the liquid being studied. The frequency of oscillation is continuously measured by computer and a change in frequency is converted to the change in mass. Since the change in mass depends only on the frequency change, resonant frequency and mass of unloaded resonator no calibration is required.

The QCM has been described as a very sensitive but not selective gravimetric device. Coating of the QCM surface can be used to tackle the selectivity issue and has resulted in a variety of uses,

from the monitoring of gas levels, to the use of conducting polymer coatings in the detection heavy metal ions. Other groups have used proteins bound to surface to study the interactions of antibodies and antigens.[13]

The device has been used in combination with a variety of other techniques. In combination with electrochemistry the term Electrochemical Quartz Crystal Microbalance, or EQCM, is commonly used. This has been done to study reactions such as electrochemical metal deposition,[14] corrosion of metals commonly used in industry,[15] and kinetics relating to the solvolysis and creation of conducting polymers.[16]

The QCM has also been studied with many in-situ surface analytical techniques including Surface Plasmon Resonance,[12] Auger Electron Spectroscopy,[17] X-ray Photoelectron Spectroscopy, Fourier-Transform IR[18] and contact angle grazing measurements.[19]

[1] R. M. M. a. W. White, *Rev. Sci. Instrum.*, 1968, **39**, 291.
[2] J. J. Kipling, 'Adsorption from Solutions of Non-Electrolytes', Academic Press, 1965.
[3] D. A. Skoog, Leary, J.J., 'Principles of Instrumental Analysis', Saunders College Publishing, 1992.
[4] A. W. S. C. D. Warner, ed. R. F. Walker, NY, 1962.
[5] J. W. S. L. Rayleigh), 'The Theory of Sound', 1945.
[6] G. Z. Sauerbrey, *Z. Phys.*, 1959, **115**, 206.
[7] M. R. Deakin and D. A. Buttry, *Analytical Chemistry*, 1989, **61**, 1147A.
[8] C. K. O'Sullivan and G. G. Guilbault, *Biosensors & Bioelectronics*, 1999, **14**, 663.
[9] Y. Okahata, K. Niikura, Y. Sugiura, M. Sawada, and T. Morii, *Biochemistry*, 1998, **37**, 5666.
[10] S. Bruckenstein and M. Shay, *Electrochimica Acta*, 1985, **30**, 1295.
[11] J. Auge, P. Hauptmann, J. Hartmann, S. Roesler, and R. Lucklum, *Sensors and Actuators, B: Chemical*, 1995, **B24**, 43.
[12] M. Minunni, M. Mascini, G. G. Guilbault, and B. Hock, *Analytical Letters*, 1995, **28**, 749.
[13] R. D. Vaughan, E. Geary, M. Pravda, and G. G. Guilbault, *International Journal of Environmental Analytical Chemistry*, 2003, **83**, 555.
[14] M. Seo, K. Yoshida, H. Takahashi, and I. Sawamura, *Journal of the Electrochemical Society*, 1992, **139**, 3108.
[15] M. Seo, K. Yoshida, and K. Noda, *Materials Science & Engineering, A: Structural Materials: Properties, Microstructure and Processing*, 1995, **A198**, 197.
[16] J. Rishpon and S. Gottesfeld, *Biosensors & Bioelectronics*, 1991, **6**, 143.
[17] J. Onsgaard and O. Ellegaard, *Nuclear Instruments & Methods in Physics Research, Section B: Beam Interactions with Materials and Atoms*, 1984, **230**, 666.
[18] T. T. Dao, C. A. Spence, and D. W. Hess, *Proceedings of SPIE-The International Society for Optical Engineering*, 1991, **1466**, 257.
[19] E. Occhiello, M. Morra, F. Garbassi, and J. Bargon, *Applied Surface Science*, 1989, **36**, 285.

Contents

A2.1 Adsorption isotherm data for Ligand **1**

Concentration/ mol dm^{-3}	Amount Adsorbed/ mol g^{-1}
2.96E-03	2.03E-05
2.36E-03	1.62E-05
1.91E-03	1.82E-05
1.64E-03	1.55E-05
7.03E-04	1.29E-05
1.93E-04	4.57E-06
1.66E-04	4.32E-06
1.59E-04	3.53E-06
1.38E-04	3.16E-06
1.24E-04	2.54E-06
1.12E-04	1.90E-06
1.13E-04	9.33E-07
8.50E-05	7.06E-07
2.96E-03	2.03E-05
2.36E-03	1.62E-05

A2.2 Adsorption isotherm data for Ligand **2**

Concentration/ mol dm^{-3}	Amount Adsorbed/ mol g^{-1}
0.00304	1.24E-05
0.00241	1.06E-05
0.00144	9.26E-06
9.35E-04	6.67E-06
3.80E-04	5.50E-06
8.02E-05	2.50E-07
8.24E-05	9.47E-07
1.10E-04	1.01E-06
1.55E-04	6.45E-07

A2.3 Adsorption isotherm data for Ligand **3**

Concentration/ mol dm^{-3}	Amount Adsorbed/ mol g^{-1}	Concentration/ mol dm^{-3}	Amount Adsorbed/ mol g^{-1}
0.001913	1.52E-05	0.000264	9.55E-07
0.001602	1.02E-05	0.000203	1.25E-06
0.001172	8.56E-06	0.000156	1.14E-06
0.000815	4.81E-06	0.000116	8.79E-07
0.000366	3.45E-06	7.27E-05	6.97E-07
0.001853	1.67E-05	3.69E-05	3.38E-07
0.001533	1.19E-05	0.001112	9.25E-06
0.001166	8.70E-06	0.001847	1.55E-05
0.000783	5.61E-06	0.00275	1.77E-05
0.000326	4.45E-06	0.00336	2.72E-05
0.000379	3.12E-06	0.000441	3.83E-06
0.000412	2.29E-06	0.000716	4.42E-06
0.000358	2.36E-06	0.000965	5.71E-06

0.000325	1.96E-06	0.001654	1.07E-05
0.000277	1.87E-06	0.001894	1.21E-05

A2.4 Adsorption isotherm data for Ligand **4**

Concentration/ mol dm^{-3}	Amount Adsorbed/ mol g^{-1}
3.69E-03	3.78E-05
2.86E-03	3.27E-05
1.99E-03	2.82E-05
1.45E-03	1.57E-05
6.99E-04	8.55E-06
3.24E-04	4.89E-06
2.82E-04	4.61E-06
2.47E-04	4.23E-06
2.32E-04	3.31E-06
1.31E-04	4.51E-06
1.77E-04	2.08E-06
1.14E-04	2.34E-06
7.79E-05	1.95E-06
6.02E-05	1.09E-06
1.77E-05	8.51E-07
2.05E-03	2.39E-05
1.62E-03	1.97E-05
1.25E-03	1.36E-05
8.48E-04	8.85E-06
4.19E-04	4.56E-06

A2.5 Adsorption isotherm data for Ligand **5**

Concentration/ mol dm^{-3}	Amount Adsorbed/ mol g^{-1}
0.00297	9.56E-06
0.00198	1.03E-05
0.00155	9.10E-06
6.09E-04	8.75E-06
3.51E-04	3.17E-06
2.43E-04	2.32E-06
2.07E-04	2.02E-06
1.84E-04	1.39E-06
1.55E-04	9.18E-07
0.00297	9.56E-06
0.00198	1.03E-05

A2.6 Adsorption isotherm data for Ligand **6**

Concentration/ mol dm^{-3}	Amount Adsorbed/ mol g^{-1}
0.00543	1.01E-05
0.00254	9.42E-06
0.00115	7.57E-06
5.68E-04	4.00E-06
5.11E-04	3.63E-06
4.45E-04	3.44E-06
3.72E-04	3.42E-06

3.22E-04	2.86E-06
2.24E-04	2.66E-06
2.07E-04	2.11E-06
1.43E-04	1.89E-06
9.04E-05	1.39E-06
5.70E-05	3.95E-07

A2.7 Adsorption isotherm data for Ligand **7**

Concentration/ mol dm^{-3}	Amount Adsorbed/ mol g^{-1}
0.005036136	1.16E-05
0.004151042	6.32E-06
0.003018781	7.11E-06
0.002102425	2.52E-06
0.001594897	1.42E-06
0.001047738	1.33E-06
0.000462366	2.19E-06
0.000438125	1.43E-06
0.000329337	1.40E-06

A2.8 Adsorption isotherm data for Ligand **8**

Concentration/ mol dm^{-3}	Amount Adsorbed/ mol g^{-1}
0.00362	1.01E-05
0.002709	7.7E-06
0.001418	2.25E-06
0.000892	2.84E-06
0.000476	6.62E-07
0.000489	3.52E-07
0.00045	6.52E-08
0.000382	5.22E-07
0.000412	-1.5E-06
0.000309	-1.7E-07
0.000241	2.62E-07
0.000208	-1.8E-07
8.46E-05	3.97E-07

A2.9 Adsorption isotherm data for Ligand **9**

Concentration/ mol dm^{-3}	Amount Adsorbed/ mol g^{-1}
7.39E-05	1.61E-07
1.25E-04	8.83E-07
1.73E-04	1.70E-06
2.15E-04	2.62E-06
5.58E-04	6.09E-06
8.95E-04	7.67E-06
0.00125	8.81E-06
0.00339	1.05E-05
0.00209	7.37E-06
0.00157	8.31E-06

A2.10 Adsorption isotherm data for Ligand **10**

Concentration/ mol dm^{-3}	Amount Adsorbed/ mol g^{-1}
4.14E-05	2.34E-07
4.86E-05	1.32E-06
6.51E-05	2.17E-06
8.78E-05	2.24E-06
8.43E-05	2.96E-06
9.31E-05	3.37E-06
7.03E-05	4.54E-06
6.57E-05	4.71E-06
2.42E-04	6.60E-06
7.24E-04	7.31E-06
9.62E-04	7.68E-06

A2.11 Adsorption isotherm data for Ligand **11**

Concentration/ mol dm^{-3}	Amount Adsorbed/ mol g^{-1}
2.98E-05	8.93E-07
4.68E-05	2.93E-06
5.94E-05	3.42E-06
6.27E-05	4.17E-06
7.06E-05	4.77E-06
9.16E-05	5.91E-06
6.83E-05	4.40E-06
1.82E-04	7.68E-06
3.93E-04	8.52E-06
6.10E-04	9.25E-06
8.37E-04	9.76E-06
3.79E-04	9.25E-06
0.00101	1.22E-05
0.00176	1.23E-05
0.00259	1.03E-05

A2.12 Adsorption isotherm data for Ligand **12**

Concentration/ mol dm^{-3}	Amount Adsorbed/ mol g^{-1}
2.96E-03	2.03E-05
2.36E-03	1.62E-05
1.91E-03	1.82E-05
1.64E-03	1.55E-05
7.03E-04	1.29E-05
1.93E-04	4.57E-06
1.66E-04	4.32E-06
1.59E-04	3.53E-06
1.38E-04	3.16E-06
1.24E-04	2.54E-06
1.12E-04	1.90E-06
1.13E-04	9.33E-07
8.50E-05	7.06E-07

2.96E-03	2.03E-05
2.36E-03	1.62E-05

A2.13 Adsorption isotherm data for Ligand **13**

Concentration/ mol dm^{-3}	Amount Adsorbed/ mol g^{-1}
3.87E-05	4.42E-07
3.17E-05	2.03E-06
5.02E-05	2.96E-06
5.92E-05	3.45E-06
5.79E-05	4.19E-06
5.54E-05	4.94E-06
7.72E-05	5.11E-06
1.67E-04	9.87E-06
5.36E-04	1.48E-05
7.39E-04	1.67E-05
9.97E-04	1.73E-05
0.00128	1.73E-05

A2.14 Adsorption isotherm data for Ligand **14**

Concentration/ mol dm^{-3}	Amount Adsorbed/ mol g^{-1}
2.65E-05	2.02E-06
6.91E-05	3.62E-06
1.28E-04	4.82E-06
2.01E-04	5.68E-06
3.14E-04	6.76E-06
5.52E-04	7.70E-06
8.56E-04	1.08E-05
1.05E-03	1.14E-05
1.29E-03	1.07E-05
1.49E-03	1.10E-05

A2.15 Adsorption isotherm data for Ligand **16**

Concentration/ mol dm^{-3}	Amount Adsorbed/ mol g^{-1}
4.92E-05	1.39E-06
8.04E-04	1.43E-05
1.36E-03	1.77E-05
1.98E-03	1.95E-05
2.59E-03	2.15E-05
4.46E-05	3.43E-06
5.09E-05	5.54E-06
6.77E-05	7.37E-06
1.03E-04	8.79E-06

A2.16 Adsorption isotherm data for Ligand **17**

Concentration/ mol dm^{-3}	Amount Adsorbed/ mol g^{-1}
0.000033875	1.14475E-06
0.000046	3.82018E-06
6.96875E-05	4.25748E-06
0.00009375	5.64321E-06
0.000135281	6.55202E-06
0.0003595	1.04162E-05
0.000654375	1.28906E-05
0.000980625	1.43552E-05
0.00131625	1.57102E-05
0.001625625	1.76563E-05
0.00195	1.93261E-05
0.002353125	1.90575E-05
0.0030275	2.15273E-05

A2.17 Adsorption isotherm data for Ligand **18**

Concentration/ mol dm^{-3}	Amount Adsorbed/ mol g^{-1}
0.0000345	6.82761E-07
4.77188E-05	1.89798E-06
0.000085	2.50542E-06
0.00011475	3.32275E-06
0.000144938	4.11508E-06
0.000121375	2.87978E-06
0.000194625	3.98299E-06
0.000247875	5.60446E-06
0.000457359	6.3022E-06
0.000652031	7.39109E-06
0.000995156	1.04205E-05

A2.18 Adsorption isotherm data for Ligand **19**

Concentration/ mol dm^{-3}	Amount Adsorbed/ mol g^{-1}
3.39E-05	1.14E-06
4.60E-05	3.82E-06
6.97E-05	4.26E-06
5.61E-05	5.54E-06
9.38E-05	5.64E-06
1.35E-04	6.55E-06
3.60E-04	1.10E-05
6.54E-04	1.37E-05
9.81E-04	1.54E-05
0.00132	1.71E-05
0.00163	1.93E-05
0.00195	2.12E-05
0.00235	2.12E-05
0.00303	2.42E-05

A2.19 Adsorption isotherm data for Ligand **20**

Concentration/ mol dm^{-3}	Amount Adsorbed/ mol g^{-1}
3.52E-05	1.12E-06
3.57E-05	3.10E-06
3.80E-05	5.00E-06
1.93E-05	6.44E-06
2.67E-05	7.31E-06
2.32E-05	8.36E-06
3.06E-05	9.11E-06
1.86E-05	9.45E-06
2.04E-04	1.47E-05
5.94E-04	2.49E-05
9.05E-04	2.74E-05
0.00117	3.07E-05
0.00144	3.38E-05
0.00178	3.56E-05
0.00228	4.26E-05

A2.20 Adsorption isotherm data for Ligand **21**

Concentration/ mol dm^{-3}	Amount Adsorbed/ mol g^{-1}
0.00322	1.85E-05
0.00271	1.88E-05
0.00221	1.89E-05
0.00182	1.63E-05
0.00137	1.53E-05
5.24E-04	1.17E-05
1.61E-04	8.33E-06
1.58E-04	8.42E-06
1.23E-04	8.05E-06
1.44E-04	6.33E-06
1.44E-04	5.05E-06
1.11E-04	4.67E-06
9.30E-05	2.63E-06
9.85E-05	1.24E-08